Theoretical and experimental investigations of Permeate Gap Membrane Distillation

Li Gao

Bachelor of Environmental Engineering

Master of Civil Engineering

The College of Engineering and Science

Institute for Sustainable Industries & Liveable Cities

Victoria University

Submitted in fulfilment of the requirements of the degree of Doctor of Philosophy

(2019)

Abstract

Membrane Distillation (MD) is a separation process driven by the vapour pressure difference established across hydrophobic membrane. In order to combine the advantages of conventional MD configurations, Permeate Gap Membrane Distillation (PGMD) modules were developed. The objectives of this study were to systematically evaluate the performance of several new hollow fibre PGMD modules.

This study consisted of four components. First of all, the membrane was systematically characterized. The membrane dimension and morphology were investigated using Scanning Electron Microscope (SEM). The membrane porosity was measured using the wetting method. The membrane hydrophobicity was determined by measuring the contact angles of the inner and outer hollow fiber surfaces. Finally, Liquid Entry Pressure (LEP) was investigated. Based on the membrane characterization, it was confirmed that the employed hollow fibre membrane was suitable for MD application.

Next, a single PGMD module was built with 8 gap channels and 1 hollow fibre within each gap channel. This module was operated in different modes (PGMD, DCMD and SGMD) to compare their performance. The results showed that the maximum flux of hollow fiber PGMD was 27% and 1.6% lower than the maximum flux of DCMD and SGMD respectively. This phenomenon was due to the higher coolant velocity for DCMD and applied air flow in the gap channel for SGMD. The mass transfer coefficient was also used as an indicator to compare performance. For PGMD, the mass transfer coefficient increased initially at the lower feed inlet temperature and then decreased when the feed inlet temperature was higher than $60°C$, which could be attributed to the combined effects of transverse vapor flux and temperature non-uniformity of the bulk flow. On the contrary, the global mass transfer coefficients of DCMD and SGMD decreased slightly as a function of feed inlet temperature. Compared to other studies, our results demonstrated that PGMD has the potential to effectively combine the advantages of different conventional MD processes.

Afterwards, we have investigated the impacts of different PGMD module designs on water productivity and energy efficiency. The results showed that module with lower hollow fibre packing density or gap channel density had a higher flux and better energy efficiency, while modules with higher hollow fibre packing density or gap channel density exhibited more energy efficient use of the membrane surface area and higher productivity. Additionally, the module with a more conductive cooling plate had a higher

flux and lower Specific Thermal Energy Consumption (STEC), which was mainly attributed to the lower thermal resistance of the cooling plate. Due to the nearly stagnant velocities within the gap and coolant channels, the impact of cooling plate material on PGMD performance was greater than that of hollow fibre packing density and gap channel density. The Gain Output Ratio (GOR) obtained for the hollow fibre PGMD module was relatively low compared to other MD studies, however, the PGMD module performance cannot be assessed purely based on GOR. A trade-off exists between GOR and flux for MD modules, and the flux obtained from our hollow fibre PGMD module was relatively high.

Finally, a set of mathematical models were developed to simulate the mass and heat transfers phenomenon in hollow fibre PGMD process. The validated model was employed to evaluate the impacts of important MD design parameters on module performance. The modelling results showed that coolant velocity and coolant temperature had less impact on flux compared to those of DCMD, because the coolant of DCMD contacts with membrane directly. The model also suggested that increasing the cooling plate thermal conductivity resulted in a higher flux. However, when the cooling plate thermal conductivity was higher than 5 W/m.K, further increases in the thermal conductivity of the cooling plate had a negligible impact on flux. A sensitivity study was undertaken to analyze the combined effects of gap channel inner/outer diameters and gap channel thermal conductivity on flux. It is concluded that the gap thermal conductivity played a more important role in PGMD performance compared to the hydrodynamic flow in permeate and coolant channels.

To further improve hollow fibre PGMD performance, six recommendations are provided for the future work.

Declaration

"I, Li Gao, declare that the PhD thesis entitled Theoretical and experimental investigations of permeate gap membrane distillation is no more than 100,000 words in length including quotes and exclusive of tables, figures, appendices, bibliography, references and footnotes. This thesis contains no material that has been submitted previously, in whole or in part, for the award of any other academic degree or diploma. Except where otherwise indicated, this thesis is my own work".
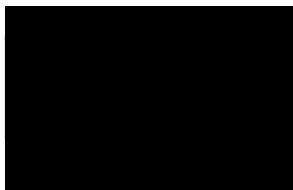
Signature: Date: 3rd January 2019

Acknowledgement

I started my Ph.D study in August 2012. After almost 6.5 years I finally reach the final stage of my study. I cannot go through a lot of 'dark moments' without the help from my supervisors, colleagues, classmates and family.

First of all, I would like to express my sincere gratitude to my principal supervisor Prof. Jun-De Li. Jun-De, I still remember our very first discussion on the possibility of my part-time Ph.D project on 6th April 2011 in your office. You have given me the opportunity to conduct this research at Victoria University and have introduced me to the membrane distillation field, which has opened a new door for me. Your great knowledge in mathematics has helped me to develop skills in computation modelling.

I am deeply grateful to Prof. Stephen R. Gray, my associate supervisor. Stephen, thanks for all the critical comments you have provided, they have improved my study significantly. Furthermore, thanks for always being 'Yes' to me. Your full support has helped me to test my ideas and to access to the broader water industry. I still need to return you the book 'Heat Transfer', which you have lent to me when we first met in 2011. It is probably overdue.

I really appreciate the help from Dr. Jianhua Zhang. Jianhua, you have taught me so much first-hand practical knowledge and skills about membrane distillation experiments, which cannot be obtained from any books or lessons. It has saved me lots of time and energy, which was particularly important for me as a part-time Ph.D student.

I also would like to give my heartfelt gratitude to my Industry Supervisor Dr. Dharma Dharmabalan, General Manager Systems Performance & Major Projects of TasWater. Dharma, you have introduced me to the Australian water industry and this Ph.D study. Without your encouragement I cannot come to this point.

I acknowledge the financial contributions to this study from my current and former employers South East Water and Coliban Water. I also greatly appreciate the generous support and encouragement from colleagues: David Sheehan, Phillip Fasham, Raj Mahendrarajah, Raymond Stephenson and Douglas Wingett from Coliban Water; Pam Kerry, Andrew Chapman, Andrew Sieber, Keith Johnson and David Bergmann from South East Water.

Li Gao

Templestowe Lower, Australia

3rd January 2019

Research Papers

Published Journal Papers arising from research described in this thesis:

[1] L. Gao, J. Zhang, S. Gray, J.-D. Li, Experimental study of hollow fiber permeate gap membrane distillation and its performance comparison with DCMD and SGMD, Separation and Purification Technology, 188 (2017) 11-23.

[2] L. Gao, J. Zhang, S. Gray, J.-D. Li, Influence of PGMD module design on the water productivity and energy efficiency in desalination, Desalination, 452 (2019) 29-39.

[3] L. Gao, J. Zhang, S. Gray, J.-D. Li, Modelling mass and heat transfers in permeate gap membrane distillation using hollow fibre membrane (submitted to Desalination).

Published Conference Paper:

[1] L. Gao, J. Zhang, S. Gray, J.-D. Li, Experimental investigation on permeate gap membrane distillation with novel hollow fibre membrane, International Membrane Science & Technology Conference, Melbourne, 2013.

[2] L. Gao, J. Zhang, S. Gray, J.-D. Li, Optimization of hollow fibre Permeate Gap Membrane Distillation (PGMD), 3rd International Conference on Desalination Using Membrane Technology, Gran Canaria, 2017.

Oral presentation

Li Gao, Jianhua Zhang, Stephen Gray, Jun-De Li, Optimization of hollow fibre Permeate Gap Membrane Distillation (PGMD), 3rd International Conference on Desalination Using Membrane Technology, 2 – 5 April 2017, Gran Canaria, Spain.

Poster presentation

Li Gao, Jianhua Zhang, Stephen Gray, Jun-De Li, Experimental investigation on permeate gap membrane distillation with novel hollow fibre membrane, International Membrane Science & Technology Conference, 25 – 29 November 2013, Melbourne, Australia.

TABLE OF CONTENTS

Chapter 5 Influence of PGMD design on the water productivity and energy efficiency   66

Chapter 6 Modelling heat and mass transfers in PGMD using hollow fibre membrane   87

List of Tables

List of Figures

Chapter 1 Introduction

Membrane distillation (MD) is an innovative process integrating membrane separation and heat-exchange for desalting highly saline water. The separation process is driven by the vapor pressure difference across a porous hydrophobic membrane [1].

Invented in early 1960s [2], MD did not gain much attention initially from either academia or industry due to two main reasons: the lack of high performance hydrophobic membrane and high energy consumption compared to other types of desalination technologies [3]. From later 1980s, the interests in MD started to recover due to the rapid developments in novel membrane materials and module configurations, and in the last decades, numerous commercially available MD systems finally emerged [4].

Although researchers have developed various new MD configurations, the following basic MD characteristics have not changed [2]:

- porous membrane is utilized;

- membrane pores cannot be wetted by process liquids;

- no condensation occurs within the membrane pores;

- liquid/vapor equilibrium of involved components cannot be altered; and

- hot feed liquid directly contacts with the membrane.

Compared to conventional evaporative process (Multi-Stage Flash Distillation or Multi-Effect Distillation) and pressure driven membrane process (Reverse Osmosis), MD demonstrates a number of key advantages [1, 3, 5, 6]:

- relatively low operating temperature compared to other thermal processes as it is not necessary to heat the solution up to the boiling point;

- the potential of utilizing low-grade waste heat or alternative energy sources, such as solar energy;

- relatively low operating pressure compared to other thermal/pressure driven processes;

- better product quality in comparison to pressure driven membrane processes (Reverse Osmosis);

- less membrane fouling and scaling; and

- lower requirements for membrane mechanical strength.

There are four conventional MD configurations as shown in Fig.1-1, including Direct Contact Membrane Distillation (DCMD), Air Gap Membrane Distillation (AGMD), Sweeping Gas Membrane Distillation (SGMD), and Vacuum Membrane Distillation (VMD). Fig.1-1 shows that the differences of these four conventional MD module designs are in the permeate arrangement on the coolant side of the membrane. Here, T_{fb}, T_{cb}, T_{fm} and T_{cm} are the temperatures of feed and coolant bulk flows, respectively, and membrane interface temperatures on the feed and cold sides, respectively. P_{vacuum} represents the vacuum pressure at the permeate side.

Each conventional MD configuration has its advantages and disadvantages. For DCMD, the coolant directly contacts with the membrane, mass transfer rate is generally high for the given temperature difference across the membrane, but heat loss by conduction is higher compared to other MD configurations. For AGMD, the existence of an air gap between the membrane and condensation surface results in less heat loss by conduction, but this leads to the higher mass transfer resistance. For VMD and SGMD, the mass transfer is improved by creating vacuum or gas sweeping on the permeate side, however, condensation takes place outside the MD module, which leads to a higher capital cost. Researchers started to develop and investigate new MD configurations, which can effectively combine advantages of different conventional MD configurations.

Permeate Gap Membrane Distillation (PGMD), also known as Water Gap Membrane Distillation (WGMD) or Liquid Gap Membrane Distillation (LGMG), is a DCMD variant, which contains a liquid gap (usually permeate water) between the membrane and coolant (see Fig. 2-4). Due to this additional permeate gap, PGMD module exhibits various advantages compared to the conventional MD configurations, including integration of heat recovery within the module compared to SGMD and VMD, lower sensible heat loss compared to DCMD, and lower mass transfer resistance compared to AGMD [6].

Although PGMD has been studied by various research groups [6-18], previous studies focused on spiral wound or flat sheet PGMD modules. Hollow fibre membrane has a relatively large specific surface area without any supporting structure, consequently, this study has developed the first hollow fibre PGMD module, which could be used for desalination, brine treatment or wastewater treatment. This study systematically investigated the module performance, and optimized its design using experimental and modelling approaches.
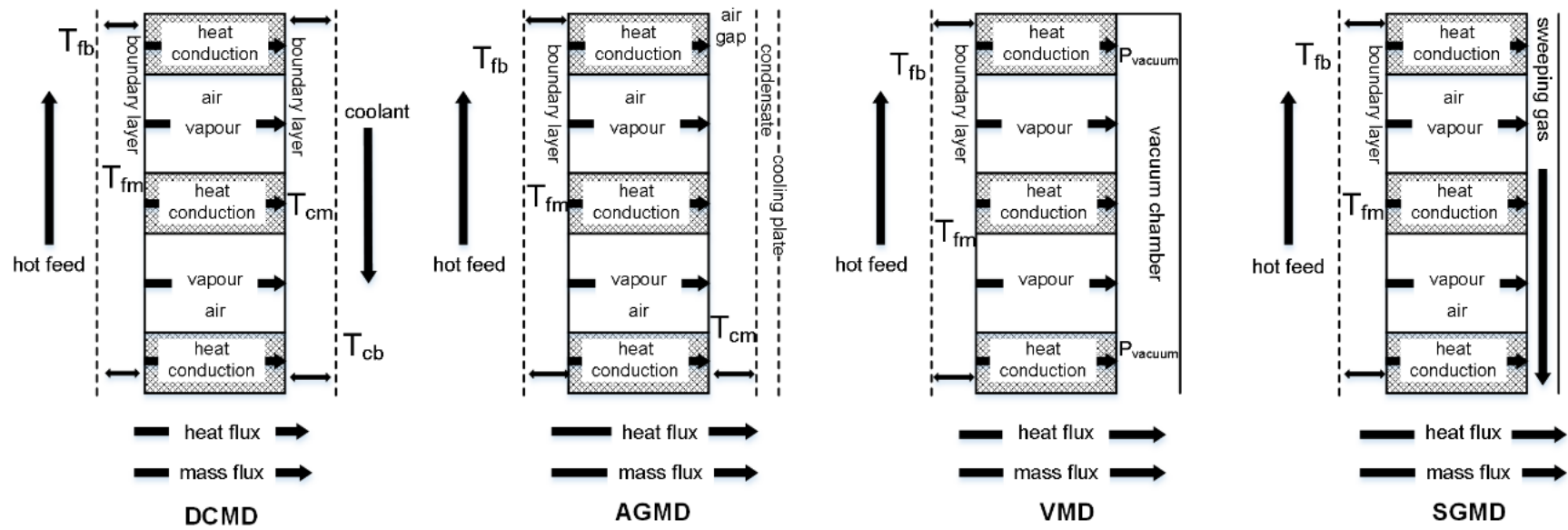
Fig.1-1. Four conventional MD configurations [4]

This study includes four major parts:

(1) to characterize the selected hollow fibre membrane to verify its suitability for MD application;

(2) to experimentally investigate the performance of a hollow fibre PGMD module and compare it with (a) same module operated in DCMD and SGMD modes; (b) other spiral wound and flat sheet PGMD studies;

(3) to assess different PGMD design parameters affecting module's productivity and energy efficiency; and

(4) to build a mathematical model to simulate heat and mass transfers within the hollow fibre PGMD module.

Through this study, the effects of different module design parameters were investigated, the advantages and limitations of hollow fibre PGMD module were presented, and recommendations were provided for module optimization.

Chapter 2 Literature review

2.1. History of MD development

The first MD patent was filed by Bruce R. Bodell in 1963 [19]. From then on, MD has gained interests from many researchers. In 1967, Findley published the first MD paper 'Vaporization through porous membranes' in the journal Industrial & Engineering Chemistry Process Design and Development using DCMD concept. Based on the experimental results, Findley has suggested the most suitable membrane characteristics for MD process. One year later, Bodell filed another U.S. patent for MD process, introducing the initial concepts of SGMD and VMD [2, 19] .

Interest in MD process faded very quickly after its initial introduction due to two main reasons. Firstly, MD process showed a significantly lower productivity compared to Reverse Osmosis (RO) process. Secondly, there was a lack of high performance hydrophobic membrane suitable for MD process.

The interests in MD process has slowly emerged again in 1980s with new developments in membrane materials and modules. The first 'Workshop on membrane distillation' was held in Rome, Italy on 5 May 1986. During this workshop terminology of MD has been discussed and standardized. The following characteristics are considered as essential for MD [4]:

- The membrane is porous;
- The membrane pores should not be penetrated by liquids;
- Condensation should not occur within the membrane pores;
- Feed solution should contact with the membrane directly;
- Membrane pores are used exclusively for vapour transport;
- The vapour equilibrium of different components in the process liquids cannot be changed by the membrane; and
- The driving force of MD is the partial vapour pressure gradient.

Since then, research publications on MD increased stably. The main MD operating parameters have been extensively studied by different researchers. Firstly, the feed temperature has a great impact on flux, which is attributed to the exponential relationship between temperature and vapour pressure. The decrease of coolant temperature could also make a noticeable change in flux, however, its impact is considerably lower than that of feed temperature [1, 20]. Secondly, the increase of feed/coolant velocities will lead to an increased flux, because the boundary layer

resistance is decreased and uniformity of temperature (concentration) within the flow channel is increased. However, an asymptotic value is usually identified for flux with the increased feed/coolant velocities, this is mainly due to that the boundary layer cannot be further reduced for the fully developed flows. Furthermore, compared to the feed/coolant temperatures, feed/coolant velocities play less important roles in flux. Thirdly, due to the different channel arrangement on coolant side, the gap width and sweeping gas velocity are considered as the critical operating parameters for AGMD/VMD and SGMD, respectively [20]. The smaller gap width will benefit the flux for AGMD and VMD, and a higher sweeping gas velocity has a decisive role in flux improvement. Last but not least, the high feed solution concentration (salinity) can reduce the vapour pressure and decrease the uniformities of temperature and concentration within the flow channel, which, subsequently, will result in a lower flux.

More recently (from 2011), there has been a research boom in MD [19], researchers started to focus on membrane and module developments, process optimization and mathematical modelling [19]. In addition, researchers have realized that better membrane material and optimized process may not be adequate enough to make MD economically viable and more competitive compared to other desalination process. A growing number of MD studies have investigated: 1) multi-stage MD processes, 2) hybrid MD systems, and 3) renewable energy powered MD systems.

Multi-stage MD process enables the recovery of residual heat from former stage to the next stage, which maximizes the internal heat recovery and increases the system Energy Efficiency (EE) accordingly. Khalifa et al. [21] compared the multi-stage AGMD and multi-stage WGMD performance and found that with a three-stage system the specific energy consumption of multi-stage WGMD was approximately 6.96 to 5 kWh/m^3, which is comparable to the typical seawater RO process. Zaragoza et al. [22] investigated the performances of different commercial MD prototypes with various configurations. Their module PT5 (flat sheet LGMD) manufactured by Keppel Seghers was designed to optimize the heat recovery by interconnecting modules in series. The study demonstrated that single module mode had the uppermost Specific Thermal Energy Consumption (STEC) of 1.1 kWh/L and the 3 module mode had the lowest STEC at approximately 0.5 kWh/L. Cipollina et al. [13] modelled the impacts of numbers of PGMD stages on system energy efficiency indicated by Gain Output Ratio (GOR). Their predictions showed that GOR can increase by almost 20 times from a laboratory-scale 1 stage unit to a 9 stage unit.

MD is considered as one of the most favorable processes for hybrid system. MD is not a pressure-driven process, it has a low pressure requirement. The process can also be easily integrated into the existing plant. Furthermore, its performance is not significantly affected by influent salt concentration, and consequently, it can improve the system's water recovery dramatically [3]. Different research groups have investigated the combination of MD with Forward Osmosis (FO) [23-26], crystallizer [27-29] or RO processes [30-32]. The hybrid system will make MD competitive in some niche applications, such as Zero Liquid Discharge (ZLD) scheme [33, 34] and special industrial wastewater treatment [19].

Renewable energy powered MD system receives considerable attention due to its potential utilization of low grade heat and minimum environmental impacts. Solar powered MD system has been extensively investigated by various researchers [13, 22, 35-41], and the utilization efficiency of solar energy is very high [3]. Use of geothermal energy for MD system has also been studied [42-44]. Sarbatly et al. [44] reported that the use of geothermal energy can meet 95% of the total energy demand. In addition to the renewable energy, the reuse of waste heat [45-49] is also one of the key advantages for MD system.

Besides the aforementioned research areas, various studies [3, 4, 19] suggested that development of MD-specific membrane and novel MD configuration, better understanding of MD fouling and wetting, and the application of MD for the purposes other than desalination (e.g. brine concentration, wastewater treatment, food processing) will be future focus areas.

2.2. Membrane configuration

A desired MD membrane configuration should have the following key features [2]:

- A high packing density (specific surface area);
- Low temperature and concentration polarization effects;
- A high mass and heat transfers within the boundary layers;
- Membrane housing should have high resistance to pressure, temperature and chemicals; and
- Uniform flows should be maintained throughout the membrane module.

Three main membrane configurations have been utilized for MD application: 1) flat sheet membrane; 2) hollow fibre membrane; and 3) spiral wound membrane. They all have been used for both laboratory testing and commercial applications [4].

Fig. 2-1 shows a schematic diagram for flat sheet membrane. Flat sheet membrane is considered as the most popular configuration in MD study. Firstly, the fabrication of flat sheet MD module is relatively simple compared to hollow fibre or spiral wound membrane configurations. Secondly, the flat sheet membrane can be easily taken out of the module for cleaning, characterization and change. The same module can be used for testing of different membranes. Furthermore, flat sheet membrane has less fouling tendency compared to hollow fibre and spiral wound membranes. On the other hand, the packing density of flat sheet membrane is approximately 100 – 400 m^2/m^3 [50], consequently, it has a lower specific surface area than hollow fibre membrane (packing density can be up to 3000 m^2/m^3).
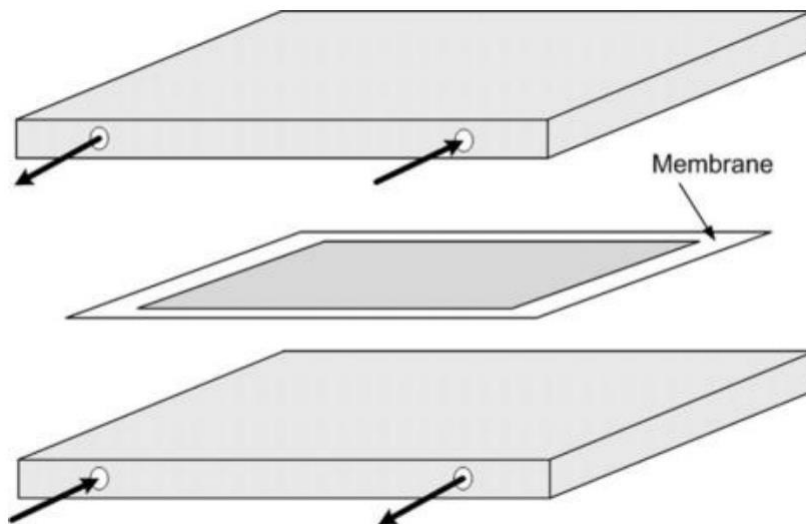
Fig. 2-1. Schematic diagram for flat sheet membrane [4]

The sketch of hollow fibre membrane configuration is shown in Fig. 2-2. As shown in the diagram, thousands of hollow fibres can be packed in membrane module housing, and as they are an integrated part of the module, no additional support is required. The inner diameter of the hollow fibre membrane is typically in the range of 50 – 100 μm [2]. The key advantage of hollow fibre configuration is the high membrane packing density (up to 3000 m^2/m^3) and subsequent compactness, which make it very attractive from a commercial point of view. However, if the fibre is wetted or broken, the whole module has to be replaced or be taken off-line to remove the broken fibres (pinning process) [2]. Because of its high packing density, the fouling tendency is also higher than flat sheet membrane. Furthermore, randomly packed hollow fibres can create flow maldistribution, which results in lower uniformity of temperature within the shell side and lowers permeation flux. Baffles, spacers and modified fibre geometries can be

applied to increase the membrane effective surface area [51] and improve the flow pattern [52]. Here, the phenomenon that the temperature on the membrane surface being close to that of the bulk flow can be defined as the uniformity of the temperature.
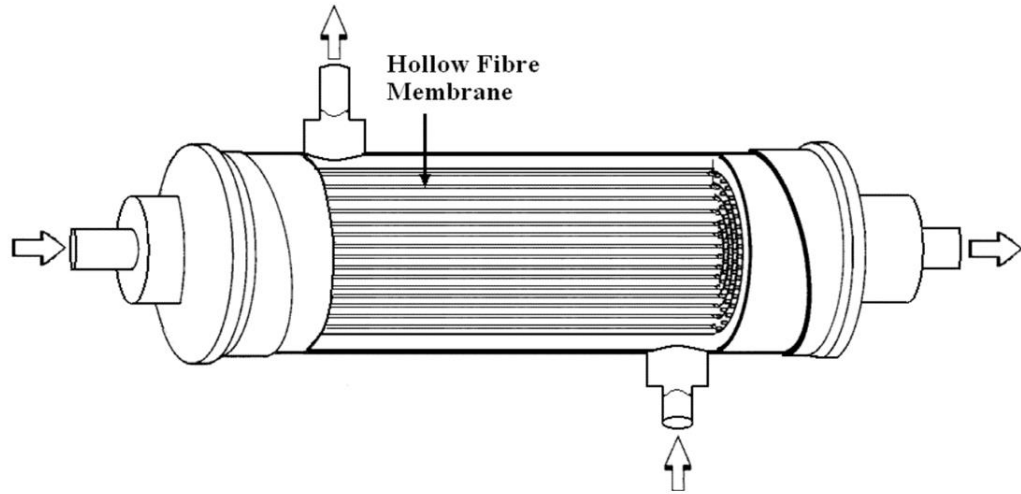
Fig. 2-2. Schematic diagram for hollow fibre membrane [4]

As shown in Fig. 2-3, spiral wound membrane is another type of flat sheet membrane, however, its structure and manufacture are more complex than that of flat sheet membrane. It has two membrane layers and they are enveloped and rolled around a perforated central permeate collection tube together with the feed flow channel spacer and porous support layer. Furthermore, the spiral wound membrane is more difficult to clean compared to flat sheet membrane. The packing density of spiral wound membrane is in the range of 300 – 1000 m^2/m^3, which is higher than conventional flat sheet membrane but lower than hollow fibre configuration. Spiral wound membrane is sensitive to the suspended particles in the feed, as a result, it is more suitable to treat feed solution with a minimum suspended matters.
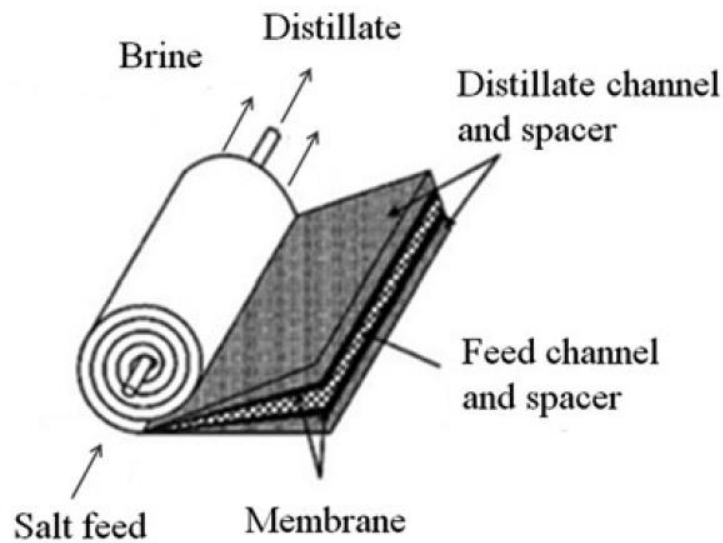
Fig. 2-3. Schematic diagram for spiral wound membrane [53]

2.3. Membrane characteristics

The lack of MD-specific membrane has been highlighted as a research gap [19] and attracted significant effort from researchers. This has been confirmed by the fact that the numbers of publications in novel MD membrane development is more than those of other MD topics [19]. Without a suitable membrane, it is difficult to apply MD into practice.

It is agreed that the membrane employed in MD applications should be hydrophobic and porous. As mass and heat transfers simultaneously occur in the MD process, the MD membrane should have a low resistance to the mass transfer and low thermal conductivity. Additionally, the membrane has to exhibit good thermal stability and high resistance to different chemicals [1, 2].

In order to satisfy the above requirements, the following characteristics are desired for MD membrane:

- High Liquid Entry Pressure (LEP)

  LEP indicates the pressure limits where liquid does not penetrate into the membrane pores. In MD process, only vapour passes through the membrane pores, a higher LEP will prevent the membrane pore from being wetted. LEP is dependent on the maximum pore size and hydrophobicity [1], which can be calculated by:

$$LEP = \frac{-2B\gamma_l}{r_{max}} \cos\theta \qquad\qquad (2\text{-}1)$$

Here, B represents the geometric factor of pore; γ_l is the surface tension of the solution; θ is the contact angle between solution and membrane surface; and r_{max} is the maximum pore radius.

- A narrow distribution of pore size with a reasonably large mean pore size
  MD membrane pore size distribution should be as narrow as possible, because oversized pores make membrane vulnerable to wetting. However, a large pore size will benefit the vapour mass transfer process. As a result, a large membrane pore size is preferred, as long as it still meets the LEP requirement.

- Low tortuosity
  The membrane flux permeation is inversely proportional to tortuosity, consequently, a low tortuosity will increase the flux.

- Higher porosity
  A higher membrane porosity will improve the flux and decrease the heat loss by conduction.

- Adequate membrane thickness
  On the one hand, thinner membrane has lower mass transfer resistance, but on the other hand, thinner membrane has lower thermal resistance, leading to a smaller temperature difference across the membrane and lower flux. Additionally, thinner membrane has less mechanical strength. A balanced decision on membrane thickness has to be made based on the above considerations.

- High hydrophobicity
  Hydrophobic membrane is used for MD process. The hydrophobicity can be indicated by membrane surface energy and contact angle of a water droplet on the membrane. If the contact angle of a water droplet is higher than 90°, the membrane shows hydrophobic characteristic. With a larger contact angle, membrane becomes more hydrophobic.

  Table 2-1 shows the typical surface energy and contact angle values for different polymers usually used for MD process.

Table 2-1 Hydrophobicity of polymers typically used for MD process [1, 54]

Polymer	Surface energy (x10^3 N/m)	Contact angle (º)
Polytetrafluoroethylene (PTFE)	19.1	138
Polyvinylidenefluoride (PVDF)	30.3	107
Polypropylene (PP)	30.0	120
Polyethylene (PE)	33.2	120

- Lower thermal conductivity

  Lower thermal conductivity can decrease the heat loss due to conduction. It will also increase the temperature difference across the membrane surfaces, leading to a higher flux.

The majority of membrane materials used for MD process are various polymers, including PTFE, PVDF and PP. PTFE has been the most popular material due to its high hydrophobicity, and thermal and chemical stability [19]. PVDF has been widely used in MD process as well. Compared to PTFE, PVDF membrane has a lower thermal conductivity and can be easily modified by changing different parameters of phase inversion process [19]. More recently ceramic membrane has also been employed for MD studies [19, 55-57] due to its superior mechanical strength and chemical resistance. However, because of its hydrophilic nature, relatively higher thermal conductivity and costs, the application of ceramic membrane in MD process is still limited.

2.4. MD module configuration

2.4.1. Conventional MD module configurations

As briefly discussed in Chapter 1, MD has four main module configurations, namely, DCMD, AGMD, SGMD and VMD.

For DCMD configuration, due to its simple structure, it is the most popular MD configuration for laboratory scale study. Both the hot feed and coolant flow tangentially to the membrane surface. The flux of DCMD is normally higher than that of AGMD, but lower than VMD under the same operating condition. Furthermore, it has the lowest uniformity of the temperature within the channel among all configurations [58].

For AGMD configuration, an air gap exists in the permeate gap and water vapour has to pass through both membrane pores and the air gap to be condensed on the condensation surface. Due to the lower thermal conductivity of air compared to that of

water, there is less heat energy loss compared to DCMD. However, air gap introduces additional mass transfer resistance, which is the main disadvantage for AGMD.

To decrease the mass transfer resistance due to the air gap of the AGMD, SGMD was developed. In SGMD module, an inert gas is used to sweep the water vapour out of the MD module to be condensed externally. Because the water vapour is mixed with a large volume of sweeping gas, a large condensation surface is required. Furthermore, external condenser, additional air blower and compressed air will result in higher capital and operational costs [59].

For VMD module, a pump is used to create a vacuum condition at the membrane permeate side. Similar to SGMD, the permeate is condensed externally. Due to the vacuum condition, the heat loss by conduction is minimum and the flux is higher compared to other MD configurations, which are considered as great advantages [1, 58]. However, VMD has a higher pore wetting probability and higher capital costs due to the vacuum pump and external condenser.

2.4.2. PGMD configuration

In order to improve energy efficiency compared to DCMD/SGMD and to increase permeation flux above that of AGMD, PGMD was proposed by numerous researchers [7, 8, 11, 13, 17, 18]. Fig. 2-4. shows the basic PGMD configuration and the temperature profile across the membrane. Here, T_{pm}, T_{pc} and T_{cc} are interface temperature between permeate and membrane, interface temperature between cooling plate and permeate, and interface temperature between coolant and cooling plate, respectively.

a) Basic configuration of PGMD module
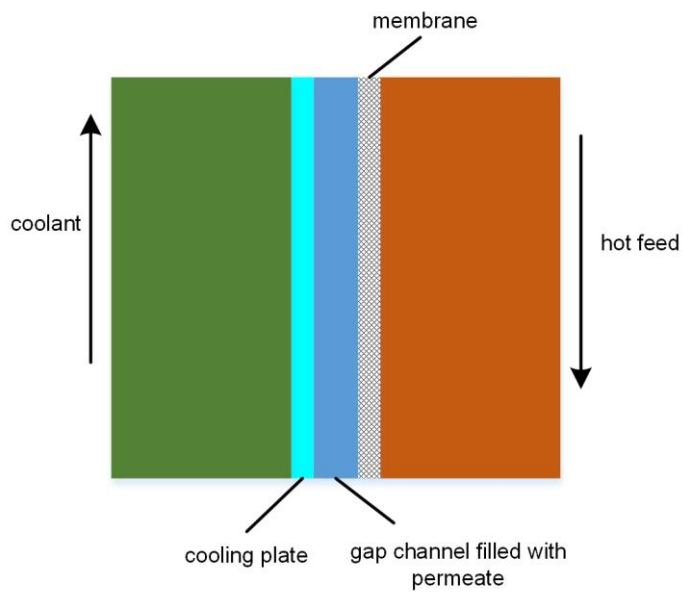
b) Temperature profile of PGMD module
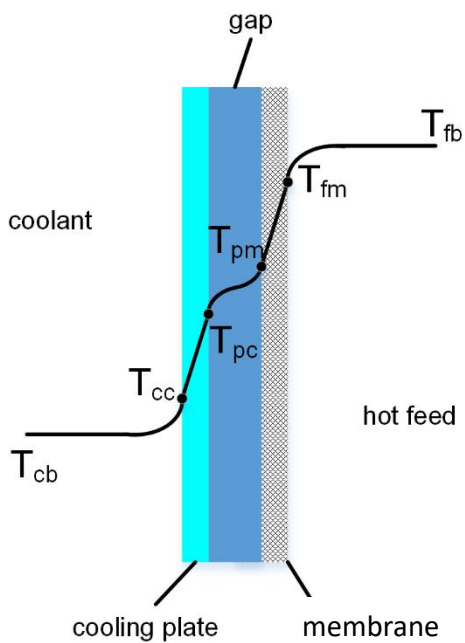
Fig. 2-4. Basic configuration and temperature profile of PGMD module

It can be seen from Fig. 2-4 that for PGMD configuration, the feed solution contacts the membrane directly, permeate is located between the membrane and the cooling plate, and the coolant water (usually feed) is on the other side of the cooling plate. The main advantages for PGMD configuration include:

- Integration of heat recovery within the module [18] compared to SGMD and VMD;

- Lower sensible heat loss compared to DCMD due to the presence of an additional permeate gap [18];

- Lower mass transfer resistance compared to AGMD by using a liquid gap rather than an air gap; and

- Separation of the permeate and the coolant water, which means the coolant can be any other liquid [18].

Consequently, the PGMD configuration effectively combines the advantages of different conventional MD processes. Although PGMD has been studied by various researchers, only flat sheet [7, 8, 11-13] and spiral wound [17, 18] membrane modules have been applied for PGMD investigation. Hollow fibre membrane has a large specific surface area without any supporting structure [60], and as a result, in this research a specifically designed PGMD module using hollow fiber membrane was manufactured and investigated under various operating conditions and module designs.

2.5. Heat and mass transfers for MD

2.5.1. Heat transfer phenomena

Normally heat transfer within a MD module can be divided into three main sub-processes. Firstly, the heat is transferred from the hot bulk flow to the interface between the membrane and hot feed. Because the temperature on the membrane surface is different from that of the bulk flow, the temperature T_{fm} at the interface between the membrane and hot feed is lower than that of feed bulk flow (T_{fb}). Secondly, the heat is transferred through the hollow fibre membrane, which can be divided into two parts: (1) sensible heat transfer via heat conduction and (2) latent heat transfer via water vapour. Afterwards, the heat is transferred from the interface between the membrane and permeate to the permeate bulk flow. For DCMD, the permeate is usually the coolant. However, due to the unique permeate gap configuration in PGMD, coolant is separated from the permeate and two additional heat transfer processes occur. The heat is transferred through the cooling plate via the conduction, thereafter, it is transferred from the interface between cooling plate and coolant to the coolant bulk flow.

In modelling the heat and mass transfers in the MD processes, it is generally assumed that there is no heat loss from the hollow fibre module to the surrounding atmosphere,

consequently, the heat transfer process through the hydrophobic membrane can be described by the following generic equation (for flat sheet DCMD as an example):

$$Q_{trans} = \alpha_f (T_{fb} - T_{fm}) = \frac{\lambda_2}{b_1}(T_{fm} - T_{pm}) + J_{vm}h_{latent} = \alpha_c (T_{cc} - T_{cb}) \quad \text{(2-2)}$$

In Eq. (2-2), the conductive heat transfer and latent heat transfer are described as $\frac{\lambda_2}{b_1}(T_{fm} - T_{pm})$ and $J_{vm}h_{latent}$, respectively. Here, Q_{trans} represents the total heat transfer; α_f and α_c represent heat transfer coefficients at hot feed side and coolant side, respectively; h_{latent} is the latent heat of vaporization of water; J_{vm} represents the water vapour flux through the membrane; λ_2 represents thermal conductivity for hollow fibre membrane; and b_1 is the thickness of the membrane.

2.5.2. Mass transfer phenomena

Similar to DCMD, the mass transfer of PGMD can be described by three steps. Firstly, the hot feed is vapourized at the interface of the hot feed and membrane; secondly, the water vapour passes through the membrane pores; and thirdly, the water vapour condenses at the interface of the permeate and membrane. Mass transfer through the membrane pores is considered as the limiting step [59].

The water vapour through the membrane is driven by the vapour pressure difference across the membrane, which can be described by:

$$J_{vm} = N(P_{fm} - P_{pm}) \quad \text{(2-3)}$$

Here, J_{vm} represents the water vapour flux through the membrane; N is the mass transfer coefficient for hollow fibre membrane; P_{fm} and P_{pm} are vapour pressures at membrane interface temperatures at hot feed side (T_{fm}) and permeate side (T_{pm}), respectively.

The MD mass transfer coefficient N has been extensively studied [1, 2, 17, 59, 61, 62] and can be described by three basic mechanisms as Knudsen diffusion, Poiseuille flow, and molecular diffusion or the combination of these mechanisms (Fig. 2-5).

Knudsen diffusion   **molecular diffusion**

viscous flow
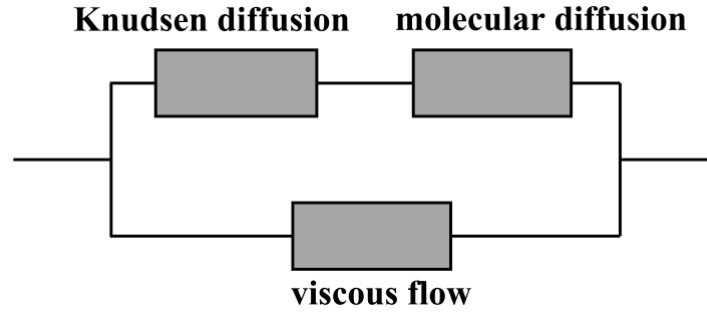
Fig. 2-5. Superposition of three basic transport mechanisms [17]

Because there is no total pressure difference within the membrane pores, the effect of Poiseuille flow can be neglected for PGMD, the mass transfer phenomenon within the membrane pores is controlled by Knudsen diffusion, molecular diffusion or Knudsen-molecular diffusion transition mechanism [17].

The Knudsen number (Kn) is utilized to determine the dominant mass transfer mechanism in the membrane pores. Kn can be calculated by:

$$Kn = \frac{l_f}{d} \tag{2-4}$$

Here, l_f represents the mean free path of the transferred gas molecules and d is the mean pore diameter of the membrane.

Table 2-2 Mass transfer mechanisms in membrane pores [61]

$Kn<0.01$	$0.01<Kn<1$	$Kn>1$
Molecular diffusion	Knudsen-molecular diffusion transition mechanism	Knudsen mechanism

The mean pore diameter of the membrane employed in the current PGMD study is 0.15 μm, and the mean free path of the water vapour is 0.11 μm at a feed temperature of 60 ˚C, the calculated Kn is approximately 0.73. Consequently, the Knudsen-molecular transition diffusion is the dominant mass transfer mechanism within the pores.

The mass transfer coefficients for Knudsen mechanism and molecular diffusion mechanism can be described as follows [17, 59, 61, 63]:

$$N_{Kn} = \frac{4}{3}\frac{d\varepsilon}{\tau b_1}\sqrt{\frac{M}{2\pi RT}} \tag{2-5}$$

$$N_m = \frac{M}{1-\chi_A} \frac{\varepsilon D_{AB}}{\tau b_1 RT} \tag{2-6}$$

Combing Eqs. (2-5) and (2-6), the mass transfer coefficient of PGMD can be described as:

$$N = (\frac{1}{N_{Kn}} + \frac{1}{N_m})^{-1} \tag{2-7}$$

$$N = (\frac{1-\chi_A}{M} \frac{\tau b_1 RT}{\varepsilon D_{AB}} + \frac{3}{4} \frac{\tau b_1}{d\varepsilon} \sqrt{\frac{2\pi RT}{M}})^{-1} \tag{2-8}$$

Here, N_{Kn} and N_m are mass transfer coefficients for Knudsen mechanism and molecular diffusion mechanism, respectively; M is the molecular mass of the water vapour; χ_A is the mole fraction of the water vapour; ε is the membrane porosity; D_{AB} is the diffusivity of the water vapour (A) relative to air (B); τ is the average tortuosity of the pores; b_1 is the thickness of the membrane; d is the mean pore diameter of the membrane; R is the universal gas constant; T is the mean temperature in the pores.

Combing Eqs. (2-3) and (2-8), the J_{vm} can be described as follows:

$$J_{vm} = (\frac{1-\chi_A}{M} \frac{\tau b_1 RT}{\varepsilon D_{AB}} + \frac{3}{4} \frac{\tau b_1}{d\varepsilon} \sqrt{\frac{2\pi RT}{M}})^{-1}(P_{fm} - P_{pm}) \tag{2-9}$$

2.6. Modelling development for MD

Different operational parameters (feed/coolant velocities, feed/coolant temperatures, feed water quality, module configuration, etc.) have significant impacts on MD performance. Experimental studies can only investigate a limited number of variables as experiments are labor intensive and time-consuming work. Furthermore, the interactions among important design and operational parameters could possibly be overlooked with limited experimental data [64]. Consequently, modelling plays an important role in MD study.

Heat transfer modelling

Although various models have been developed to simulate heat transfer in MD process, they are all based on the calculation of the Nusselt's number (*Nu*) [64]. Nusselt's number is a dimensionless number, which represents the ratio of the convective to

diffusive heat transfer. Nu under fully developed flow and uniform heat flux condition can be calculated by [65, 66]:

$$Nu = 4.36 + \frac{0.036(\text{Re Pr } d_h / l)}{1 + 0.0011(\text{Re Pr } d_h / l)^{0.8}}$$
(2-10)

where l is the module length; Re and Pr represent Reynolds number and Prandtl number; and d_h is the hydraulic diameter for the flow channel.

Based on the Nusselt's number, the heat transfer coefficient (e.g. α_f) can be calculated by:

$$\alpha_f = \frac{Nu_f \lambda_1}{d_{hf}}$$
(2-11)

Here, Nu_f is the Nusselt's number for hot feed channel; λ_1 is the thermal conductivity for the hot feed; and d_{hf} is the hydraulic diameter for the feed channel.

With the calculated heat transfer coefficients for hot and coolant channels, the interface temperature between hot feed and membrane and the interface temperature between coolant and membrane can be calculated. As shown in Eq. (2-2), flux is included during the calculation of interface temperatures. An initial guess for the first iteration or flux obtained from experiments could be used. The simulation process will be concluded when the difference between calculated and experimental results are within a pre-defined range.

Mass transfer modelling (the formulae given earlier are for mass transfer modelling)

Numerous models have been developed to simulate the mass transfer phenomenon within the membrane pores. Three popular mass transfer models are: (1) Fick's law model; (2) Dusty Gas Model (DGM); and (3) empirical models.

Fick's law model is one of the simplest method to describe MD mass transfer phenomenon. The membrane region is represented by a space full of the stagnant air [64]. The flux is initially calculated using a theoretically calculated diffusion coefficient. After that the theoretical diffusion coefficient is calibrated using initial calculated flux

and flux obtained from experiments. The calibrated diffusion coefficient is then applied for flux modelling [64].

DGM is most widely applied method to simulate MD mass transfer phenomenon. The principle of DGM is that the porous membrane behaves as an array of dusty particles kept stationary in space, the particles act as giant gas molecules and interacts with gas and surface. During the modelling of mass transfer process, DGM takes viscous flow, molecular and Knudsen diffusion into account [59, 64]. One of the limitations of DGM is that the model was developed based on isothermal conditions. Although the mass transfer phenomenon in MD has been successfully simulated using the average temperature, the actual temperature throughout the membrane is not the same.

Empirical models have also been developed to simulate MD mass transfer phenomenon, such as Artificial Neural Network (ANN) model [67, 68] and Response Surface Methodology (RSM) visualization technique [69, 70]. Empirical models do not represent the actual physical phenomena and are purely based on data. The key limitations of empirical models are: (1) a large number of data is required to calibrate the model; (2) the obtained results are only valid for the calibrated data range; and (3) the developed model cannot be applied to other systems [64].

2.7. Objectives

The overall objective of this study is to develop a hollow fibre PGMD module, evaluate its performance and optimize its design. The specific objectives include:

- to investigate the physical and structure characteristics of employed hollow fibre membrane to confirm its applicability for MD process;

- to understand the unique characteristics, advantages and limitations of hollow fibre PGMD compared to other conventional MD modes and configurations;

- to evaluate the effects of hollow fibre packing density, gap channel density and gap materials on hollow fibre PGMD module performance; and

- to further optimize PGMD module design using modelling approach.

Chapter 3 Characterization of selected hollow fibre membrane

As a membrane-based process, the characteristics of membrane play a decisive role in system performance. In this study a commercially available PVDF membrane has been utilized to manufacture the PGMD modules. This membrane was prepared by Tianjin Polytechnic University using the non-solvent induced phase separation (NIPS) method. In order to confirm its suitability for MD application, membrane characterization was undertaken as the first stage of this research.

The following parameters have been measured to examine the membrane characteristics: (1) dimension (inner/outer diameters and thickness); (2) membrane porosity; (3) mean membrane pore size; (4) contact angles (inner and outer surfaces); (5) LEP; and (6) cross sectional area and surface investigation using Scanning Electron Microscope (SEM).

3.1. Methodology

3.1.1. Membrane dimension

To prepare for the measurement of the membrane thickness, three hollow fibre samples were firstly immersed and frozen in the liquid nitrogen. Then three different sections were cut from each hollow fibre to form smooth and intact cross sections. The inner and outer diameters of the hollow fibre were measured by a LEICA SEM (S440 W) via imaging of each membrane cross section and the average inner and outer diameters were used to calculate the membrane thickness.

3.1.2. Membrane porosity

The membrane porosity was determined by the wetting method [71]. The hollow fibre membrane sample was firstly soaked in the deionized water. Due to the hydrophobic properties of PVDF membrane, water cannot penetrate into membrane pores, total unwetted fibre volume (including pore volume) was measured. The hollow fibre membrane sample was then dried and soaked in the ethanol. Due to the low surface tension of ethanol, the PVDF membrane was completely wetted and membrane pores were filled by ethanol, the total wetted fibre volume (mass volume) was measured. The porosity was calculated by

$$\varepsilon = 1 - \frac{V_{mass}}{V_{total}}$$

(3-1)

where the V_{mass} and V_{total} are the mass volume and total fibre volume, respectively.

In order to minimize the error, the porosities of four different fibres were measured (lengths of the fibres: 217.72 cm, 317.51 cm, 304.81 cm and 661.83 cm) and the average porosity was reported as the membrane porosity.

3.1.3. Membrane mean pore size

The membrane mean pore size was measured by gas permeation method [61, 62, 72] using compressed nitrogen gas. According to [73] the mass transfer of nitrogen gas within the membrane pores can be described as the sum of fluxes due to viscous and Knudsen flows, and the membrane mean pore size can be calculated accordingly [62]. Zhang et al. [62] also found that shorter membrane sample resulted in a higher gas permeation due to the average driving pressure approaching the inlet pressure when membrane sample became shorter.

In this study, the gas inlet pressure was varied between 5 – 90 kPa and the pressure difference across the membrane was set at 1.00 ± 0.01kPa. Two digital manometers (645, TPI) were used to measure the inlet pressure and the pressure difference, respectively. Two hollow fiber membranes were randomly selected for testing, and three samples with different lengths were made from each fiber. In order to eliminate the length dependency, the calculated membrane pore sizes were plotted against the sample length, and a linear fitting curve was then employed to extrapolate the membrane length (variable) to zero. This method was described in [62].

3.1.4. Contact angle

The contact angles of the inner and outer surfaces were measured by the same methods described in [74].

For inner surface contact angle measurement, part of the hollow fibre was firstly enclosed in a clear cylinder (Fig. 3-1), then epoxy resin was used to seal the space between the fibre and the cylinder; afterwards, the fibre was slowly submerged into deionized water. When water firstly protruded from the top of the fibre, the height difference between the top of the fibre and water surface was recorded. The inner surface contact angle was determined accordingly by [75]

$$h = \frac{-4\gamma_1 \cos\theta}{\rho g d_{fi}} \tag{3-2}$$

Here, h is the height difference between the top of the fibre and water surface; γ_1 is the surface tension of the solution; θ is the contact angle between the solution and the membrane surface (see Fig. 3-1); ρ is the water density; g is the acceleration due to the gravity; and d_{fi} is the inner diameter for the hollow fibre.
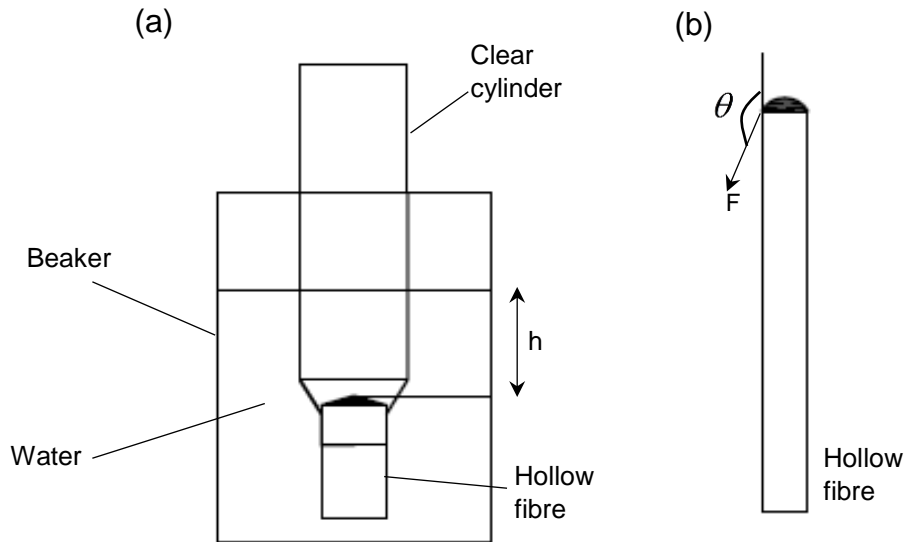
Fig. 3-1. Schematic diagrams for (a) inner surface contact angle measurement apparatus and (b) force balance at interface boundary

For outer surface contact angle measurement, a copper wire was inserted into the lumen side of the hollow fibre (Fig. 3-2), and part of the fibre was submerged into deionized water. The mass change arising from submersion of the fibre was recorded, and the mass reduction due to the surface tension effects was measured. The outer surface contact angle was then calculated by [75].

$$F = \pi d_{fo} \gamma_1 \tag{3-3}$$

$$\Delta m = F \cos \theta \tag{3-4}$$

Here, F is the force from surface tension; d_{fo} is the outer diameter for the hollow fibre; and Δm is the mass change due to the F.
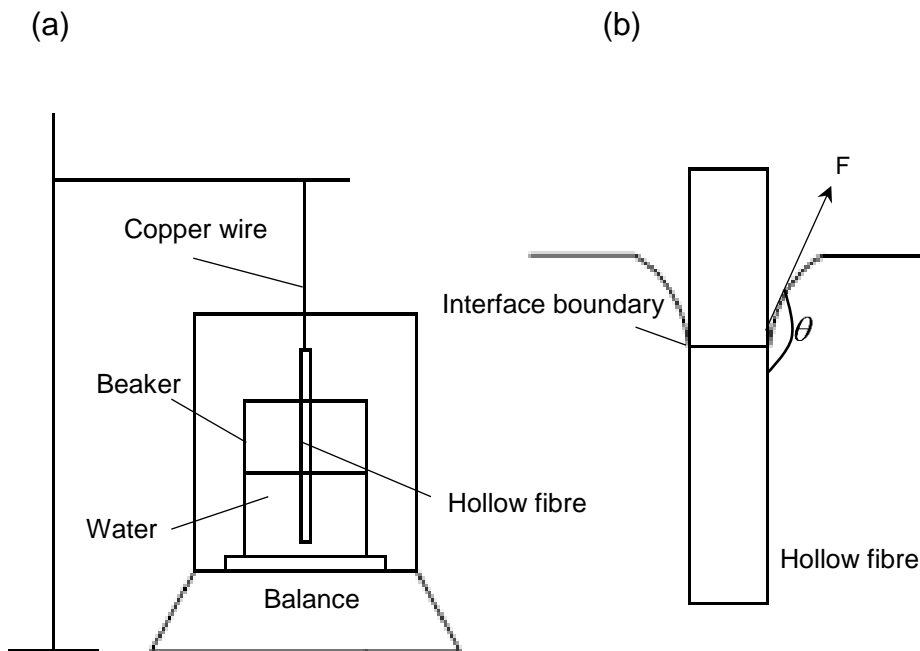
Fig. 3-2. Schematic diagrams for (a) outer surface contact angle measurement apparatus and (b) force balance at interface boundary

3.1.5. LEP

LEP was determined by a change of conductivity and Fig. 3-3 shows the schematic diagram of the experiment installation. Firstly, the hollow fibre membrane was inserted into a copper tube holder. A salt solution (20% NaCl solution) was injected into the hollow fibre lumen side, and the holder with hollow fibre was submerged into a beaker with 200 mL deionized water that was continuously stirred by a magnetic stirrer. Pressure was then applied on the hollow fibre lumen side to force the salt solution through the membrane. A HACH HQ14d conductivity meter was used to monitor the conductivity change of the deionised water. The applied pressure was gradually increased in increments of 5 kPa and was kept constant for 1 minute before the next pressure increase. The LEP was determined when a conductivity increase in the deionized water was detected. The measured LEP was converted into the LEP under experimental condition (1% NaCl solution) [5].
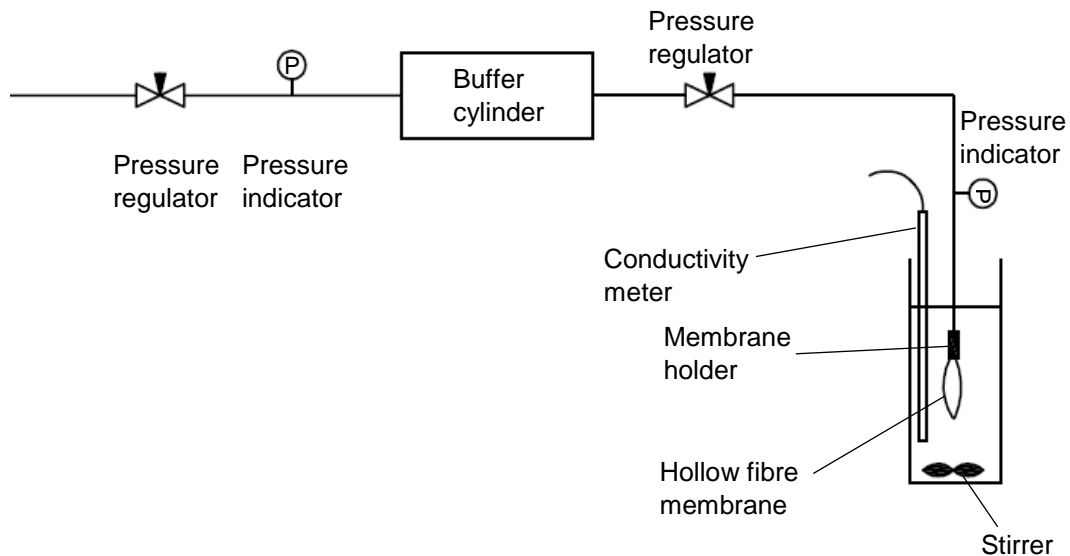
Fig. 3-3. Schematic diagram of LEP testing installation

3.1.6. SEM Investigation

Surfaces (outer and inner) and cross sectional structures of the applied membrane were observed by a LEICA SEM to investigate the membrane morphology and verify the results from gas permeation experiments.

3.2. Results and discussion

Table 3-1 lists the measured membrane properties as well as some data provided by the manufacturer. Here, d_{fi} and d_{fo} are the inner and outer diameters of the hollow fiber membrane, respectively. It shows that the data provided by the manufacturer and our corresponding measured data are very similar. Compared to other PVDF membranes employed in MD process [76-80], the membrane used in this study has a relatively high porosity of 82%, which is mainly caused by the inner/outer finger-like macrovoid layers of the membrane to be shown later. This high porosity is desirable for MD and will result in lower mass transfer resistance as well as less sensible heat loss through the membrane. The membrane mean pore size is 0.15 μm, and is within the typical mean pore size range of 0.07 – 0.32 μm [5, 77, 79-82] for PVDF membrane employed in MD process.

Table 3-1 Membrane properties obtained from characterization and manufacturer

Membrane properties	Dimension (mm)			Porosity (%)	Mean pore size (μm)	Contact angle		LEP (kPa)	
	d_{fi}	d_{fo}	b_1			Inner	outer	Measured	Calculated[5]
Manufacturer	0.80	1.16	0.18	82.0	0.16	-	-	-	-
Measured	0.81	1.11	0.15	81.7	0.15	132˚±3˚	94˚±2˚	240.8	224.0

The larger inner surface contact angle indicates a higher hydrophobicity, which can effectively prevent water from penetrating into the membrane pores as the feed solution is pumped through the hollow fiber lumen.

Fig. 3-4 shows some SEM images of the inner surface, outer surface and cross sections of the employed hollow fiber membrane. Figs. 3-4a and 3-4b show the three layer structure of the hollow fiber membrane. These figures show that the employed hollow fiber membrane consisted of a finger-like macrovoid inner layer, a sponge-like middle layer and a finger-like macrovoid outer layer. Figs. 3-4c and 3-4d show further details of the macrovoid layer and the sponge-like layer.

It can be clearly seen that there are two distinctive pore size groups: the relatively large pore size for the macrovoid layers and the small pore size for the sponge-like layer. It can also be seen that the tortuosity of the finger-like macrovoid layer is close to 1 and that of sponge-like middle layer is much greater than 1. The images show that the porosity of the macrovoid finger-like layers is much higher than that of sponge-like middle layer. The higher porosity and smaller tortuosity within the finger-like layers will increase the flux and lower the sensible heat loss; on the other hand, the smaller porosity and larger tortuosity of the sponge-like middle layer can provide the desired mechanical strength [76].

The inner and outer surface structures are shown in Figs. 3-4e and 3-4f, respectively. It can be seen that the inner surface is smoother than the outer surface. Additionally, the inner surface is more porous than the outer surface.

Based on the above investigation and discussion, it can be concluded that the employed PVDF membrane is suitable for MD applications.

a) Cross section
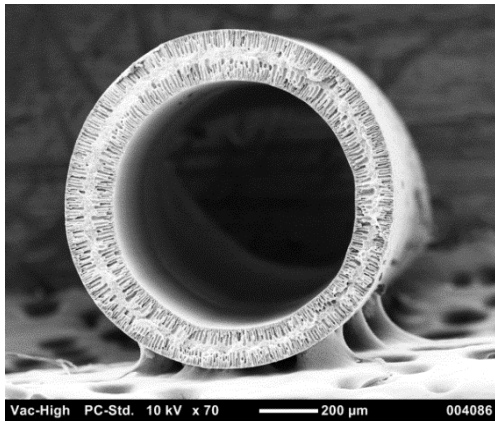
b) Triple-layer structure
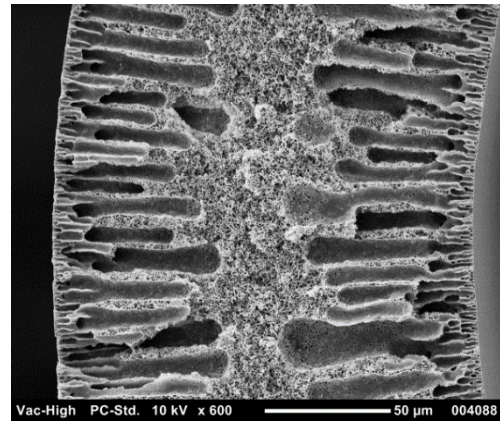
c) Macrovoid finger-like layer
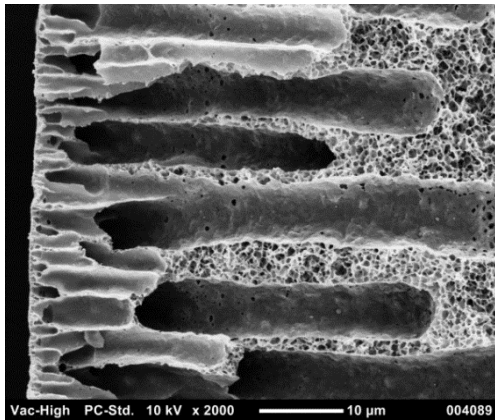
d) Sponge-like layer
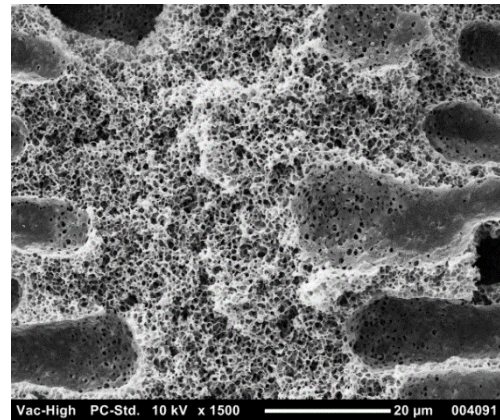
e) Inner surface
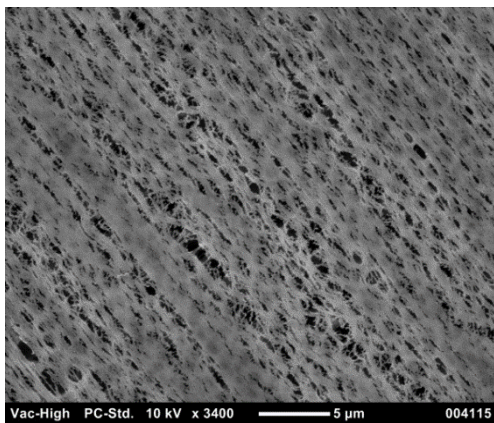
f) Outer surface
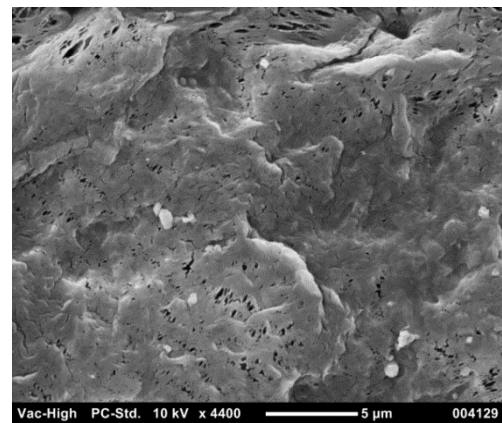
Fig. 3-4. SEM images of membrane cross section, inner and outer surfaces

Chapter 4 Experimental study of hollow fibre PGMD and its performance comparison with DCMD and SGMD

4.1. Introduction

As described in Chapter 2, numerous benefits have been identified for PGMD compared to DCMD and SGMD. However, due to the different membrane characteristics and operating conditions, it is difficult to make a direct performance comparison between PGMD, DCMD and SGMD from different studies. In this study, we have operated a single MD module in different modes (PGMD, DCMD and SGMD) to facilitate the discussion. As the first reported hollow fibre PGMD module, we have also compared our hollow fibre PGMD performance to other flat sheet and spiral wound PGMD studies to demonstrate the advantages of hollow fibre PGMD module.

4.2. Experimental methods and setup

4.2.1. Hollow fibre PGMD module

The specifically designed hollow fiber PGMD modules were fabricated using hollow fiber membrane (d_{fi}=0.81 mm and d_{fo}= 1.11 mm), High Density Polyethylene (HDPE) tube (d_{gi}=2.84 mm and d_{go}=3.40 mm) as the gap channels, and PE pipe (d_{pi}=25 mm) as the module shell. The effective length of the hollow fiber membrane (hot channel) is 0.425 m. Here, d_{fi}, d_{fo}, d_{gi} and d_{go} are the inner and outer diameters of the hollow fiber membrane and the HDPE gap channel, respectively; and d_{pi} is the inner diameter of the PE pipe.

Fig. 4-1. shows a photograph of the PGMD module and a sketch of its basic internal arrangement.
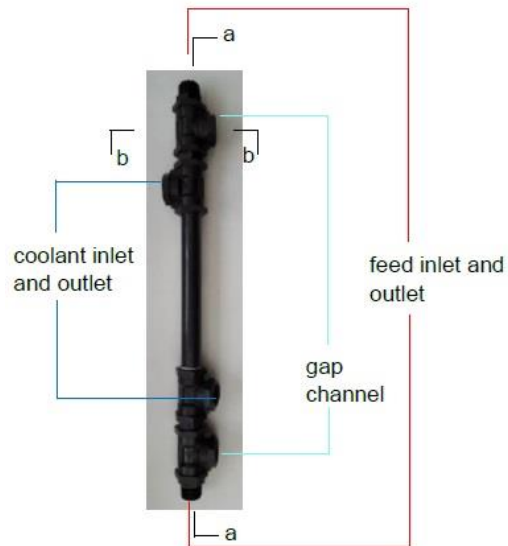
a) Module overview   b) a-a cross section
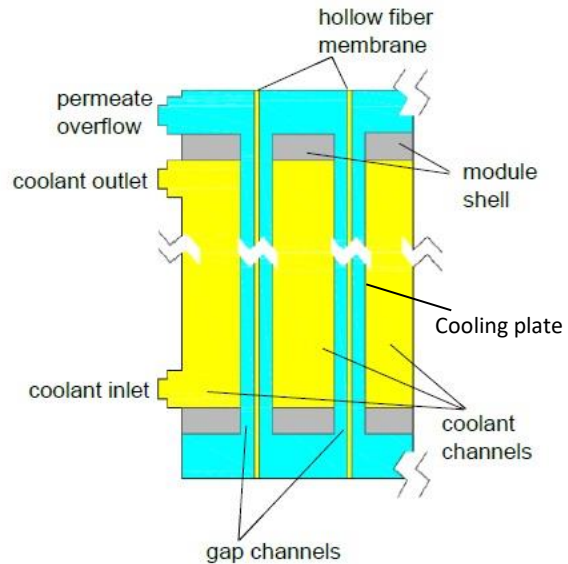
c) b-b cross section
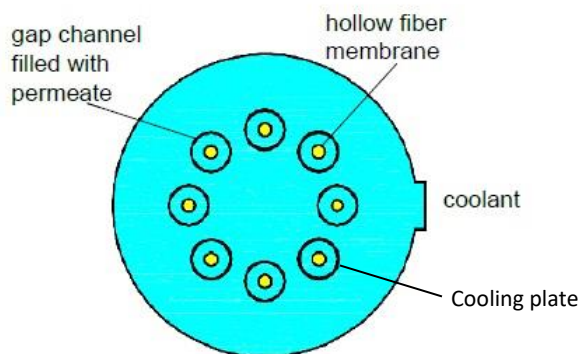
Fig. 4-1. Basic channel arrangement of hollow fiber membrane PGMD module

This channel arrangement enables the utilization of the coolant liquid as the hot feed solution, which facilitates sensible and latent heat recovery within the same module. Besides the aforementioned PGMD mode, this module can be operated under DCMD and SGMD modes when the gap channels are used as coolant channels or gaps for sweeping gas, respectively.

4.2.2. MD testing setup

A PGMD membrane module with 8 gap channels and 1 hollow fiber in each gap channel was tested to investigate the performance under different operating

conditions. The same module was operated under DCMD and SGMD modes to enable performance comparison. Higher hollow fibre packing density/gap channel density configuration was not applied here, because this study focused only on the investigation of unique characteristics of hollow fibre PGMD module rather than a full-scale study.

The velocity of the feed solution through the membrane lumen side was varied in the range of 0.28 – 0.81 m/s (70 – 200 mL/min); the temperature of the feed inlet was varied in the range of 40 – 70°C, and the inlet temperature of the coolant water remained at 20°C. The feed brine was prepared by dissolving 100 g NaCl into 10 L deionized water, and the produced permeate was periodically added back into the feed brine reservoir along with the brine concentrate to maintain a constant feed brine concentration. The temperatures of the feed, coolant and permeate were monitored at their respective inlets and outlets; the pressure of the feed inlet was measured to ensure that the operating pressure was lower than the LEP of the membrane; and a conductivity sensor was also used to measure the salt rejection. The flux was determined by weight in a permeate reservoir over time. The permeate reservoir was covered to eliminate the loss due to evaporation. All the data were obtained after the flux had stabilized, and the reported flux is the averaged value measured every hour over a 2-4h period following stabilization. The salt rejection was checked and was higher than 98% in all the experiments conducted in this study. To ensure experimental reproducibility, all the experiments were repeated at least once and the reproducibility was within $\pm 9\%$.

PGMD testing

Fig. 4-2 shows a sketch of the counter-current PGMD experimental apparatus. A peristaltic pump was used to send brine from the feed tank through the PGMD module coolant channel via a chiller. The coolant water out of the PGMD module was heated before it was sent to the membrane lumen side as the hot feed. Water out of the membrane lumen side was circulated back to the feed tank and naturally cooled down. The produced permeate filled the gap channels gradually, and then overflowed into the permeate reservoir. As the coolant was gradually heated through the coolant channel by the feed due to this unique module design, less heat energy was required to heat it to the pre-set feed inlet temperature, the heat recovery occurred within the membrane module.
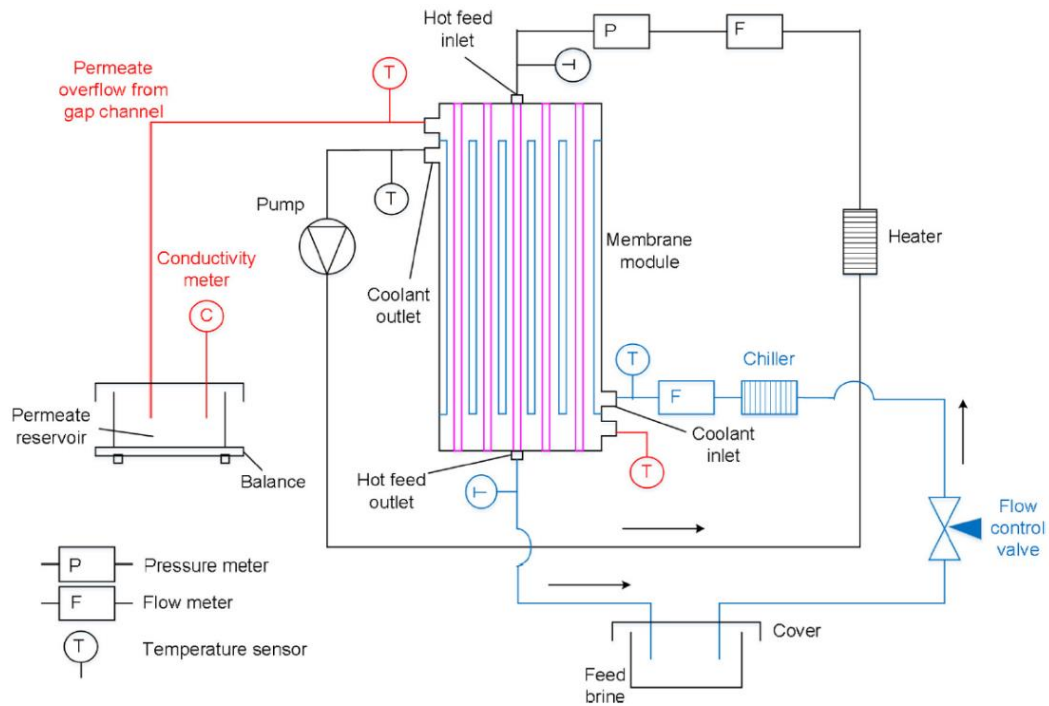
Fig. 4-2. Flow diagram of PGMD mode

DCMD testing

A sketch of the counter-current DCMD experimental apparatus is shown in Fig. 4-3. For DCMD tests, two peristaltic pumps were used to send brine and permeate through the module feed channel and the gap channel, respectively. Please note that the coolant channel in the PGMD mode was not used in DCMD mode.
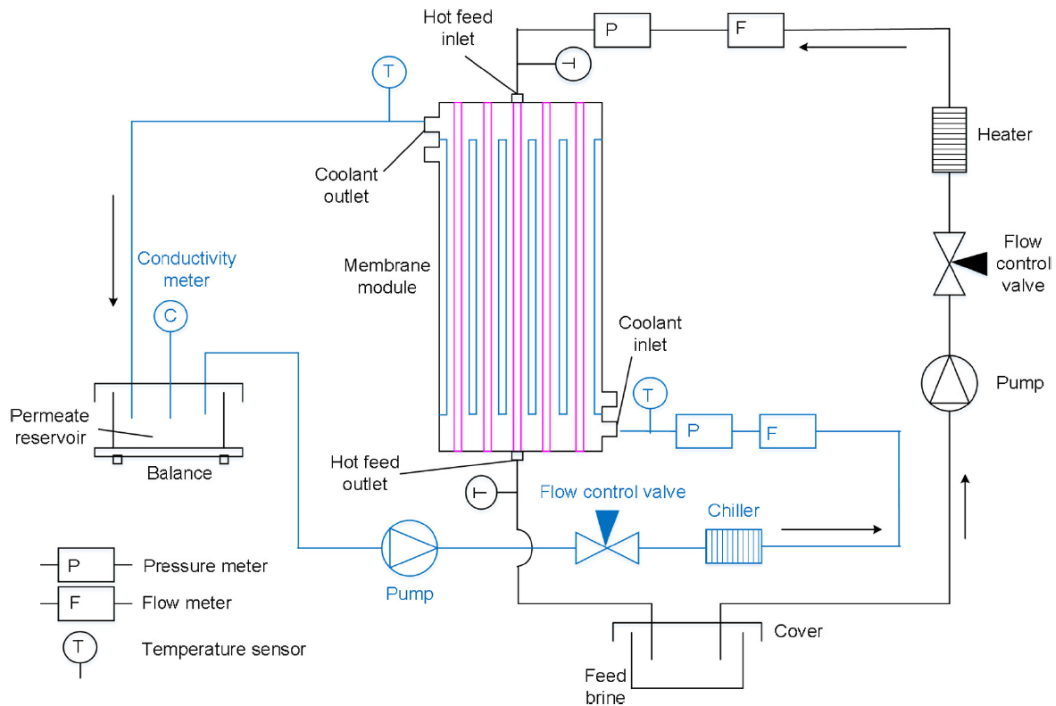
Fig. 4-3. Flow diagram of DCMD mode

SGMD testing

For SGMD tests (Fig. 4-4), two peristaltic pumps were used to send the brine and coolant water (demineralized water) through the feed channel and coolant channel, respectively. The produced permeate vapour was condensed on the surface of the cooling plate at the permeate side, then it flowed downward along the gap channels into the permeate reservoir. Due to the small gap (0.87 mm) between the hollow fiber and the gap channel (HDPE tube), the produced permeate may not flow smoothly and the gap channel could be blocked and flooded by the water droplets. In order to prevent this happening, a small air pump (air flowrate: 1.3 L/min (0.52 m/s)) was used to sweep the produced permeate out of the gap channel. Based on this setup, the experiments were not conducted under standard SGMD or AGMD mode, but rather the setup configuration is a combination of AGMD and SGMD. However, SGMD is used here to simplify the terminology.

Similar to PGMD and DCMD, the same volumetric flow rates of the lumen and cold sides and same feed/coolant water temperatures were used in the SGMD mode.

It is worthwhile mentioning that, as a non-typical SGMD module, a portion of the permeate vapour could be lost due to the partial condensation. The air entered the module with lower temperature was saturated by permeate vapour at a higher temperature inside the gap channel, and then was directed into the bottom of the

permeate tank before bubbling through the permeate and being discharged to the atmosphere. The permeate tank was covered by a plastic film to minimize evaporation. It was assumed that the permeate vapour loss due to air flow was low. To verify this assumption, the permeate vapour loss was calculated based on: (a) the air inlet temperature of 20 ˚C; (b) the air outlet temperature of 41 ˚C being the average temperature of the feed outlet temperature (62 ˚C) and the coolant inlet temperature (20 ˚C) since both air outlet temperature and permeate temperature were not monitored during the experiments; (c) inlet air humidity being 70% as average air humidity in August in Bendigo and (d) the air was saturated coming out of the permeate tank. The effect of the calculated maximum permeate loss on flux was 3.5%. Consequently, it could be concluded that the effect of permeate loss on flux was less than 5%, which is within the experimental error.
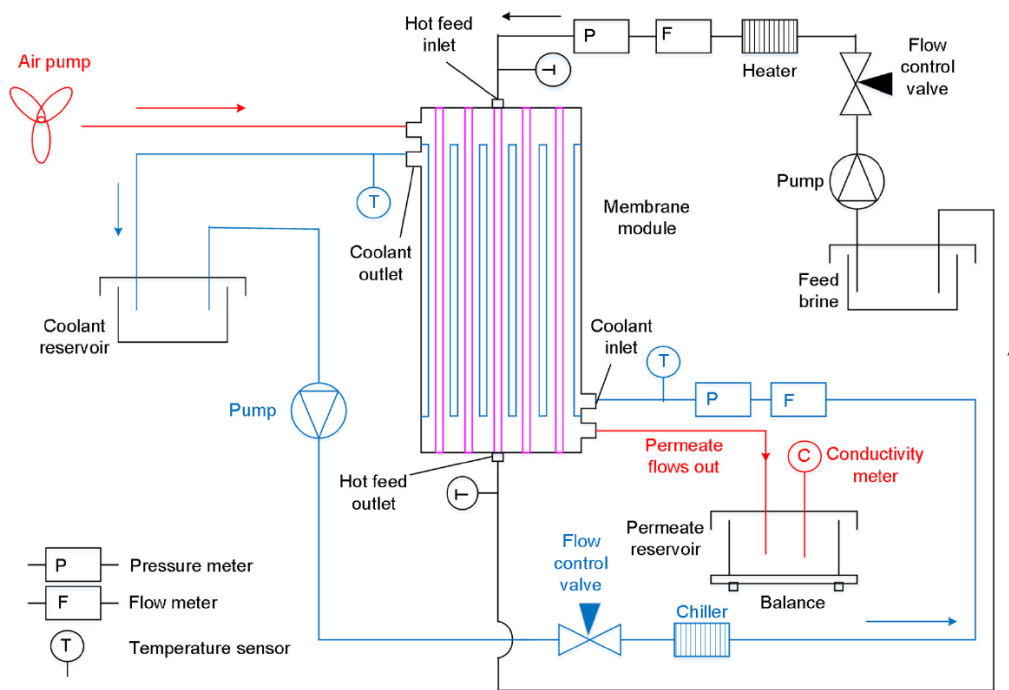
Fig. 4-4. Flow diagram of SGMD mode

4.3. Results

4.3.1. Influence of feed inlet temperature on flux
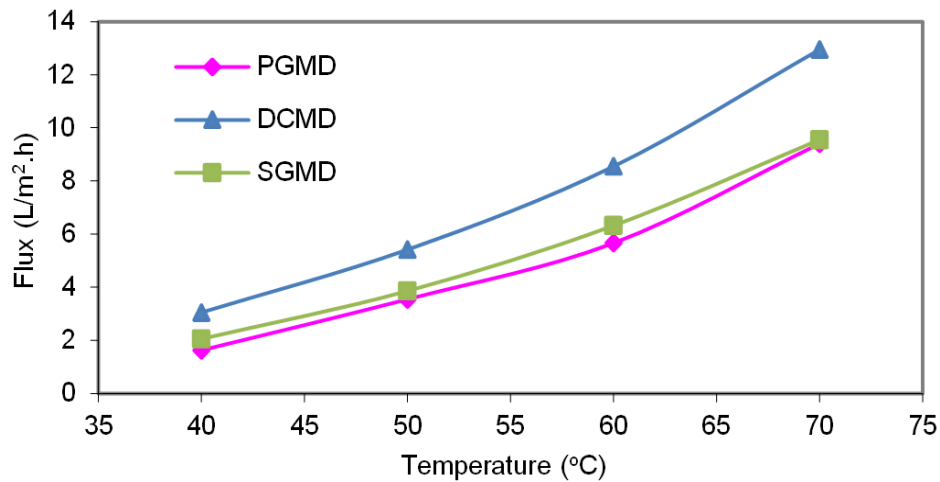
Fig. 4-5. Influence of feed inlet temperature on flux (feed velocity 0.81 m/s)

The flux variation as a function of feed inlet temperature under different operating modes is shown in Fig. 4-5 for a feed velocity of 0.81m/s. Due to the different cross sectional areas of coolant flow channels under different modes, the coolant velocities were different and were significantly less than that of hot feed (see Table 4-1).

Fig. 4-5 shows that the flux increased with increasing feed inlet temperature for all three different modes, and the flux increased more significantly at higher temperature. This phenomenon is because MD is driven by vapor pressure difference, which increases exponentially with the feed temperature [7, 26, 33].

Fig. 4-5 also shows that the module operated under the DCMD mode exhibited the highest flux as expected. This phenomenon was probably due to the coolant velocity for DCMD being 10 to 100 times higher than the coolant velocity of SGMD and permeate overflow velocity of PGMD respectively (see Table 4-1), which resulted in higher uniformity of the temperature at the cold side and increased driving force across the membrane. Additionally, the increased coolant velocity also led to a shorter residence time within the membrane module and consequently a higher temperature difference between the membrane surfaces. The flux of SGMD was 26% and 1.6% higher than those of PGMD at 40˚C and 70˚C feed inlet temperatures, respectively. This phenomenon was probably due to that the use of air to blow the permeate out of the coolant channel for the SGMD experiments, which has significantly decreased the mass transfer resistance.

Table 4-1 Velocities and Re numbers at 70˚C inlet temperature

Hot inlet temperature 70˚C	Velocity (m/s)														
	PGMD	DCMD	SGMD	PGMD	DCMD	SGMD	PGMD	DCMD	SGMD	PGMD	DCMD	SGMD	PGMD	DCMD	SGMD
Feed channel	0.81	0.81	0.81	0.69	0.69	0.69	0.53	0.53	0.53	0.40	0.40	0.40	0.28	0.28	0.28
Coolant channel	0.0080	0	0.0080	0.0068	0	0.0068	0.0052	0	0.0052	0.0040	0	0.0040	0.0028	0	0.0028
Permeate gap	0.00062	0.078	0	0.00057	0.066	0	0.00052	0.050	0	0.00044	0.039	0	0.00038	0.027	0
	Re (-)														
Feed channel	1468	1388	1484	1230	1159	1214	937	897	959	687	637	694	466	400	451
Coolant channel	87	-	88	75	-	76	58	-	59	45	-	46	33	-	32
Permeate gap	2.2	154	-	2.0	132	-	1.8	103	-	1.5	79	-	1.2	57	-

4.3.2. Influence of feed velocity on flux
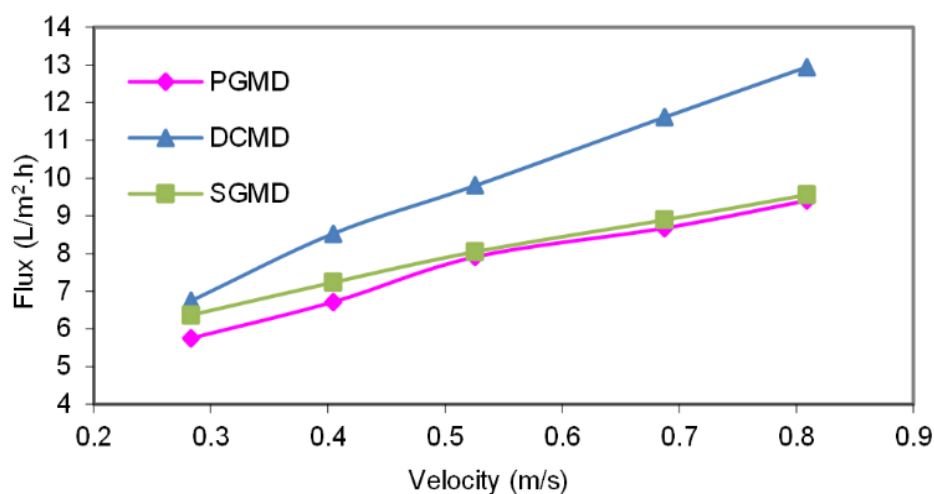
Fig. 4-6. Influence of feed velocity on flux (feed inlet temperature 70 ˚C)

In order to evaluate the influence of feed velocity on flux under different operating modes, the flux measured at 70 ˚C feed inlet temperature with different feed velocities was shown in Fig. 4-6.

Fig. 4-6 shows that the flux increased with feed velocity. This phenomenon is due to the higher velocity leading to a better uniformity of the temperature at the feed side and increased vapour pressure difference across the membrane.

It also can be seen that the rate of flux increase slowed at higher feed velocities for SGMD and PGMD but not for DCMD experiments. The possible reason is that the same velocity (feed and coolant) and flow channel were used for SGMD and PGMD experiments, but the coolant velocity of the DCMD was much higher than those of the SGMD and PGMD, which should have a significant impact on the uniformity of the temperature on the cold side.

Many studies [11, 24, 33] have identified some asymptotic flux values with increasing feed velocity. This is mainly because the boundary layer could not be further reduced when feed velocity results in a fully developed flow, and the uniformity of the temperature will not be improved accordingly. Higher feed velocity was not applied for different operating modes in this study to avoid wetting the membrane pores at the higher applied pressures. The same volumetric flow rates were applied for lumen and cold sides, which resulted in a significantly low coolant velocities for both SGMD and PGMD. Consequently, uniformity of the temperature on the cold sides of the SGMD

and PGMD cannot be effectively improved over the applied coolant velocity. On the other hand, it is expected that the flux will reach a plateau for DCMD if a higher feed velocity is applied.

4.3.3. Influence of operating conditions and modes on energy performance
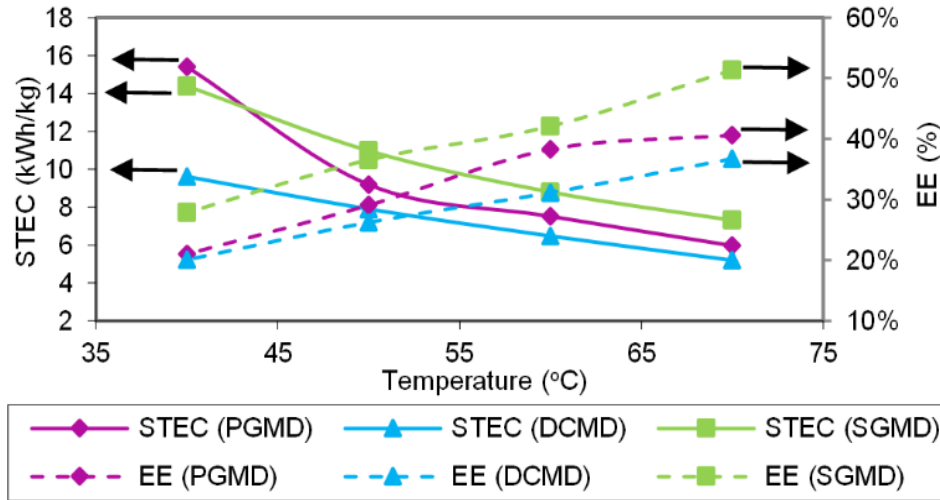
Fig. 4-7. Influence of feed inlet temperature on Specific Thermal Energy Consumption (STEC) and Energy Efficiency (EE) (feed velocity 0.81 m/s)

In order to compare the energy performance, STEC and EE were calculated for different operating modes.

STEC is the energy required to produce 1 kg of permeate water, and can be calculated by:

$$STEC = \frac{\dot{Q}_{heat}}{\dot{m}_{permeate}}$$
(4-1)

Here, $\dot{Q}_{heat}$ is the external thermal energy input; and $\dot{m}_{permeate}$ is the mass flow rate of the produced permeate. $\dot{Q}_{heat}$ is calculated by:

$$\dot{Q}_{heat} = \dot{m}_{feed} c_p (T_{Hi} - T_{Co})$$
(4-2)

Here, $\dot{m}_{feed}$ is the feed mass flow rate, c_p is the specific heat capacity which depends on temperature and salinity [63], and T_{Hi} and T_{Co} are the inlet and outlet temperatures of the feed and coolant solutions, respectively. Here, the coolant is gradually heated through the coolant channel, and then is used as the feed, and the

thermal energy input is that used to heat the feed stream following heat recovery in the PGMD module.

EE is the ratio of the latent heat energy to the total heat loss, and low efficiency occurs when there is high heat loss through conduction. EE is also a measure of the energy utilization during the condensation process and can be calculated by:

$$EE = \frac{\dot{m}_{permeate} h_{latent}}{\dot{Q}_{total.heat.loss}} \qquad (4\text{-}3)$$

Where, $\dot{Q}_{total.heat.loss}$ is the total heat loss of the feed and can be calculated by:

$$\dot{Q}_{total.heat.loss} = \dot{m}_{feed} c_p (T_{Hi} - T_{Ho}) \qquad (4\text{-}4)$$

Here, T_{Ho} is the outlet temperature of the feed solution.

The STEC was calculated based on the external thermal energy input for 1 kg permeate produced. For the PGMD mode, external energy input was calculated based on the temperature difference between the feed inlet and coolant outlet due to the energy recovery enabled by the unique module design. For DCMD and SGMD, the external energy was calculated based on the temperature difference between the feed inlet and the brine within the brine reservoir. As the brine temperature was not measured during the experiments, the laboratory room temperature of 20 ˚C was used as the brine temperature and it simulated a constant temperature feed in single pass arrangement. It is worthwhile mentioning that the actual brine temperature should be higher than 20 ˚C for DCMD and SGMD, because the heated brine out of the feed channel was circulated back to the brine reservoir. The EE was calculated based on the ratio of the latent heat and the total heat loss. For all the different operating modes, total heat loss was calculated based on the temperature difference between the feed inlet and outlet.

It can be seen from Fig. 4-7 that STEC decreased with increasing feed inlet temperature for different modes. On the other hand, EE increased as a function of feed inlet temperature. At higher feed inlet temperature, the external energy input was higher, however, the flux increased more rapidly compared to the increase of external energy input. Consequently, the STEC was lower while EE was higher at higher feed inlet temperature. This is consistent with results from other investigations [7, 26, 33] that flux has an exponential relationship with feed inlet temperature compared to the linear relationship between conductive heat losses and the feed inlet temperature.

Fig. 4-7 shows that DCMD had the lowest STEC. The main reason was due to the significantly higher flux obtained under DCMD mode compared to SGMD and PGMD. The STEC of PGMD was normally lower compared to that of SGMD except at 40 ˚C. The calculation of external energy input of PGMD included the energy recovery from the coolant, however, energy recovery was not considered for SGMD and DCMD for this study and the temperature of the brine within the brine feed reservoir before pumping into the module was assumed at 20 ˚C. For the PGMD experiments, the coolant outlet temperature was always higher than 20 ˚C and it was closer to 20 ˚C when the feed inlet temperature was lower as less internal thermal energy was recovered. Consequently, although flux was slightly higher for SGMD compared to PGMD, the external energy input was much higher for SGMD, and subsequently, the STEC of PGMD was lower than that of SGMD except at 40 ˚C feed inlet temperature when the influence of internal energy recovery was negligible.

It can also be seen from Fig. 4-7 that SGMD had the highest EE, which was 26% and 40% higher than those of PGMD and DCMD, respectively, at 70 ˚C feed inlet temperature and 0.81 m/s feed velocity. When the feed inlet temperature was decreased to 40 ˚C, the EE of SGMD was 33% and 39% higher than those of PGMD and DCMD, respectively. This phenomenon was probably due to the fact that the heat loss by conduction was less for SGMD due to the existence of the sweeping gas gap compared to PGMD and DCMD. The feed inlet temperature was the same for the different modes, DCMD and SGMD had the lowest and highest outlet temperatures for feed channel respectively (Table 4-2). This indicated that DCMD and SGMD had the highest and lowest total heat energy loss respectively. In the meantime, DCMD and SGMD had the lowest and highest EE respectively. Based on the above, it could be concluded that DCMD and SGMD had the highest and lowest heat loss due to the conduction, respectively.

Table 4-2 Outlet temperature for feed channel under different modes with 0.81 m/s feed velocity

Feed inlet temperature (˚C)	40	50	60	70	40	50	60	70
	Outlet temperature for feed channel (˚C)				Outlet temperature for coolant channel (˚C)			
PGMD	37.28	44.10	52.97	59.97	22.62	26.09	28.86	29.87
DCMD	34.01	41.19	47.06	51.98	25.92	28.89	31.66	35.48
SGMD	38.12	45.95	53.51	62.22	21.96	24.10	26.61	28.86

4.4. Discussion

4.4.1 Performance evaluation by global mass transfer coefficient

The impact of operating conditions and modes on module performance can be evaluated by the global mass transfer coefficient, an indicator frequently adopted for MD module evaluation.

As per Eq. (2-3), the permeation flux J_{vm} is assumed to be proportional to the vapour pressure difference across the membrane. However, the temperatures at membrane interfaces (T_{fm} and T_{pm}) are difficult to measure accurately [5, 74], it is more practical and simple to use bulk temperature. Hence, the global mass transfer coefficient is used in this study to investigate the performance of the MD process.

$$J_{vm} = N(P_{fm} - P_{pm}) = C_{global}(P_{T_{fb}} - P_{T_{pb}}) = C_{global}\Delta P_{avg} \tag{4-5}$$

For counter-current flow, the ΔP_{avg} can be calculated by

$$\Delta P_{avg} = \frac{(P_{Hi} - P_{Po}) - (P_{Ho} - P_{Ps})}{\ln \dfrac{P_{Hi} - P_{Po}}{P_{Ho} - P_{Ps}}} \tag{4-6}$$

Here, N is the membrane mass transfer coefficient, which is only related to membrane characteristics and gas conditions in the membrane pores [74]; $P_{T_{fb}}$ and $P_{T_{pb}}$ are vapour pressures at T_{fb} and T_{pb}, respectively; T_{pb} is the average bulk temperature within the permeate gap; C_{global} is the global mass transfer coefficient which combines the effects from the boundary layer and membrane [5, 74]; ΔP_{avg} is the average vapor pressure difference between the feed bulk flow and the permeate gap; P_{H_i} and P_{H_o} are inlet and outlet vapour pressures for hot feed channel, respectively; and P_{P_o} and P_{P_s} are overflow vapour pressure and bottom vapour pressure of the permeate gap, respectively.
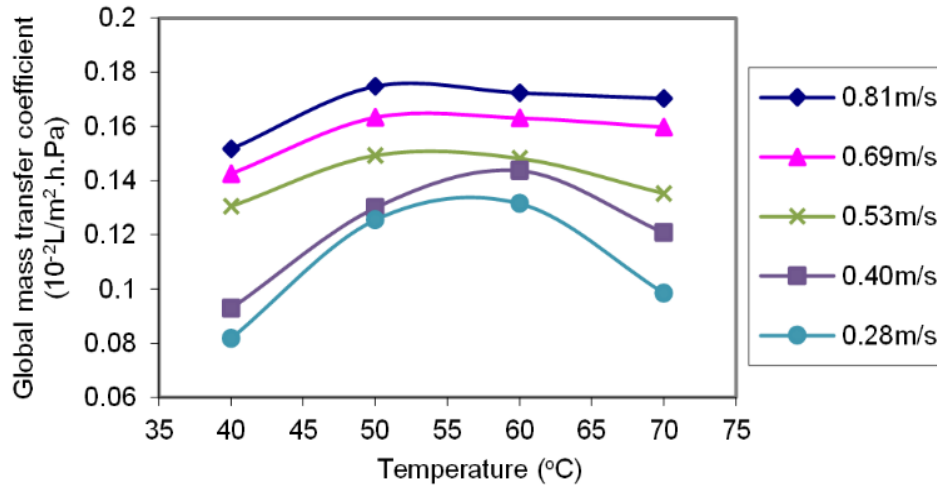
Fig. 4-8. Influence of feed inlet temperature on PGMD global mass transfer coefficient

The global mass transfer coefficient as a function of feed inlet temperature for PGMD is shown in Fig. 4-8 at different inlet velocities. It can be seen that the global mass transfer coefficient increased initially with temperature, and then decreased at higher temperature. This phenomenon is probably due to the combined effects of transverse vapor flux and uniformity of the temperature within the channel. The higher transverse vapor flux will break down the laminar boundary layer and enhance the heat transfer [60]. On the other hand, with increasing feed inlet temperature, the uniformity of the temperature within the feed channel decreases accordingly [74] and the global mass transfer coefficient decreases. The results of this study suggest that the effects of transverse vapor flux played a more decisive role at lower temperature and effects of uniformity of the temperature became more critical at higher temperature.

It also can be seen that the mass transfer coefficient increased with increasing feed velocity. Higher velocity increased the uniformity of the temperature, resulted in shorter residence time within the channels and increased temperature difference between membrane surfaces, consequently, mass transfer coefficient was improved by higher velocity.

The mass transfer coefficient was more stable at higher feed velocity, and there are two possible reasons for this phenomenon. Firstly, the boundary layer cannot be further reduced when feed velocity increases beyond the velocity required for fully developed flow; secondly, permeation flux was higher with a higher feed velocity, so the effect of decreased uniformity of the temperature at the higher temperature become less compared to that with lower feed velocity.
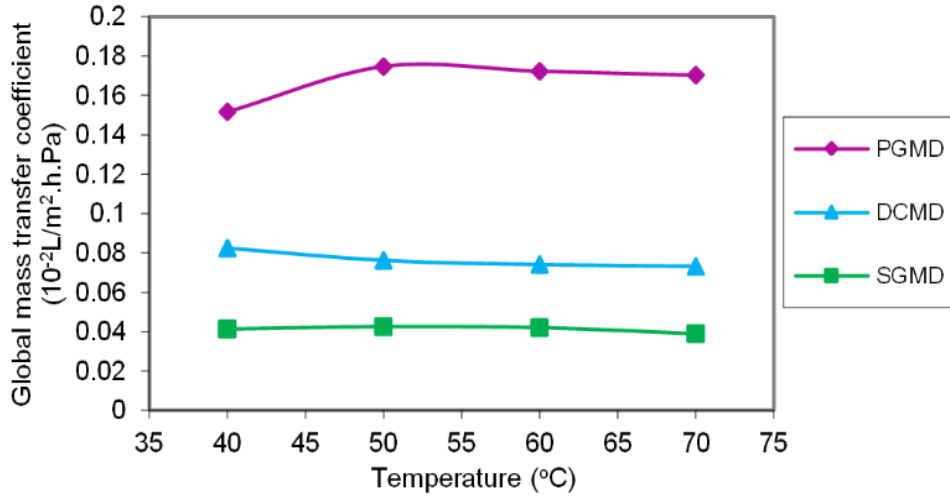
Fig. 4-9. Global mass transfer coefficient comparison between different operating modes (feed velocity 0.81 m/s)

The global mass transfer coefficients for PGMD, DCMD and SGMD are shown in Fig. 4-9. ΔP_{avg} for PGMD is the average vapor pressure difference between the feed bulk flow and the permeate gap, while ΔP_{avg} of DCMD and SGMD is the average vapor pressure difference between the feed bulk flow and coolant bulk flow. Due to the above difference, the trends of global mass transfer coefficient rather than the actual values have been used here to identify the unique module characteristics of PGMD.

Fig. 4-9 shows that the global mass transfer coefficients of the DCMD and SGMD decreased slightly as a function of feed inlet temperature, which is similar to the results by Zhang et al. [74]. This phenomenon is probably due to the decreased uniformity of the temperature at higher temperatures and fluxes [83].

The different trends of the global mass transfer coefficients for PGMD, DCMD and SGMD were due to the nearly stagnant permeate overflow within the permeate channel for PGMD compared to the significantly higher coolant circulation velocity and air velocity for DCMD and SGMD, respectively. In order to evaluate the flow characteristics of different channels under different modes, Reynolds numbers (Re) were calculated by:

$$\mathrm{Re} = \frac{d_h v \rho}{\mu} \tag{4-7}$$

Here, d_h is the hydraulic diameter of the flowing channels, v is the velocity, ρ is the density of the fluid, and μ is the viscosity of the fluids. The hydraulic diameter was calculated by:

$$d_h = \frac{4A}{P_w} \tag{4-8}$$

Here, A is the cross sectional area of the channel, and P_w is the wetted perimeter of the cross section.

The calculated Re (Table 4-1) shows that the flows of all three channels under different modes were within the laminar flow regime. It is considered that the transverse vapor flux within the permeate gap under PGMD mode should have a greater impact on boundary layer, especially within the laminar flow regime, and the uniformity of the temperature is relatively high at lower feed inlet temperature. Due to the unique module characteristics of the PGMD, considerations should be given to optimizing the flow within the permeate gap to improve the PGMD performance. Increased hollow fiber packing density, increased gap channel density and the introduction of turbulence promotors could be applied. Furthermore, utilization of cooling plate with a higher thermal conductivity and the adoption of multi-stage process could potentially improve the PGMD performance as well.

4.4.2 Comparison of PGMD, DCMD and SGMD

In order to compare the PGMD performance to DCMD and SGMD, the flux and STEC results obtained under different modes from this study are plotted into Fig. 4-10. Additionally, results from various DCMD [84, 85] and SGMD [86, 87] from the literature are also plotted for comparison.

It is worthwhile mentioning that due to the different membrane characteristics and operating conditions, it is difficult to make a direct comparison between different studies. Nevertheless, a qualitative comparison rather than a quantitative one is shown here. Furthermore, STECs were not given for some of the studies. To facilitate the comparison, STECs were calculated based on the data from those studies and the same approach was applied for all these studies (laboratory room temperature of 20 ˚C was used as the brine temperature and there is no heat recovery).

The membrane characteristics and operating conditions for the above DCMD [84, 85] and SGMD [86, 87] are summarized in Table 4-3.
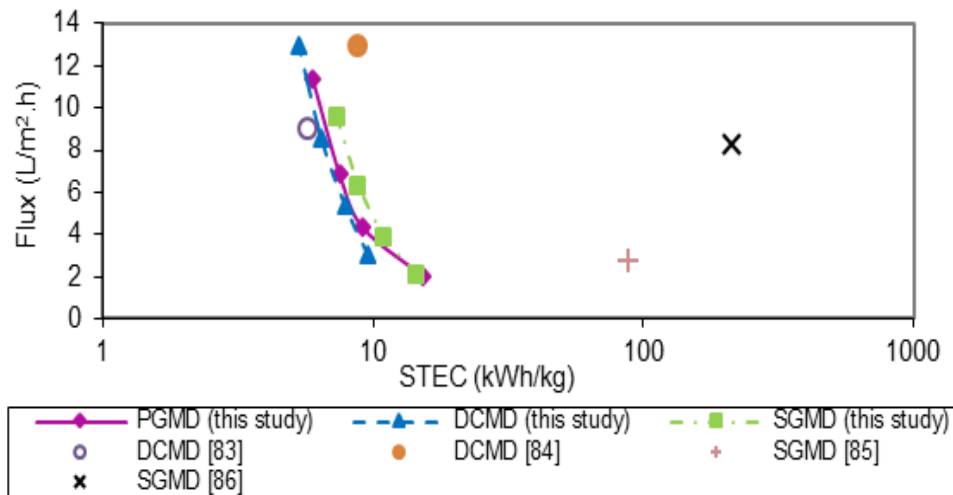
Fig. 4-10. Flux versus STEC for PGMD, DCMD and SGMD

The flux versus STEC obtained with different feed inlet temperature (40 - 70 ˚C) and 0.81 m/s feed velocity for PGMD, DCMD and SGMD is shown in Fig. 4-10. The desired MD module should have a high flux with a low STEC, which fits into the upper left corner of Fig. 4-10.

From Fig. 4-10, it can be seen that the highest flux was obtained under DCMD mode, however, the lowest STEC was obtained under PGMD mode if the flux was the same. Furthermore, compared to the results from other DCMD [84, 85] and SGMD [88, 89], results from our PGMD also showed a relatively good balance in terms of flux and STEC.

Many studies have focused on the comparison between PGMD and AGMD rather than SGMD. Francis et al. [7] investigated the AGMD performance using a flat sheet membrane module and compared it to the Material Gap Membrane Distillation (MGMD), which utilized the same module as AGMD but the gap was filled with other materials such as polyurethane (sponge), polypropylene mesh, sand and de-ionized water. They identified that a maximum increase of 820% in the flux was observed during WGMD compared to AGMD under the same operating conditions. Essalhi and Khayet [11] compared LGMD with AGMD using a porous composite hydrophobic/hydrophilic flat sheet membrane. Their results showed that the permeation flux of LGMD was only slightly higher than that of AGMD (2.2 – 6.5%). They concluded that the higher water production rate may be due to two main factors: firstly, the higher thermal conductivity of water compared to that of air resulting a lower temperature at the permeate side of the membrane and increased transmembrane driving force, and secondly, smaller established distance between the liquid/vapor interfaces at both sides of the membrane as water penetrates inside the membrane

hydrophilic layer. The above discussion suggested that due to the different membrane materials in these studies, the difference between PGMD and AGMD performance varies significantly.

In terms of energy performance, Essalhi and Khayet [11] showed that the EE of LGMD was higher than that of AGMD and it was suggested that this may be attributed to the less uniformity of the temperature of AGMD. Cipollina et al. [13] investigated the influences of feed flow rate (400 – 1200 mL/min and coolant and feed flow rates were identical) and feed inlet temperature (50 - 80 ˚C) on the permeation flux and the STEC of a flat sheet membrane under PGMD and AGMD modes, respectively. Their study showed that the permeation flux of PGMD was higher than that of AGMD while the STEC of AGMD was higher than that of PGMD.

All the above studies suggest that PGMD has a higher flux and lower STEC compared to AGMD. Generally, mass transfer rate and energy consumption of SGMD are higher than those of AGMD [4]. Consequently, the flux of SGMD from our study is slightly higher than that of PGMD, but, as shown in Fig. 4-10, the STEC of PGMD was lower than those of SGMD and DCMD when the flux is the same.

Based on the above consideration, it could be concluded that PGMD has the potential to effectively combine the advantages of conventional MD processes (DCMD, AGMD and SGMD), with a lower STEC than DCMD and SGMD, when flux is the same. Additionally, different approaches (see Chapter 4.4.1) could be utilized to further improve both the flux and the energy performance of the PGMD module.

4.4.3 Comparison of PGMD in different module designs

As the first developed hollow fiber PGMD module, its performance has been compared to other PGMD studies (flat sheet [7, 11, 13] and spiral wound [17, 18]) to evaluate the unique hollow fiber module characteristics. The membrane characteristics and operating conditions for the above studies can be found in Table 4-3.

As mentioned in Section 4.4.2, different PGMD studies had different operating conditions and membrane/module characteristics, a qualitative comparison rather than a quantitative one was made here. Furthermore, the comparison was based on two general parameters: flux and STEC, which were always used for MD performance evaluation.

The STEC of PGMD studies should be calculated based on the difference between feed channel inlet temperature and coolant channel outlet temperature due to the internal energy recovery. Some of the above studies did not calculate the STEC and

the coolant channel outlet temperatures were not reported, therefore, the STEC was calculated based on the method adopted as that for the DCMD and SGMD modes.
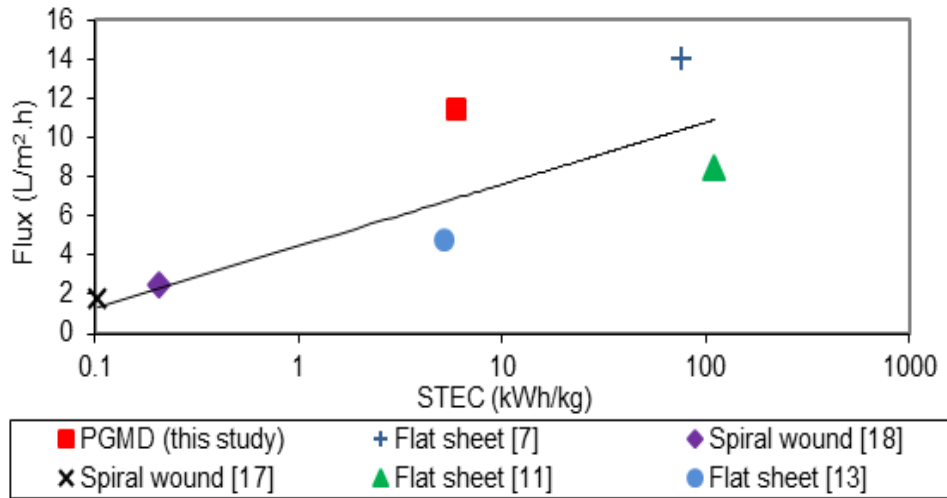
Fig. 4-11. Flux versus STEC for PGMD in different module designs

Fig. 4-11 shows that hollow fiber PGMD module had a relatively high flux compared to that of flat sheet and spiral wound PGMD. The flux obtained with flat sheet WGMD module [7] under 70 °C feed inlet temperature was approximately 14.5 L/m^2.h, which was 50% higher than that obtained from our study under same feed inlet temperature. However, the coolant velocity applied for that study was 0.25 m/s, which was significantly higher than our study, and it could increase the uniformity of the temperature at the coolant side. Essalhi and Khayet [11] obtained a flux of around 8.5 L/ m^2.h with 65 °C feed inlet temperature under flat sheet LGMD mode, which was slightly higher than that from our study. This phenomenon could be due to the unique membrane properties as a composite hydrophobic/hydrophilic membrane was employed in that study. Furthermore, distilled water was used as the feed solution compared to the 10 g/L NaCl brine used in our study, which could also improve the permeation flux. Cipollina et al. [13] achieved the fluxes of approximately 4.8 and 8.6 L/m^2.h with 400 and 1200 mL/min feed flow rates for 70 °C feed inlet temperature respectively. The results confirmed that the feed velocity had a significant influence on flux by increasing the uniformity of the temperature. Although the minimum feed flow rate (400 mL/min) was higher than the maximum feed flow rate used in our study (200 mL/min), the flux obtained from our study was around 100% higher than that obtained from [13] with similar feed and coolant inlet temperatures. Winter et al. [17, 18] used spiral wound membrane to investigate the PGMD concept, with 80°C and 25°C as hot and cold inlet temperatures, respectively, and achieved a considerably lower permeation flux in the range of 1.8 to 3.0 kg/m^2.h. The possible reason for this low

permeation flux could be due to that the longer membrane module led to a less temperature difference across the membrane, resulting in a low flux.

In terms of energy efficiency, Fig. 4-11 demonstrated that STEC of the hollow fiber PGMD is better than that from most flat sheet PGMD studies, however, it is significantly higher than that of spiral wound PGMD. Essalhi and Khayet [11] found that the EE of their flat sheet LGMD increased with increasing feed temperature, which was similar to our study. However, their EE was in the range of 10 – 25%, which was lower than our results. Cipollina et al. [13] showed that the STEC of their flat sheet PGMD module decreased with increasing feed inlet temperature, which was similar to our study. Their highest STEC was approximately 17 kWh/L with 1200mL/min feed flowrate and 50˚C feed inlet temperature, and the lowest STEC was around 5 kWh/L with 400mL/min feed flowrate and 80˚C feed inlet temperature. The results for our PGMD system resulted in a STEC of 9.19 kWh/L for 200mL/min feed flowrate and 50˚C feed inlet temperature. It is assumed that the STEC will increase if higher feed velocity is applied. Both spiral wound PGMD studies [17, 18] found a lower STEC in the range of 0.1 - 0.23 kWh/L compared to ours and that of Cipollina et al. [14]. These results indicate that the internal heat recovery was maximized by spiral wound module design, however, the penalty is a considerably lower flux. It also indicated that the longer hollow fibre module could potentially increase the latent heat and sensible heat recovery, but decrease the module flux.

A trend line shown in Fig. 4-11 was made based on the data obtained from various flat sheet [7, 11, 13] and spiral wound [17, 18] PGMD studies. The line clearly demonstrates that a trade-off exists between flux and STEC for different PGMD modules. Spiral wound PGMD module normally has a better STEC but lower flux due to its module configuration; the above flat sheet PGMD modules show either a high flux and high STEC or a low flux and low STEC. Although the performance of spiral wound or flat sheet module is highly dependent on module size and operating conditions and could be further optimized, hollow fibre PGMD module appears to achieve a better balance between flux and STEC compared to the flat sheet and spiral wound modules (above the trend line). Due to the various potential advantages of hollow fiber membrane (high specific area and small footprint), it is desired to further optimize this hollow fiber PGMD module.

Table 4-3 Operating conditions and membrane characteristics of MD studies

Reference	Operating condition*					Membrane characteristics*			
	Membrane configuration	Hot feed / coolant temperature (˚C)	Hot feed concentration (g/L)	Hot feed flowrate (mL/min)	Coolant flowrate (mL/min)	Pore size (μm)	Porosity (%)	Membrane area (m^2)	Thickness (μm)
Francis et al. [7]	PGMD	70 / 20	-	1500	1500	0.2	-	0.005	100
Winter et al. [18]	PGMD	80 / 25	0	8333	8333	0.2	80	10	70
Winter et al. [17]	PGMD	80 / 25	0	5000	5000	0.2	75-80	10	70
Essalhi and Khayet [11]	PGMD	65 / 20	0	1666	-	0.04-0.05	-	0.0055	58.4-71
Cipollina et al. [13]	PGMD	70 / 17-20	35	400	400	0.2	80	0.042	250
Duong et al. [84]	DCMD	50 / 25	35	1250	1250	0.3	85	0.05	76
Al-Obaidani et al. [85]	DCMD	70 / 15	35	3219	1580	0.2	70	0.1	650
Zhao et al. [86]	SGMD	65 / 21 (gas)	0	333	1000 (gas)	0.1	85-93	0.0042	109-111
Khayet et al. [87]	SGMD	71.6 / 17.3 (gas)	30	2750	36000 (gas)	0.45	80	0.0055	178

* The permeation flux from these studies was plotted into Figs.4-10 and 4-11, the corresponding operating conditions and membrane

characteristics are referred here.

4.5. Summary

A new PGMD module using hollow fiber membrane was successfully developed and tested with different feed velocities and feed inlet temperatures. The same module was also tested under DCMD and SGMD modes to enable performance comparison.

The maximum hollow fiber PGMD flux of 9.4 L/m^2.h was obtained for the experimental conditions of 70°C feed inlet temperature and 0.81 m/s feed velocity, which was 27% and 1.6% lower than the maximum flux of DCMD and SGMD respectively. This phenomenon was due to the higher coolant velocity for DCMD and applied air flow in the gap channel for SGMD.

The experiments also showed that the STEC of our PGMD was higher than that of DCMD but lower than that of SGMD (except at 40 °C feed inlet temperature), this is mainly due to the higher flux of the DCMD. The EE of PGMD was always higher than that of the DCMD and lower than that of the SGMD, which was attributed to the lower heat loss due to the conduction for SGMD.

The mass transfer coefficient of the present PGMD was compared to those from DCMD and SGMD. For PGMD, the mass transfer coefficient increased with the increasing feed velocity and stabilized at the higher feed velocity. Additionally, the mass transfer coefficient increased initially at the lower feed inlet temperature and then decreased when the feed inlet temperature was higher than 60°C, which could be attributed to the combined effects of transverse vapor flux and uniformity of the temperature. On the contrary, the global mass transfer coefficients of DCMD and SGMD decreased slightly as a function of feed inlet temperature, which was probably due to the decreased uniformity of the temperature at higher temperature. The different trends for global mass transfer coefficients versus feed inlet temperature for PGMD, DCMD and SGMD was probably due to the nearly stagnant permeate overflow within the permeate channel for the present PGMD compared to the much higher coolant circulation velocity and air velocity for DCMD and SGMD, respectively.

Compared to other studies, our results successfully demonstrated that PGMD has the potential to effectively combine the advantages of different conventional MD processes, a lower STEC compared to DCMD and SGMD when flux was the same. Furthermore, hollow fiber PGMD module could achieve a better balance between flux and STEC compared to flat sheet and spiral wound PGMD modules. Different approaches could be adopted to further optimize this hollow fiber PGMD module, such as increased hollow fiber packing density, increased gap channel density, an

introduction of turbulence promotors, cooling plate with a higher thermal conductivity and multi-stage process.

Chapter 5 Influence of PGMD module design on its performance

5.1. Introduction

As discussed in Chapter 4, a comparison has been made in the performance of PGMD to DCMD and SGMD using a single module. The results showed that hollow fibre PGMD can effectively combine the advantages of different conventional MD configurations together.

In this study, five different PGMD modules with different design parameters were manufactured and tested under the same operating conditions as those in the Chapter 4 to evaluate the influence of different module designs on its performance, and specifically on water productivity and energy efficiency.

Previously, researchers have implemented different approaches to improve PGMD performance. Material Gap Membrane Distillation (MGMD) and Conductive Gap Membrane Distillation (CGMD) were developed based on PGMD design. MGMD and CGMD have a similar channel arrangement except the gap channel of MGMD is filled by materials with low thermal conductivities, such as polypropylene, polyurethane (sponge) or mesh [7]; and the conductive gap channel of CGMD is filled with highly conductive materials, such as metal mesh [16], Francis et al. [15] showed that the flux of MGMD with de-ionized water gap was significantly higher than those of MGMD with other low conductivity material gaps. CGMD study undertaken by Swaminathan et al. [16] demonstrated that the permeate production only increased approximately 15% when the gap conductivity increased from 0.6 to 10 W/m.K. The insert of highly conductive material could require more mechanical support as the module is generally heavier. In addition, the costs of highly conductive material will be significantly higher than that of PGMD that is composed of mainly plastic materials.

In this study, the design parameters of the PGMD modules were varied in the numbers of gap channels (gap channel cross section relative to the cross sectional area of the housing Polyethylene (PE) pipe), the numbers of hollow fibres (hollow fibre cross section relative to the inside cross sectional area of each High Density Polyethylene (HDPE) or Stainless Steel (SS) tube), and cooling plate materials to evaluate their effects on the mass and heat transfers. This study could provide a guidance for further optimization of hollow fibre PGMD module.

5.2. Parameters for PGMD performance evaluation

Four parameters, Gain Output Ratio (GOR), STEC, Temperature Polarization Coefficient (TPC), and C_{global} are utilized here to evaluate the energy performance and heat/mass transfers phenomenon of different PGMD modules.

The definitions of STEC and C_{global} have been provided in Chapter 4, therefore, only GOR and TPC are defined as follows.

GOR

GOR is often used to indicate the energy performance of MD process, and is determined by [17, 90]:

$$GOR = \frac{\dot{m}_{permeate} \cdot h_{latent}}{\dot{Q}_{heat}} \tag{5-1}$$

GOR indicates the ratio of the thermal energy used for permeate production to the external heat energy input.

TPC

TPC is used as an indicator to assess the uniformity of temperature, which can be calculated based on the temperature difference across the membrane and the bulk temperatures of feed and permeate channels [71].

$$TPC = \frac{T_{fm} - T_{pm}}{T_{fb} - T_{pb}} = \frac{\Delta T_1}{\Delta T_2} \tag{5-2}$$

ΔT_1 and ΔT_2 can be estimated by:

$$\Delta T_1 = \frac{\dot{Q}_{trans} - J_{vm} h_{latent} A_m}{\dfrac{\lambda_2 A_m}{b_1}} \tag{5-3}$$

$$\Delta T_2 = \frac{(T_{H_i} - T_{P_o}) - (T_{H_o} - T_{P_s})}{\ln \dfrac{T_{H_i} - T_{P_o}}{T_{H_o} - T_{P_s}}} \tag{5-4}$$

Here, A_m is the membrane surface area; and T_{P_o} and T_{P_s} are the permeate overflow and bottom temperatures of the permeate gap, respectively. It should be pointed out

that the temperature differences given in Eqs. (5-3) and (5-4) are the average temperatures along the MD module.

STEC and C_{global} can be calculated by Eqs. (4-1) and (4-5), respectively.

5.3. Experimental methods and setup

5.3.1. Hollow fibre membrane characteristics

The employed hollow fibre membrane has been characterized and the details have been reported in Chapter 3.

5.3.2. Hollow fibre membrane PGMD modules

Five different PGMD modules were manufactured in the laboratory of Victoria University and their characteristics are listed in Table 5-1. The materials of the gap channel are either HDPE (outer and inner diameters of 3.40 mm and 2.84 mm, respectively) or SS 316 (outer and inner diameters of 6.35 mm and 4.55 mm, respectively) tubes. PE pipe (inner diameter of 25 mm) is used to make the module shell. All the materials used for module fabrication were commercially available.

Table 5-1 Properties of membrane modules

Module number	Material of cooling plate	Number of gap channels	Percentage of PE pipe filled by gap channels (%)	Number of hollow fibres within each channel	Percentage of single gap channel filled by hollow fibres (%)	Module length (hot channel) (m)	Membrane surface area (m^2)
1	HDPE	6	11.1	1	15.3	0.425	0.0076
2	HDPE	8	14.8	1	15.3	0.425	0.0102
3	HDPE	8	14.8	2	30.6	0.425	0.0203
4	HDPE	8	14.8	3	45.8	0.425	0.0305
5	SS	8	51.6	1	6.0	0.425	0.0102

As shown in Figs. 5-1a (side view) and 5-1b (top view), different numbers of HDPE or SS tubes were firstly inserted into a PE pipe to form the permeate gap channels. Two spacers made from HDPE sheet were applied at both ends of the tube bundles to ensure the optimal contact of coolant water and gap channels. Epoxy resin compound was then poured into module shell at one end to fill the gap between module shell and the gap channels firstly. The excess HDPE or SS pipes and resin were trimmed off when the epoxy resin was cured. Same process was then repeated at the other end of the module. Afterwards, as shown in Figs. 5-1c (side view) and 5-1d (top view),

different numbers of hollow fibres were inserted into each gap channel, and both ends of the hollow fibre bundles were then potted by epoxy resin compound. The excess hollow fibre and resin were also trimmed off when the epoxy resin was cured. Fig. 5-1e shows the overview of a finalized module.

As shown in Table 5-1, PGMD modules with different numbers of HDPE tubes, different numbers of hollow fibres, and different gap channel materials were built in order to perform a comprehensive performance comparison. Module 2 (8 gap channels, each gap channel contains 1 hollow fibre) has been utilized to benchmark the performance of other PGMD modules. This is also the module used to compare the PGMD results to DCMD and SGMD as in Chapter 4.
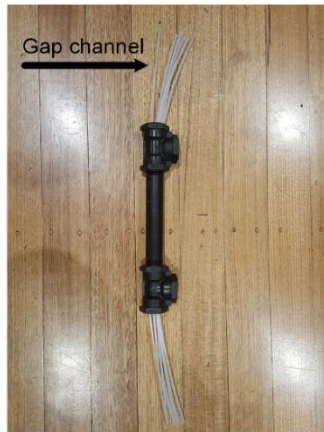
a) gap channel density (side view)

b) gap channel density (top view)

c) hollow fibre packing density (side view)

d) hollow fibre packing density (top view)

e) module channel overview

Fig. 5-1. Module channel arrangement overview

5.3.3. PGMD testing setup and data analysis

The procedure for testing the PGMD has been described in Chapter 4. During the experiments, one pump was utilized to circulate brine through both the coolant and hot channels, and thus the volumetric flow rates of coolant and feed were identical. The volumetric flow rates were adjusted in the range of 70 – 600 mL/min, depending on the gap channel density and hollow fibre packing density to achieve the same linear velocity. The velocity of the hot feed (0.28 – 0.81 m/s) was significantly greater than that in the coolant channel (0.002 – 0.024 m/s), because of the significantly larger cross sectional area of the coolant channel.

The results presented here were obtained from experiments directly or calculated based on the experimental data. The flux was calculated based on the weight measurements of the distillate over 2-3 hours period after the stabilization of the temperature. GOR and STEC were calculated using Eqs. (5-1) and (4-1), respectively, based on the calculated flux and monitored temperatures at the inlets and outlets of different channels.

5.4. Results and discussion

5.4.1. Effects of hollow fibre packing density on flux and TPC

Fig. 5-2 shows the flux and TPC as a function of feed velocity for module 2, 3 and 4. The TPC was calculated based on Eq. (5-2).
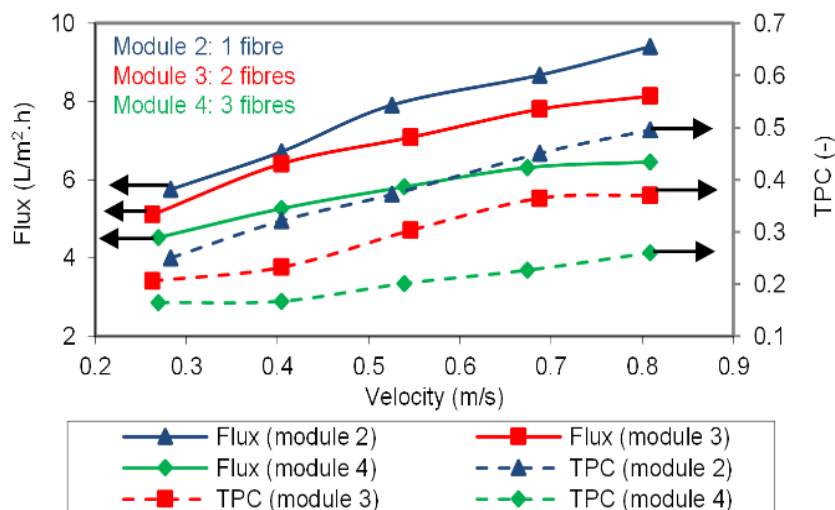
Fig. 5-2. Effects of hollow fibre packing density on flux and TPC (feed inlet temperature 70 ˚C)

The results in Fig. 5-2 show that both the flux and TPC increase with increasing feed velocity. For the TPC, because boundary layer can be reduced by the high flow velocity, the TPC was increased accordingly. The TPCs was in the range of 0.2 – 0.5, which was lower than that of DCMD [1]. Francis et al. [7] suggested that the uniformity of the temperature of MGMD is expected to decrease at permeate side for two main reasons: (1) no forced-convective heat transfer at permeate side as in DCMD configuration, and (2) no heat transfer via vapour mass transfer as in AGMD configuration. Similarly, the lower uniformity of the temperature in our PGMD study was mainly due to the nearly stagnant flow (Table 5-2) within the permeate gap compared to the higher coolant circulation velocity for DCMD. However, the existence of permeate gap can reduce the sensible heat loss compared to DCMD and decrease the mass transfer resistance compared to AGMD [6].

Zhang et al. [5] observed that the uniformity of the temperature at feed side has a greater impact on flux compared to that at the coolant side. Although the uniformity of the temperature within the permeate gap cannot be effectively improved, a higher velocity within the feed channel (0.26 – 0.81 m/s, Re<1531, still within laminar flow regime) can improve the uniformity of temperature at feed side and increase the flux. Higher velocity also resulted in a higher temperature difference between the membrane surfaces, which improved the flux subsequently.

Module 2 has 8 HDPE gap channels and each channel contains 1 hollow fibre. It had the highest flux, and was 15% and 46% higher than those of module 3 and module 4 with 2 and 3 fibres within each gap channel, respectively, at a feed velocity of 0.81 m/s. The flux of module 2 was 13% and 27% higher than those of module 3 and 4, respectively, if the feed velocity was reduced to 0.26 m/s. Module 2 also had a highest TPC of approximately 0.50, which indicated the highest uniformity of temperature. The TPC of module 2 was 35% and 42% higher than those of module 3 and module 4, respectively, at 0.81 m/s feed velocity.

The inner diameter of the HDPE gap channel and outer diameter of PVDF hollow fibre are 2.84 mm and 1.11 mm, respectively. Therefore, a maximum of 3 fibres could be inserted into each HDPE gap channel. For the module with more than 1 fibre within each gap channel, the surfaces of the hollow fibres could contact with each other, which will reduce the effective membrane surface area contacting with the permeate liquid and decrease the uniformity of temperature at permeate side. Furthermore, module with a higher hollow fibre packing density had a higher permeate productivity (see Table 5-3), it resulted in a greater temperature increase within the permeate gap

due to the same cooling plate surface area, which substantially reduced the driving force across the membrane. Consequently, compared to module 2 with single fibre in the gap channel, module 3 and 4 showed a lower flux.
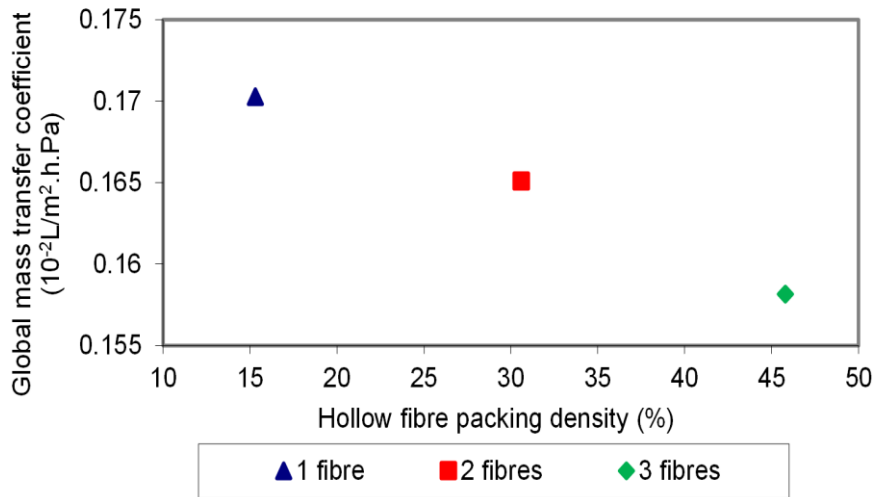
Fig. 5-3. Effects of hollow fibre packing density on C_{global} (feed inlet temperature 70 °C and feed velocity 0.81 m/s)

Moreover, different fibre packing density will create different hydrodynamic behaviours, and thus impacting the mass transfer of the PGMD module. Yang et al. [60] investigated the influence of hollow fibre packing density on MD performance and concluded that higher packing density may lead to uneven flow distribution around each fibre. Zheng et al. [91] used the random cell model to analyse the flow pattern for a hollow fibre membrane module. They found that mal-distribution appeared at the shell side of a randomly packed hollow fibre membrane module and it became more significant along with an increase in mean packing density.

The global mass transfer coefficients (Fig. 5-3) obtained from our study decreased with increasing hollow fibre packing density, indicating a higher mass transfer resistance within the boundary layer of the module with a higher fibre packing density. Yang et al. [60] identified the similar phenomenon that mass transfer coefficient decreased as a function of packing density, and they suggested that this is probably due to the local turbulence caused by the transverse flow for the loosely packed module where each fibre had a full contact with the two fluids [60]. Although the velocities within the permeate gaps of this study were very low, the better breakdown of the boundary layer and enhanced mixing on the membrane surface will improve the mass transfer, and subsequently, leading to a higher flux and TPC for the module with a lower hollow fibre packing density. It is worthwhile mentioning that a higher flux

normally leads to a lower TPC due to the higher thermal energy demand [4, 92], our results demonstrate that the optimized hydrodynamic condition of the module with a lower hollow fibre packing density had a greater impact on TPC.

Based on the above discussion, it can be concluded that the combined effects of reduced effective membrane surface, lower vapour pressure difference and deteriorated hydrodynamics were considered as the reasons for reduced flux and lower TPC for the module with a higher hollow fibre packing density.

Table 5-2 Flow velocities and Reynolds (*Re*) numbers for different modules (feed inlet temperature of 70 ˚C)

Module no.	1	2	3	4	5
	Velocity (m/s)				
Feed channel	0.81	0.81	0.81	0.81	0.81
Gap channel	0.0007	0.0006	0.0013	0.0020	0.0003
Coolant channel	0.0057	0.0080	0.0159	0.0239	0.0140
	Re (-)				
Feed channel	1471	1467	1517	1531	1444
Gap channel	2	2	3	3	2
Coolant channel	76	88	174	256	62

5.4.2. Effects of gap channel density on flux and TPC
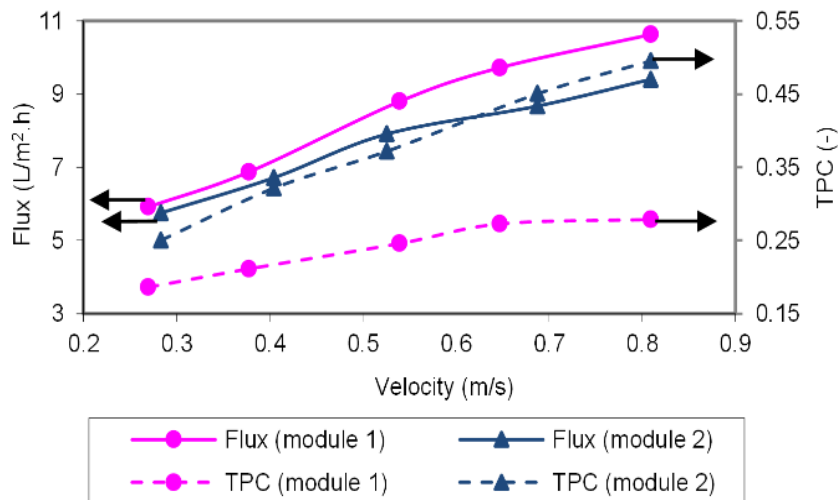
Fig. 5-4. Effects of gap channel density on flux and TPC (feed inlet temperature 70 ˚C)

The variations of flux and TPC as a function of feed velocity for modules with different gap channel densities are shown in Fig. 5-4 for a feed inlet temperature 70 ˚C.

Fig. 5-4 demonstrates that the fluxes of modules 1 and 2 with 6 and 8 gap channels, respectively, increased as a function of feed velocity, and the fluxes of module 2 were

2.9% and 11.6% lower than those of module 1 with 0.28 m/s and 0.81 m/s feed velocity, respectively. The TPCs of both modules also increased with the increasing feed velocity, and the TPCs of module 2 were approximately 77% and 34% higher than those of module 1 with 0.28 m/s and 0.81 m/s feed velocity, respectively.

Higher gap channel density resulted in a higher permeate productivity (see Table 5-3), and more latent heat was then released into the permeate gap. This led to a smaller temperature difference across the membrane for the module with higher gap channel density. Therefore, the flux of module 1 with 6 gap channels was higher than that of module 2 with 8 gap channels.

Table 5-3 Permeate productivity for different modules (feed inlet temperature of 70 ˚C)

Module no.		1	2	3	4	5
		Permeate productivity (L/h)				
Velocity (m/s)	0.28	0.045	0.058	0.103	0.137	0.064
	0.40	0.052	0.068	0.130	0.161	0.077
	0.53	0.067	0.080	0.144	0.177	0.090
	0.69	0.074	0.088	0.158	0.192	0.106
	0.81	0.081	0.096	0.165	0.197	0.114

In terms of TPC, as only 1 fibre was within each gap channel for both modules 1 and 2, the membrane had the full contact with permeate water and there was less flow mal-distribution. The hot feed velocities for modules 1 and 2 were similar, the flows within the gap channels of modules 1 and 2 were nearly stagnant, as a result, the difference of hydrodynamics between modules 1 and 2 was negligible. The higher flux of module 1 resulted in a greater heat transfer through liquid phase, increasing the temperature gradient in the boundary layer [93]. Consequently, the TPC of module 2 was higher than that of module 1.

5.4.3. Effects of cooling plate material on flux and TPC
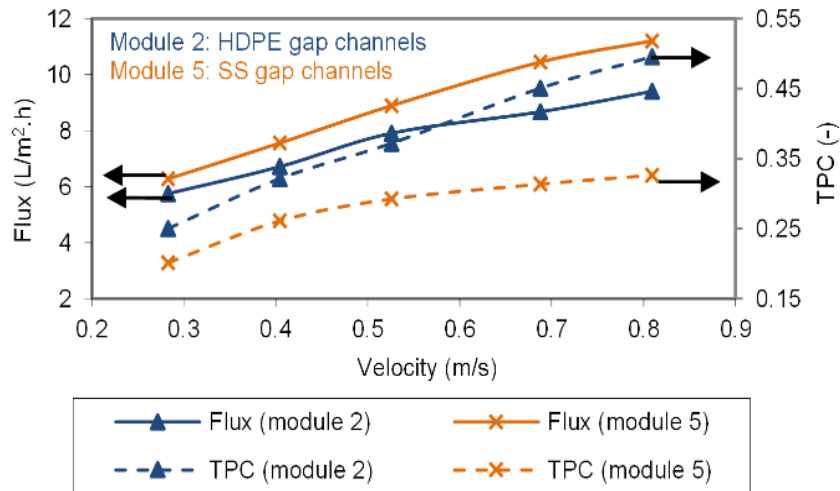
Fig. 5-5. Effects of cooling plate material on flux and TPC (feed inlet temperature 70 ˚C)

To evaluate the effects of cooling plate material on flux, module 5 with SS cooling plate was tested under the same operating conditions as module 2 with HDPE cooling plate.

Fig. 5-5 shows that modules 2 and 5 had the similar flux and TPC trends over the applied feed velocity, with the flux and TPC increasing as the feed velocity was increased.

The fluxes of module 2 were 8.4% and 16.1% lower than those of module 5 with 0.28 m/s and 0.81 m/s feed velocity, respectively. The TPCs of module 2 were approximately 34% and 20% higher than those of module 5 at 0.28 m/s and 0.81m/s feed velocity, respectively.

The thermal conductivity of SS cooling plate is considerably higher than that of HDPE cooling plate, which is considered as the main reason for the higher flux of module 5. The thermal conductivities for HDPE and SS are 0.38-0.51 W/m.K [94] and 15 W/m.K [95], respectively. The thicknesses for HDPE and SS cooling plates are 0.28 mm and 0.90 mm, respectively. Based on the thermal conductivities and thicknesses of HDPE and SS, the value of λ/b of SS cooling plate was approximately 10 times more than that of HDPE cooling plate (here, 0.45W/m.K is used for HDPE thermal conductivity as the average value of 0.38 W/m.K and 0.51 W/m.K [94]), which indicated that there was less thermal resistance in module 5 using SS as cooling plate material than that using HDPE. It resulted in a lower temperature within the gap channel and a higher temperature difference across the membrane, which subsequently led to a greater

vapour pressure difference between membrane surfaces. Our experimental results (see Table 5-4) confirmed that module 2 had a higher average temperature in the gap channel, but a lower average temperature in the coolant channel. Swaminathan et al. [16] used a slightly different method to improve the gap thermal conductivity by inserting highly conductive materials into PGMD gap, they also found that the flux of a module with a higher thermal conductivity gap was higher compared to traditional PGMD module. This was further confirmed by another study undertaken by Francis et al. [7]. They filled less thermally conductive material (sand) into the gap of a PGMD module, and found that the module exhibited a lower flux compared to that filled with a higher thermally conductive material (water).

Similarly, the higher flux of the module 5 led to a greater heat transfer through the liquid phase, which subsequently had increased the temperature gradient and decreased the TPC.

Table 5-4 Comparison of average temperatures of coolant and permeate channels between modules 2 (HDPE) and 5 (SS) with 70 ˚C feed inlet temperature

Feed velocity (m/s)	0.28	0.40	0.53	0.69	0.81	0.28	0.40	0.53	0.69	0.81
	Coolant channel average temperature (˚C)					Gap channel average temperature (˚C)				
Module 2	28.61	26.78	26.47	25.77	24.93	51.85	55.11	57.59	58.72	60.07
Module 5	28.95	27.82	27.48	26.69	25.96	48.65	52.29	54.44	54.95	55.36
Difference	-0.34	-1.04	-1.01	-0.92	-1.03	3.2	2.82	3.15	3.77	4.71

5.4.4. Effects of module design on energy performance

a) Effects of fibre packing density on STEC and GOR
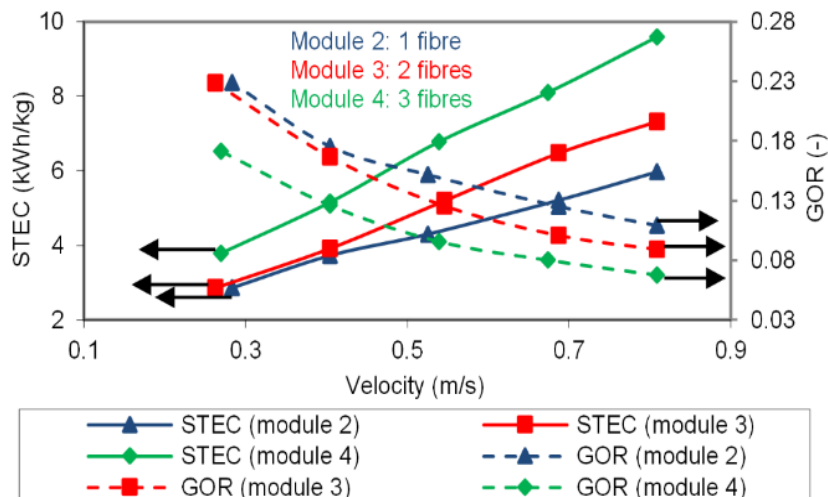
b) Effects of gap channel density on STEC and GOR
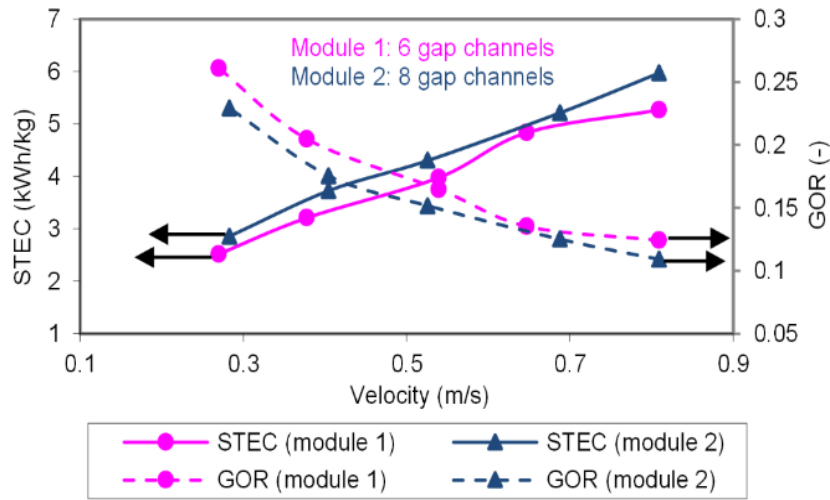
c) Effects of cooling plate material on STEC and GOR
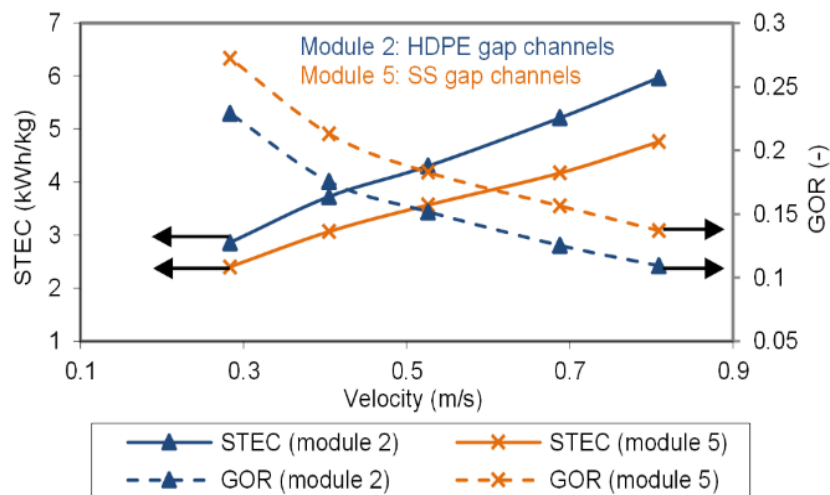
Fig. 5-6. Effects of PGMD module design on STEC and GOR (feed inlet temperature 70 ˚C)

Fig. 5-6 shows the effects of different module designs on energy performance, in terms of STEC and GOR. For all modules, STEC increased with the increase of feed velocity, and GOR decreased as a function of feed velocity.

When the feed velocity was higher, the internal heat recovery was less, and the coolant outlet temperature was lower. The higher feed velocity also resulted in a larger volume of coolant to be heated. Therefore, the external thermal power input increased when the feed velocity was higher. Although the increased feed velocity resulted in a higher flux, the external thermal power input grew more rapidly than the increase of flux. Winter et al. [18] investigated PGMD performance using a spiral wound module, and

they also found that STEC increased with increasing feed flowrate. They suggested that the improvement of heat transfer and the increase of energy input due to the higher feed flowrate are not adequate enough to increase the driving force accordingly. Consequently, the STEC increased with the increasing feed velocity, but GOR decreased with the increasing feed velocity.

Fig. 5-6a demonstrates that the modules with less fibre packing density showed a better energy efficiency (a lower STEC and a higher GOR). The outlet temperature of the coolant channel for the module with high fibre packing density was lower compared to that of the module with low fibre packing density. The reason is that the volumes of the brine feed and coolant for modules 3 and 4 were 2 and 3 times more, respectively, than that of module 2 under the same feed velocity. Therefore, due to the same cooling plate surface area and heat transfer loss, coolant was heated to lower temperatures for modules 3 and 4 compared to that for module 2. This resulted in a higher specific external thermal power inputs for modules 3 and 4. At the same time, the flux of module 2 was higher compared to those of module 3 and 4. Consequently, module 2 with a lower fibre packing density showed a better energy performance.

Fig. 5-6b shows that the module with lower gap channel density had a better energy performance. T_{Co} for module 2 was higher than that of module 1, consequently, the specific external thermal power input for module 2 was lower compared to that of module 1. However, the decrease of flux was more rapid than the decrease of external thermal power input when the number of gap channels increased from 6 to 8. Consequently, the module with less gap channels showed a better energy performance.

Fig. 5-6c shows that the STEC of module 2 with HDPE cooling plate were 19% and 25% higher than those of module 5 with SS cooling plate with feed velocities of 0.28 m/s and 0.81 m/s, respectively, and feed inlet temperature of 70 ˚C. Furthermore, the GORs of module 5 were 17% and 27% higher than those of module 2 with feed velocities of 0.28 m/s and 0.81 m/s, respectively, at feed inlet temperature of 70 ˚C.

A cooling plate with a higher thermal conductivity resulted in a lower temperature within the permeate gap and a higher temperature within the coolant channel, therefore, less external thermal power input was required to re-heat the brine coming out of the coolant channel. Additionally, the flux of module 5 was higher than that of module 2. Consequently, module 5 showed a better energy performance.

The above discussions show that more conductive cooling plate material can improve the energy efficiency of PGMD compared to the hollow fibre packing density and gap channel density.

Different studies [96, 97] suggested that the GOR of laboratory scale MD tests is usually lower than 1. The maximum GOR obtained from our study was 0.27 for module 5, which was relatively low compared to other MD studies [16, 17, 98-101]. This phenomenon is probably due to three main reasons: (1) membrane modules tested in this study had a small surface area, normally, larger membrane surface area will lead to a longer residence time of the feed, which will result in a better heat recovery, and subsequently, a higher GOR [13, 96]; (2) heat loss due to the two steps of heat transfer (heat transfer from feed channel to permeate channel, and from permeate channel to coolant channel); and (3) insufficient internal heat recovery due to the lower TPC (the TPCs of PGMD from this study were generally lower than that of DCMD) and less conduction surfaces of hollow fibre membrane and cooling plate. However, PGMD module performance cannot be purely evaluated by GOR. Various studies observed a compromise between GOR and flux as it is difficult to achieve a better GOR and a high flux simultaneously [90, 101]. With a low GOR, the flux obtained from this study is relatively high compared to other PGMD studies [6].

GOR obtained from [15] also showed a downward trend as a function of feed flowrate. Their GOR results were also comparable to that from the present study, decreasing from around 0.35 to 0.27 when feed flowrate increased from 600 mL/min to 900 mL/min, with 15 °C and 82 °C as the cold and hot inlet temperatures, respectively, and 30 g/L feed water salinity. In [15], it was suggested that the low GOR was due to the great heat loss rate for laboratory scale setup and poor internal heat recovery by the developed PGMD module with special geometry. Winter et al. [17] investigated the impacts of deaeration of the hot feed on their spiral wound PGMD module, and found that GOR decreased as a function of feed flowrate, regardless of deaeration. The GOR from [17] decreased from approximately 5.5 to 3.2 when feed flowrate increased 200 kg/h (3.33 L/min) to 500 kg/h (8.33 L/min) with 25 °C and 80 °C as the cold and hot inlet temperatures, respectively. The higher GOR from that study was probably due to two main reasons. Firstly, the longer membrane module (larger membrane surface) led to a better internal heat recovery, resulting in a higher coolant outlet temperature. Secondly, although the flux of that study was considerably lower, the distillation output was high due to the larger membrane surface area (5-10 m^2).

In this study, the membrane surface area was between 0.008 - 0.030 m^2. High packing density and large specific surface area are considered as the main advantages for hollow fibre membrane module, as they have a key role in total productivity and subsequently energy performance [70, 102]. Although the current study showed that module with lower hollow fibre packing density/gap channel density had a better energy performance under current experimental conditions, GOR could be improved for modules with high hollow fibre packing density/gap channel density. If a lower brine circulation flowrate is used for the module with much higher hollow fibre packing density/gap channel density, the flux will be lower, but the total heat energy input could be the same or less while the total produced permeate is higher due to the larger membrane surface, which could result in a better energy performance. This will be further discussed in Chapter 5.4.5. Swaminathan et al. [16] also investigated the impacts of gap thermal conductivity on GOR, they identified that the increase of the thermal conductivity can result in a considerably higher GOR, while the effect was negligible when the gap conductivity was higher than 10 W/m.K. With the more conductive cooling plate material, GOR of module 5 from our study achieved the highest GOR compared to other modules.

It is also worthwhile mentioning that due to the size of current PGMD modules, the energy consumption obtained from this study cannot be considered as representative for full scale hollow fibre PGMD module operation. The energy consumption data from this study was only indicative and used for comparisons between different modules. It will help to optimize the module design during the upscaling.

5.4.5 Considerations for PGMD module optimization

In this study, efforts have been made to optimize the hollow fibre PGMD performance, focusing on hydrodynamic conditions on channel densities (permeate gap and coolant channel) and the thermal conductivity of cooling plate.

The experiments showed that different gap channel density and hollow fibre packing density had minimum impacts on velocities within the permeate gap and coolant channel due to the significantly larger cross sectional areas of the permeate gap and coolant channel compared to the hot feed channel. Therefore, flows within the gap channel and coolant channel for different modules were all within the laminar flow regime, and the uniformity of the temperature was not effectively improved. This PGMD investigation was a laboratory scale study, but a full scale industrial module could have significantly higher hollow fibre packing density and gap channel density that could change the flow regimes accordingly, especially that in the coolant channel.

It is also worthwhile mentioning that although modules with the greater gap channel density or hollow fibre packing density in this study had higher STEC, they were more productive. Here, a new parameter S was defined to enable the comparison of energy performance among different modules when membrane surface area was taken into account:

S= STEC/membrane surface area (kWh/kg.m^2)   (5-5)

S could be used as an indicator to show the effective use of membrane surface area, with low S values indicative of more energy efficient use of the membrane surface area.
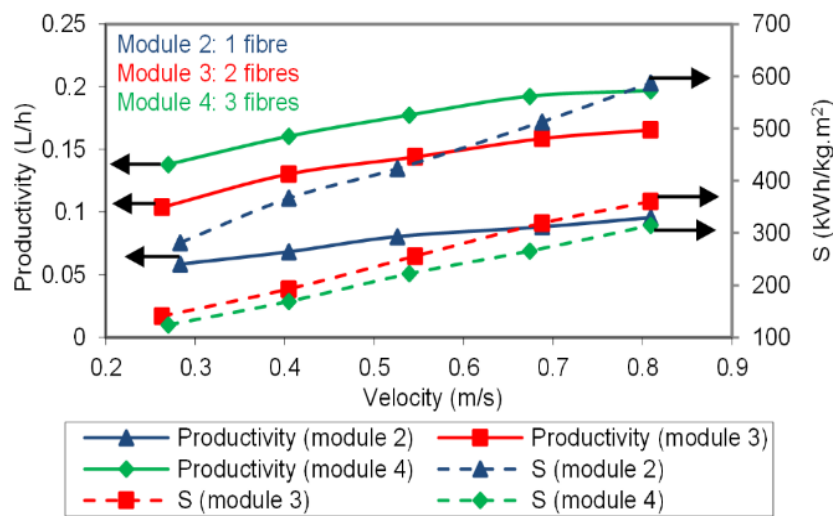
Fig. 5-7. Effect of membrane surface on module performance

Fig. 5-7 clearly shows that module with larger membrane surface area were more productive. It also had a lower S, which indicated a more energy efficient use of membrane surface area. The next step in module optimization and full scale design should take this factor into consideration.

With the current system design, only one pump is used to circulate brine through both the coolant and hot channels. Although this method can save one pump and enable internal energy recovery, the same volumetric flow rate for coolant channel and feed channel caused extremely low circulation velocity in the coolant channel, which led to a less uniformity of the temperature in the coolant channel. Our study showed that hollow fibre PGMD had a relatively high flux. It is expected that the flux will be further improved if the uniformity of the temperature can be improved in the coolant channel. Use of a separate pump to circulate the brine in the coolant channel with a higher velocity could effectively improve the uniformity of temperature accordingly. In order to recover heat energy from coolant outlet under a two pumps system, a second tank is

required for the coolant circulation. A third pump is also required to pump the extra water from coolant circulation tank back to the brine feed tank to keep the water balance, and this approach has no effect on the uniformity of temperature within the permeate gap.

Introduction of different turbulence promotors (such as baffles, spacers and modified hollow fibre geometries) could also improve the uniformity of temperature, especially within the permeate gaps. Teoh et al. [51] investigated the influences of baffles, spacers and modified hollow fibre geometries on the permeation flux of DCMD hollow fibre modules. The results showed that the flux of the module with baffles increased by 20% to 28% compared to module without baffles and using spacers among fibres may increase the effective membrane area 18-33%. Ali et al. [52] highlighted the impact of different hollow fibre membrane configurations and flow patterns on the MD performance, and they found that flux enhancements of 47% and 52% were obtained for modules with helical and wavy configurations compared to the conventional straight hollow fibre membrane. Although the above experiments were undertaken with significantly higher flow velocities for the membrane shell side compared to the permeate overflow velocity in this study, baffles, spacers or modified hollow fibre geometries can still be applied to prevent fibres from sticking together and create the additional surface for permeate production. Moreover, baffles and spacers could be considered for gap channel (HDPE/SS tubes), combined with a higher coolant circulation velocity, the uniformity of temperature could be significantly improved.

This study confirmed that cooling plate material with a higher thermal conductivity could improve PGMD performance, in terms of flux and energy efficiency. Cheaper and lighter but more conductive materials, such as aluminum alloy [103] or high thermal conductivity plastics [104, 105], could be also used as the cooling plate materials. In addition, a set of mathematical models will be developed in Chapter 6 to further investigate the effects of different cooling plate materials on PGMD performance.

Systems with GOR lower than 1 will not be considered by the industry, another approach to improve the energy performance (STEC/GOR) for this module is to further utilize the heat energy coming out of the hot feed channel. In this study, the feed brine was firstly pumped through coolant channel, then flowed through the feed channel before returning to the feed brine reservoir. The feed outlet temperature was in the range of 45 – 58 °C for module 5 (SS gap channel) with 70 °C feed inlet temperature

and 70 – 200 mL/min (0.28 – 0.81 m/s) feed flowrate. An external heat exchanger could be engaged to further recover the heat energy from feed outlet stream.

Heat recovery efficiency can be influenced by many factors [106], including flowrate, material, and number of stages, and it could be as high as 95%. To evaluate the effect of heat recovery on GOR, it was conservatively assumed that 80% of the thermal energy can be transferred from hot feed outlet to coolant outlet, which is subsequently used as the hot feed. Fig. 5-8 shows the improved GOR for module 5 with 8 SS gap channels and 70 ˚C feed inlet temperature.
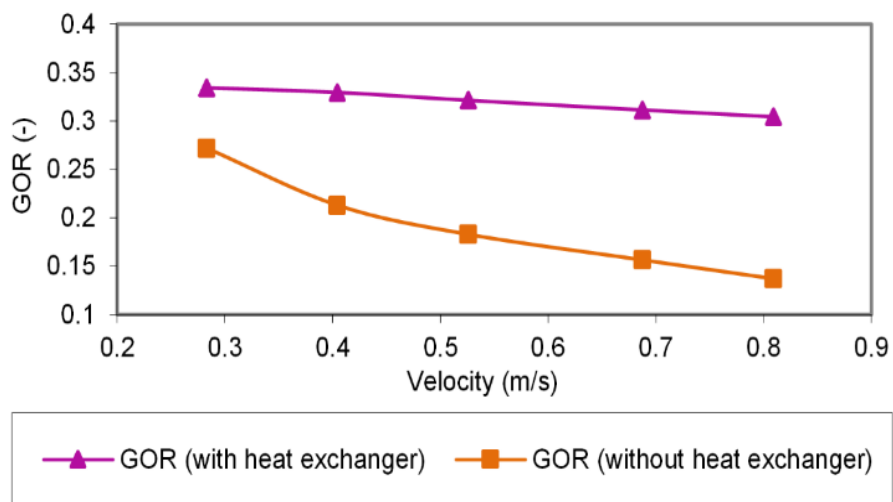
Fig. 5-8. Effect of external heat exchanger on GOR (feed inlet temperature 70 ˚C)

It can be seen from Fig. 5-8 that GOR increased significantly if an external heat exchanger is applied. GOR with external heat exchanger increased by 23% for 0.28 m/s feed velocity, while the GOR increased by 122% when feed velocity was increased to 0.81 m/s. The reason for this phenomenon is that high feed velocity led to a higher hot feed outlet temperature, resulting in a greater energy recovery. It should be pointed out that the results shown in Fig. 5-8 are only for a single pass heat recovery. To further increase the GOR, more passes of heat recovery are required.

One of the key advantages of PGMD configuration is the integration of heat recovery within the module [6]. As an initial study of hollow fibre PGMD, the lengths of the hot channel of the tested modules are all 0.425 m, which is considerably shorter than commercial hollow fibre modules (1.5-2.3 m) [107]. The longer hollow fibre module could result in a better latent heat recovery, leading to a better GOR. Although the flux will be decreased due to the lower vapour pressure difference across the membrane, the total produced distilled water could still be higher due to the larger membrane surface area.

Multi-stage process could also be considered to improve both flux and energy performance. The longer residence time (lower feed velocity) will increase the internal heat recovery, and consequently, less external thermal power input is required. On the contrary, the permeation flux decreases with the lower feed velocity due to the less uniformity of temperature and less vapour pressure difference. A multi-stage process could overcome this problem. Several hollow fibre PGMD modules could be connected in series (see Fig. 5-9), the coolant would be pumped from the brine reservoir to the coolant channel of the last module via a chiller, then gradually flows through the coolant channel of each module. After it exits the coolant channel of the first module (last module that the coolant passes through), it flows into the hot feed channel of the first module via a break tank and heater, then it gradually flows through all the modules and returns to the brine reservoir. The brine reservoir is interconnected with the feed break tank to keep the water balance. Based on this multi-stage design, greater internal heat recovery can be realized, which would decrease the external thermal power input and increase the GOR (lower the STEC). Zaragoza et al. [22] investigated the performances of different commercial MD prototypes with various configurations. Their module PT5 (flat sheet LGMD) manufactured by Keppel Seghers was designed to optimize the heat recovery by interconnecting modules in series. The study demonstrated that single module mode had the uppermost STEC of 1.1 kWh/L and the 3 module mode had the lowest STEC at approximately 0.5 kWh/L. Cipollina et al. [13] modelled the impacts of numbers of PGMD stages on GOR and their predictions showed that GOR can increase by almost 20 times from a laboratory-scale 1 stage unit to a 9 stages unit.
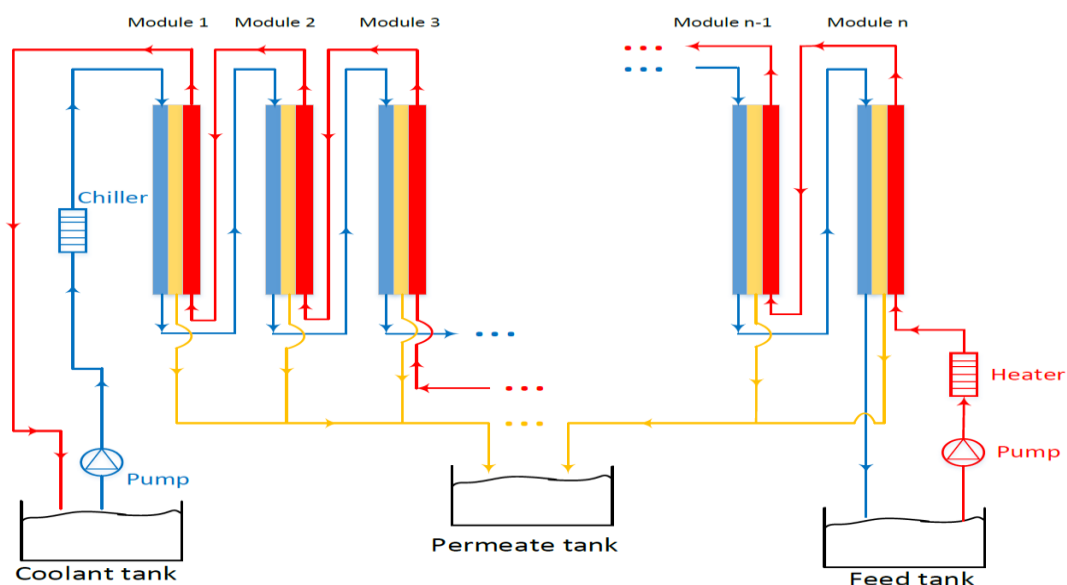
Fig. 5-9. Schematic diagram for multi-stage PGMD process

The structure of conventional hollow fibre module is more complex than that of flat sheet module. The hollow fibre failure could lead to the loss of system integrity, and increase of the repair costs and system down-time. The hollow fibre PGMD module has an additional permeate gap, which makes the module structure more complex. To ensure the successful application of hollow fibre PGMD module during the system scale-up, modular gap channel with pre-installed hollow fibres could be considered. The failed gap channel with broken fibres can be easily replaced by the pre-manufactured modular gap channel, which eliminates the replacement of the whole module and decreases the repair costs and system down-time.

5.5. Summary

In this chapter, five different hollow fibre PGMD modules were tested under the same operating condition to investigate the effects of different PGMD module designs on its performance. The module with lower hollow fibre packing density or gap channel density had a higher flux and better energy efficiency, while modules with higher hollow fibre packing density or gap channel density exhibited a more energy efficient use of membrane surface area and higher productivity. For the future scale up of hollow fibre PGMD installation, the higher hollow fibre packing density/gap channel density will be applied, efforts will be made to optimize the heat transfer from gap channel to coolant and improve the uniformity of temperature in gap and coolant channels.

Additionally, the module with a more conductive cooling plate had a higher flux and lower STEC, which was mainly attributed to the lower thermal resistance of the cooling plate. Due to the nearly stagnant velocities within the gap and coolant channels, the impact of cooling plate material on PGMD performance was greater than that of hollow fibre packing density and gap channel density.

The GOR obtained from this study was relatively low compared to other MD studies, which was mainly attributed to the small membrane surface area, high heat loss for two steps of heat transfer and insufficient internal heat recovery. However, the PGMD module performance cannot be assessed purely based on GOR. A trade-off exists between GOR and flux for MD modules, and the flux obtained from this study was relatively high.

Further improvements to this hollow fibre PGMD module could be achieved by approaches such as hydrodynamic improvements in the coolant channel, effective surface increase for hollow fibres and gap channels, heat recovery of hot feed outlet and multi-stage processes.

Chapter 6 Modelling the heat and mass transfers in PGMD using hollow fibre membrane

6.1. Introduction

As shown in Chapter 5, various PGMD modules were tested to investigate the impacts of different design parameters on the productivity and energy efficiency. Based on the results, it can be concluded that different module designs can influence PGMD performance significantly. In order to optimize PGMD module design more efficiently, a set of mathematical models have been developed to simulate the mass and heat transfers phenomenon in the PGMD process of this study.

The developed model was firstly validated by the experimental data. Afterwards, the validated model was employed to evaluate the impacts of important design parameters on module performance. The objective is to use this model for future scale up of hollow fibre PGMD installation.

The heat and mass flows for hollow fibre PGMD are shown diagrammatically in Fig. 6-1.
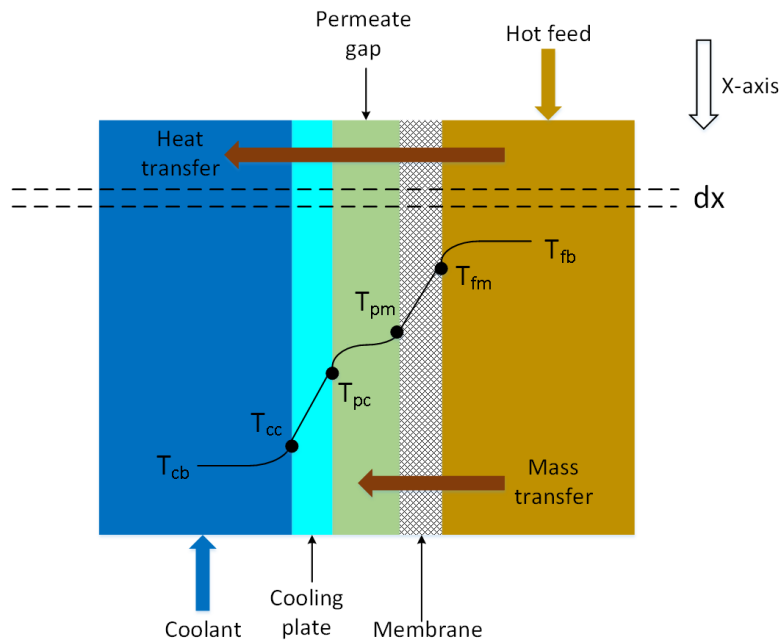
Fig. 6-1. Overview of heat and mass transfers for hollow fibre PGMD

In Fig. 6-1, dx represents a small distance along the membrane module; T_{fb}, T_{fm}, T_{pm}, T_{pc}, T_{cc}, and T_{cb} are the temperatures for bulk feed, membrane surface at feed side and permeate side, cooling plate surface at permeate side and coolant side, and bulk coolant, respectively.

6.2. PGMD process simulation

6.2.1. Theoretical analysis of mass and heat transfers of PGMD

In this study, it is assumed that the feed flows counter-current to the coolant stream.

The heat and mass transfers of PGMD process can be analyzed in each small segment dx along the module (see Fig. 6-2) based on the following 5 sub-processes.
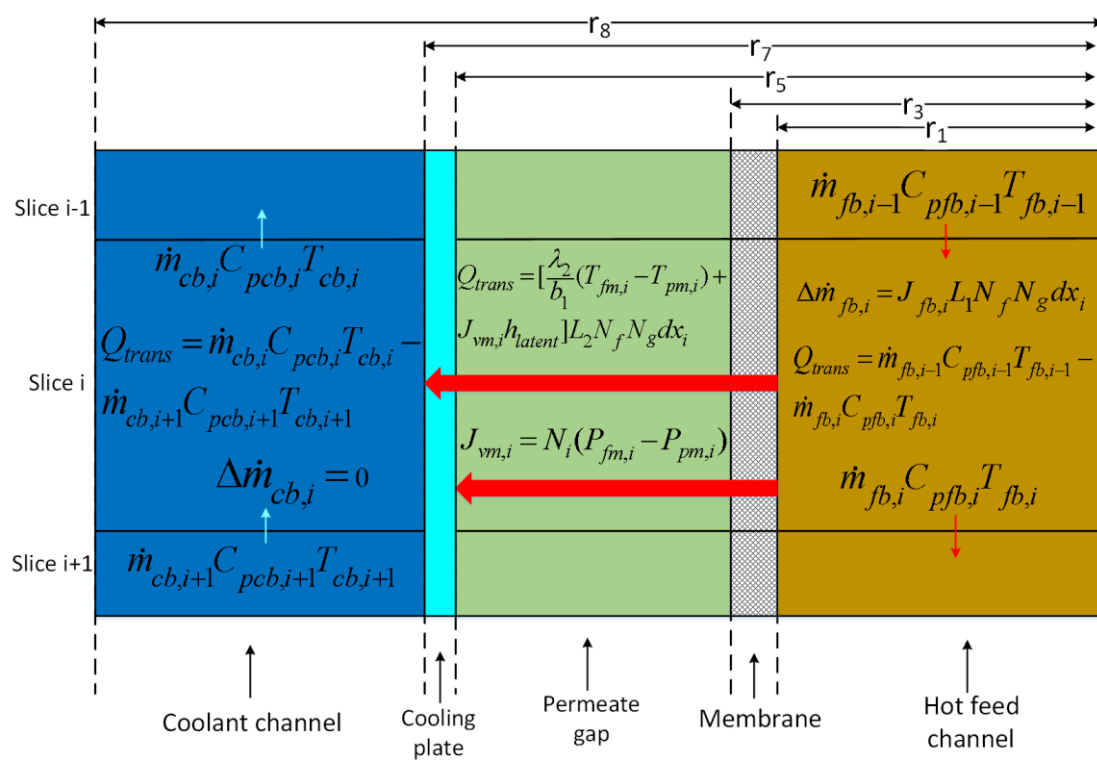
Fig. 6-2. Analysis of heat and mass transfers from slice $i\text{-}1$ to slice $i\text{+}1$ along PGMD module

6.2.1.1.   Mass and heat transfers in the hot feed channel

The mass transfer in the hot feed channel for slice i can be described by:

$$\Delta \dot{m}_{fb,i} = \dot{m}_{fb,i-1} - \dot{m}_{fb,i} = J_{fb,i} L_1 N_f N_g dx_i \tag{6-1}$$

The heat transfer of slice i for the hot feed channel is described below:

$$Q_1 = \dot{m}_{fb,i-1} C_{pfb,i-1} T_{fb,i-1} - \dot{m}_{fb,i} C_{pfb,i} T_{fb,i} \tag{6-2}$$

$$L_1 = 2\pi r_1 \tag{6-3}$$

Here, the subscript i represents the ith slice; $\Delta \dot{m}_{fb,i}$ represents the change of mass flow rate for the feed bulk flow; $J_{fb,i}$ is the vapour mass flux in the hot feed channel; $\dot{m}_{fb,i}$ and $\dot{m}_{fb,i-1}$ represent the mass flow rates of the bulk feed flow coming out and into the slice, respectively; Q_1 represents total heat transfer rate in the hot feed channel; L_1 is the circumference of hollow fibre membrane based on its inner diameter; $C_{pfb,i}$ and $C_{pfb,i-1}$ are the specific heat capacities of feed bulk flow coming out and into the slice, respectively; $T_{fb,i}$ and $T_{fb,i-1}$ are temperatures for feed bulk flow coming out and into the slice, respectively; N_f represents the number of hollow fibre within each gap channel; N_g represents the number of gap channel; dx_i represents the length of the slice i; and r_1 is the radius based on inner diameter of hollow fibre membrane.

The hot feed is vapourized at the interface between the membrane and feed brine, the heat transfer from hot bulk flow to the membrane surface on the hot feed side can be described by:

$$Q_2 = \alpha_{f,i}(T_{fb,i} - T_{fm,i})L_1 N_f N_g dx_i \tag{6-4}$$

Here Q_2 represents total heat transfer from the bulk hot flow to the membrane surface; $T_{fm,i}$ represents the membrane interface temperature on the feed side; and $\alpha_{f,i}$ is the heat transfer coefficient at the hot feed side, which can be calculated by [63]:

$$\alpha_{f,i} = \frac{Nu_f \lambda_1}{d_{hf}} \tag{6-5}$$

Here λ_1 is the thermal conductivity of the feed brine; d_{hf} is the hydraulic diameter for the hot channel, which can be determined by:

$$d_{hf} = \frac{4A_1}{L_1} = 2r_1 \tag{6-6}$$

Here, A_1 is the cross sectional area for the hot channel based on its inner diameter. Nu_f is the Nusselt's number of the hot feed. Previous experimental results [6] suggested that the water within the feed channel, permeate gap and coolant channel all had laminar flow regimes. Consequently, Nu_f under fully developed flow and uniform heat flux condition can be calculated by [65, 66]:

$$Nu_f = 4.36 + \frac{0.036(\mathrm{Re}\,\mathrm{Pr}\,d_{hf}/l)}{1 + 0.0011(\mathrm{Re}\,\mathrm{Pr}\,d_{hf}/l)^{0.8}} \tag{6-7}$$

where l is the module length; Re and Pr represent Reynolds number and Prandtl number, which can be calculated by:

$$\mathrm{Re} = \frac{\rho d_h v}{\mu} \tag{6-8}$$

$$\mathrm{Pr} = \frac{C_p \mu}{\lambda} \tag{6-9}$$

Here, ρ, d_h, v, μ, C_p, and λ are density, hydraulic diameter, velocity, viscosity, specific heat capacity, and thermal conductivity of water, respectively. The thermodynamic properties and viscosities are allowed to vary with temperature which changes along the module length, Re and Pr are respectively calculated for hot and coolant channels using Eqs. (6-8) and (6-9).

6.2.1.2   Mass and heat transfers through the hollow fibre membrane

The mass transfer of the slice i through the hollow fibre membrane can be expressed by:

$$J_{vm,i}L_3 N_f N_g dx_i = N_i (P_{fm,i} - P_{pm,i})L_3 N_f N_g dx_i \tag{6-10}$$

Here, $J_{vm,i}$ is the water vapour mass flux through the membrane, which is slightly different from $J_{fb,i}$ due to difference between L_1 and L_3; N_i is the mass transfer coefficient for hollow fibre membrane; $P_{fm,i}$ and $P_{pm,i}$ are vapour pressures at the membrane interfaces corresponding to temperatures at the hot feed side ($T_{fm,i}$) and permeate side ($T_{pm,i}$), respectively; and L_3 is the outer circumference based on the outer (r_3) radius of the hollow fibre membrane:

$$L_2 = 2\pi r_3 \tag{6-11}$$

As mentioned in Chapter 2, there is no total pressure difference within the membrane pores, the effect of Poiseuille flow can be neglected for PGMD, the mass transfer phenomenon within the membrane pores is controlled by Knudsen-molecular diffusion transition mechanism [17]. As a result, N_i can be calculated by [63]:

$$N_i = (\frac{1-\chi_A}{M}\frac{\tau b_1 RT}{\varepsilon D_{AB}} + \frac{3}{4}\frac{\tau b_1}{d\varepsilon}\sqrt{\frac{2\pi RT}{M}})^{-1} \tag{6-12}$$

Here M is the molecular mass of the water vapour; χ_A is the mole fraction of the water vapour; ε is the membrane porosity; D_{AB} is the diffusivity of the water vapour (A) relative to air (B); τ is the average tortuosity of the pores; b_1 is the thickness of the membrane; d is the mean pore diameter of the membrane; R is the universal gas constant; T is the mean temperature in the pores.

D_{AB} can be determined from [61, 66]:

$$D_{AB} = \frac{1.895 * 10^{-5} T^{2.072}}{P}$$ (6-13)

Here, P is the total pressure, and

χ_A can be determined by [63]:

$$\chi_A = \frac{P_v}{P}$$ (6-14)

Here P_v represents the water vapour partial pressure.

The membrane tortuosity τ can be estimated by [1] :

$$\tau = \frac{(2\text{-}\varepsilon)^2}{\varepsilon}$$ (6-15)

With the combination of Eqs. (6-10) and (6-12), the flux $J_{vm,i}$ can be written as:

$$J_{vm,i} = (\frac{1 - \chi_A}{M} \frac{\tau b_1 RT}{\varepsilon D_{AB}} + \frac{3}{4} \frac{\tau b_1}{d\varepsilon} \sqrt{\frac{2\pi RT}{M}})^{-1}(P_{fm,i} - P_{pm,i})$$ (6-16)

Therefore, N_i can also be expressed by:

$$N_i = 7.58 * 10^{-5} \frac{d\varepsilon}{\tau b_1} \frac{MT^{1.072}}{4Rd(P - Pv) + 5.685 * 10^{-5} T^{1.072} \sqrt{2\pi MRT}}$$ (6-17)

The heat transfer of the slice i through the hollow fibre membrane can be divided into sensible heat transfer via heat conduction and latent heat transfer, which is described by:

$$Q_3 = [\frac{\lambda_2}{b_1}(T_{fm,i} - T_{pm,i}) + J_{vm,i} h_{latent}]L_3 N_f N_g dx_i$$ (6-18)

Combing Eqs. (6-11) and (6-18) gives:

$$Q_3 = [\frac{2\pi\lambda_2}{\ln(r_3 / r_1)}(T_{fm,i} - T_{pm,i}) + J_{vm,i} h_{latent} 2\pi r_3]N_f N_g dx_i$$ (6-19)

Here Q_3 represents the total heat transfer through the hollow fibre membrane of slice i; h_{latent} is the latent heat of vaporization; λ_2 represents the average hollow fibre thermal conductivity, which can be calculated by:

$$\lambda_2 = \varepsilon \lambda_{air} + (1-\varepsilon)\lambda_m \tag{6-20}$$

Here λ_{air} and λ_m are thermal conductivities for air and the membrane material, respectively.

6.2.1.3 Mass and heat transfers within the permeate gap

The water vapour is distilled into permeate at the interface of permeate and membrane, the mass transfer of slice i can be described by:

$$\Delta \dot{m}_{fb,i} = \dot{m}_{pg,i} - \dot{m}_{pg,i+1} = J_{pg,i} L_3 N_f N_g dx_i \tag{6-21}$$

Here $J_{pg,i}$ is defined as the water vapour flux for slice i in permeate gap; and $\dot{m}_{pg,i+1}$ and $\dot{m}_{pg,i}$ represent the mass flow rates of the permeate coming in and out the slice i, respectively, because the permeate flows in opposite direction to that of the feed.

For the heat transfer within the permeate gap, it was identified that the permeate within the gap channel was nearly stagnant, therefore, the convective heat can be neglected, and the heat transfer was mainly caused by conduction, which can be determined by:

$$Q_4 = \frac{2\pi\lambda_3}{\ln(r_5/r_3)}(T_{pm,i} - T_{pc,i})N_f N_g dx_i \tag{6-22}$$

Here Q_4 represents the heat transfer rate within the permeate gap of slice i; λ_3 represents the permeate thermal conductivity; $T_{pc,i}$ is the cooling plate surface temperature at the gap channel side of slice i ; and r_5 represents the inner radius of the cooling plate.

6.2.1.4 Heat transfer through the cooling plate

The heat transfer through the cooling plate of slice i can be described by:

$$Q_5 = \frac{2\pi\lambda_4}{\ln(r_7 / r_5)}(T_{pc,i} - T_{cc,i})N_g dx_i \tag{6-23}$$

Here, Q_5 represents total heat transfer through the cooling plate of slice i; λ_4 represents the cooling plate thermal conductivity; $T_{cc,i}$ is the cooling plate surface temperature at the coolant channel side of slice i ; and r_7 represents the outer radius of the cooling plate.

6.2.1.5   Heat transfer within the coolant channel

The heat transfer from the interface between the cooling plate and the coolant to the coolant bulk flow of slice i can be described by:

$$Q_6 = \alpha_{c,i}(T_{cc,i} - T_{cb,i})L_7 N_g dx_i \tag{6-24}$$

Here, Q_6 represents the total heat transfer from the interface between cooling plate and coolant to the coolant bulk flow of slice i; $T_{cb,i}$ is the temperature for the bulk coolant flow of slice i; and $\alpha_{c,i}$ is the heat transfer coefficient on the coolant side, which can be calculated similarly as $\alpha_{f,i}$; and L_7 is the circumference of the cooling plate based on its outer radius (r_7).

The heat transfer of slice i for the coolant bulk flow can be calculated as:

$$Q_7 = \dot{m}_{cb,i}C_{pcb,i}T_{cb,i} - \dot{m}_{cb,i+1}C_{pcb,i+1}T_{cb,i+1} \tag{6-25}$$

Here, Q_7 represents total heat transfer for the coolant bulk flow of slice i; $\dot{m}_{cb,i}$ and $\dot{m}_{cb,i+1}$ represent the mass flow rate of coolant bulk flow coming out and into the slice i, respectively; $C_{pcb,i}$ and $C_{pcb,i+1}$ are defined as the specific heat capacities of coolant bulk flow coming out and into the slice i, respectively; and $T_{cb,i}$ and $T_{cb,i+1}$ are temperatures for coolant bulk flow coming out and into the slice i, respectively.

6.2.2. Numerical solutions

The following assumptions have been made to simulate the heat and mass transfers of hollow fibre PGMD module:

- no heat loss to the surrounding atmosphere via the module shell;
- no heat loss due to the permeate production from the system;
- no changes in membrane thickness, tortuosity and porosity; and
- the heat transfer within the permeate gap is caused by conduction and latent heat transfer.

As it is assumed that there is no heat loss to the surrounding atmosphere or due to the permeate production, it can be concluded that:

$$Q_1 = Q_2 = Q_3 = Q_4 = Q_5 = Q_6 = Q_7 = Q_{trans} \tag{6-26}$$

Here, Q_{trans} represents the total heat transfer of slice i.

From Eqs. (6-4), (6-18), (6-22), (6-23) and (6-24), the following equations can be obtained:

$$\frac{Q_2}{\alpha_{f,i} L_1 N_f N_g dx_i} = T_{fb,i} - T_{fm,i} \tag{6-27}$$

$$\frac{\dfrac{Q_3}{L_3 N_f N_g dx_i} - J_{vm,i} h_{latent}}{\dfrac{\lambda_2}{b_1}} = T_{fm,i} - T_{pm,i} \tag{6-28}$$

$$\frac{Q_4}{\dfrac{2\pi\lambda_3}{\ln(r_5 / r_3)} N_f N_g dx_i} = T_{pm,i} - T_{pc,i} \tag{6-29}$$

$$\frac{Q_5}{\dfrac{2\pi\lambda_4}{\ln(r_7 / r_5)} N_g dx_i} = T_{pc,i} - T_{cc,i} \tag{6-30}$$

$$\frac{Q_6}{\alpha_{c,i} L_7 N_g dx_i} = T_{cc,i} - T_{cb,i} \tag{6-31}$$

Combing Eqs. (6-27) – (6-31) gives:

$$Q_{trans} = U(T_{fb,i} - T_{cb,i} + J_{vm,i} h_{latent} \frac{b_1}{\lambda_2}) \tag{6-32}$$

Here, U can be determined by:

$$U = (\frac{1}{\alpha_{f,i}L_1N_fN_g dx_i} + \frac{1}{L_3N_fN_g dx_i}\frac{b_1}{\lambda_2} + \frac{1}{\frac{2\pi\lambda_3}{\ln(r_5/r_3)}N_fN_g dx_i}$$
$$+ \frac{1}{\frac{2\pi\lambda_4}{\ln(r_7/r_5)}N_g dx_i} + \frac{1}{\alpha_{c,i}L_7N_g dx_i})^{-1}$$

(6-33)

Considering a vertical module, the hot feed is assumed to flow into the module from the top, and the coolant flows counter-currently from the bottom of the module. Thus, the input conditions, the feed and coolant inlet temperatures, are at different x-positions. In order to solve the differential equations for the mass and heat transfers, a matching scheme from the feed inlet x=0 requires a value for the coolant exit temperature, which is an unknown to begin with. To start the numerical solution, an initial guess of $T_{cb,1}$ is made, which is in general taken as the average temperature of the hot feed and coolant inlet temperatures. Based on this assumption, the solution can be marched till the exit of the feed at $x_n= l$ and an estimated coolant inlet temperature can be obtained. This estimated value is compared with the actual coolant inlet temperature which is an input boundary condition, and if the difference between the estimated coolant inlet temperature and the actual coolant inlet temperature is more than 0.00001 ˚C, the solution process is repeated with a new guess on the coolant exit temperature at x=0 until convergence. A flowchart of the numerical solution process is shown in Fig. 6-3.
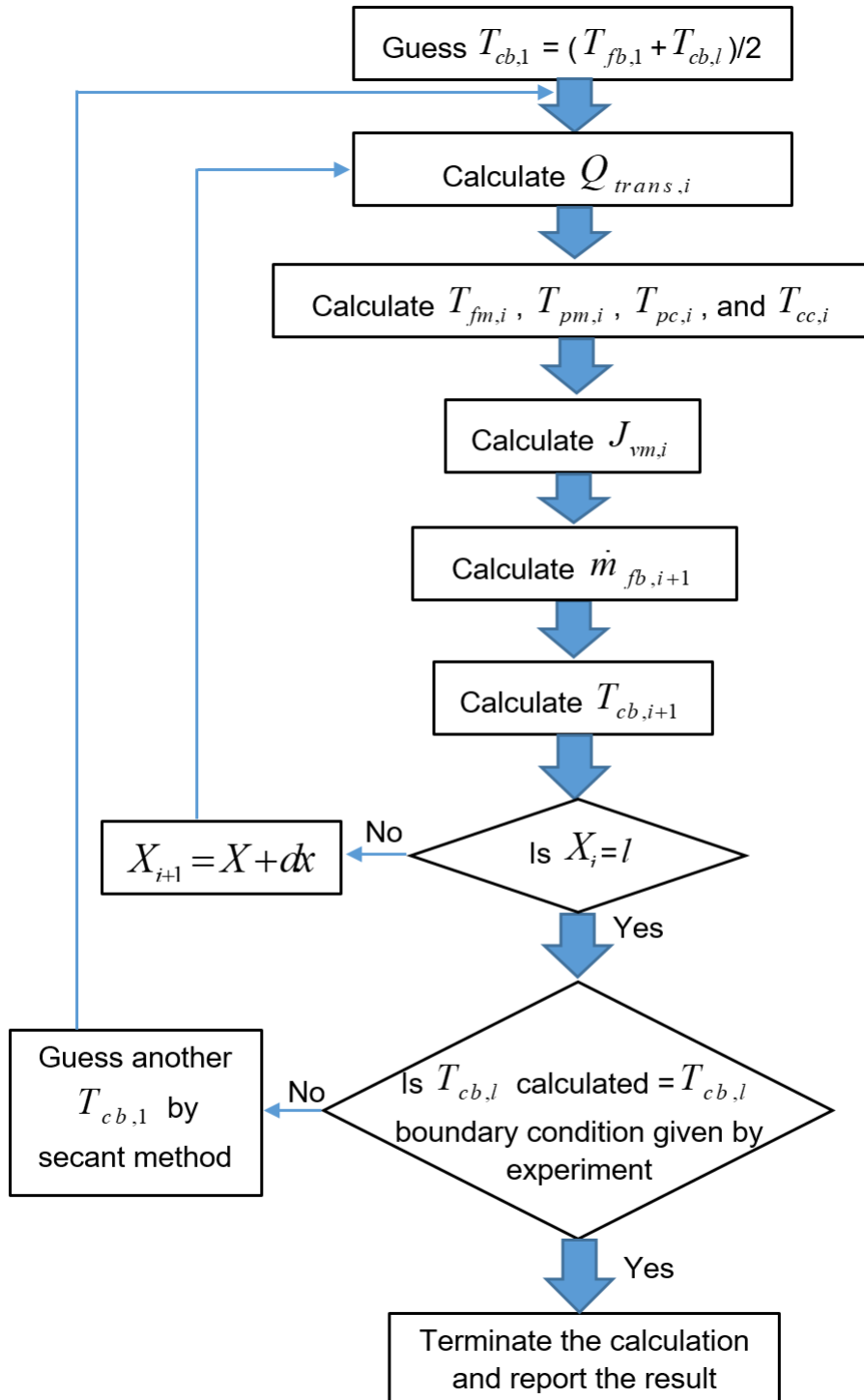
Fig. 6-3. Simulation procedure for hollow fibre PGMD model

6.3. Material and experiments

The detailed membrane characteristics, different module properties and PGMD experimental operating conditions have been reported in previous chapters. Here, Tables 6-1, 6-2 and 6-3 show module properties, gap channel characteristics and testing conditions briefly.

It is worthwhile mentioning that the coolant length 0.35m is used as the effective membrane length for the model simulation. As shown in Fig. 5-1e, there is length difference between hot channel and coolant channel (length difference 0.0375 m), and coolant channel is shorter than hot channel. The water vapour mass transfer in PGMD module is due to the temperature difference established by the hot and coolant channels. As a result, the length of coolant channel is used here to accurately simulate the heat transfer phenomenon.

Table 6-1 Properties of manufactured hollow fibre membrane modules

Module number	Material of cooling plate	Number of gap channels	Percentage of PE pipe filled by gap channels (%)	Number of hollow fibres within each channel	Percentage of single gap channel filled by hollow fibres (%)	Module length (m)
1	HDPE	8	14.8	1	15.3	0.35
2	HDPE	8	14.8	2	30.6	0.35
3	HDPE	8	14.8	3	45.8	0.35
4	Stainless Steel (SS)	8	51.6	1	6.0	0.35

Table 6-2 Properties of gap channels

	Inner diameter (mm)	Outer diameter (mm)	Thickness b_2 (mm)	Conductivity λ_4 (W/m.K)
HDPE gap channel	2.84	3.40	0.28	0.445 [108]
SS gap channel	4.55	6.35	0.90	15 [108]

Table 6-3 PGMD testing conditions

	Inlet temperature (˚C)	Volumetric flow rate (mL/min)	Brine concentration (g/L NaCl)
Hot channel	40, 50, 60, 70	70-500 (0.28-0.69 m/s)	10
Coolant channel	20	70-500 (0.003-0.020 m/s)	10

6.4. Results and discussion

6.4.1. Model validation with experimental data

To validate the developed model, the simulated results are compared with the experimental data.

Experimental results of module 1 (8 HDPE gap channels and 1 hollow fibre within each gap channel) are used to validate the effects of feed velocity and feed inlet temperature.

Fig. 6-4 shows that experimental data of module 1 obtained at 70 ˚C hot inlet temperature with different velocities are very close to the simulated results obtained from the model, and Table 6-4 demonstrates that the errors between the experimental outcomes and modelled results are in the range of ± 5%, which are smaller than the typical experimental error of ± 10%. The model predicts an asymptotic flux trend as the feed velocity increases. This phenomenon has been identified by many other studies [8, 20, 74], which is due to the uniformity of the temperature across the feed channel being unable to be further improved for a fully-developed flow condition.
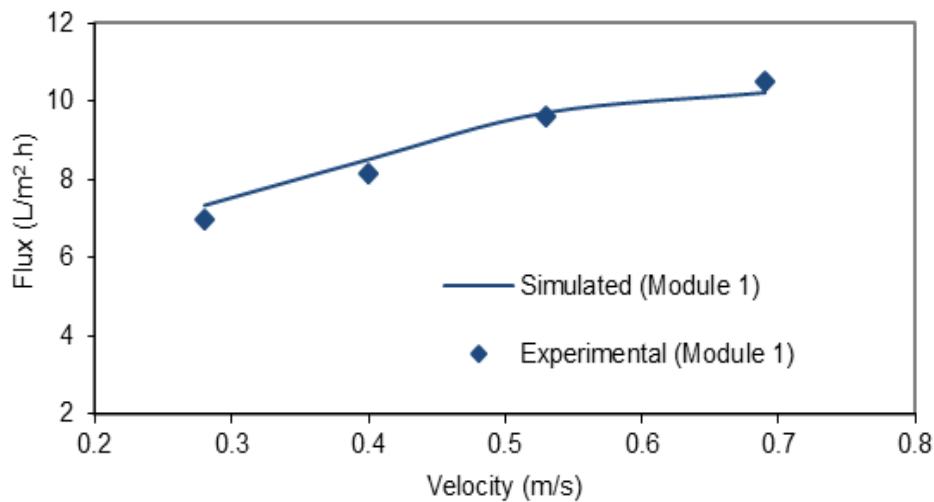
Fig. 6-4. Simulated and measured results with different feed velocities (70 ˚C hot inlet temperature)

Table 6-4 Relative errors between predicted and experimental results (70 ˚C hot inlet temperature)

Hot feed velocity (m/s)	0.28	0.40	0.53	0.69
Error (%)	-5.04	-4.46	-1.18	2.89

Fig. 6-5 demonstrates that the difference between the modelled results and experimental results of module 1 obtained at different feed inlet temperatures but a fixed feed velocity of 0.69 m/s. The comparison (Table 6-5) shows that, again, the model predictions agree with the experimental results to within $\pm 10\%$ for the given experimental conditions. The model also successfully predicts a more significant flux increase with higher feed inlet temperature, which is due to the exponential relationship between feed inlet temperature and vapour pressure [76, 109].
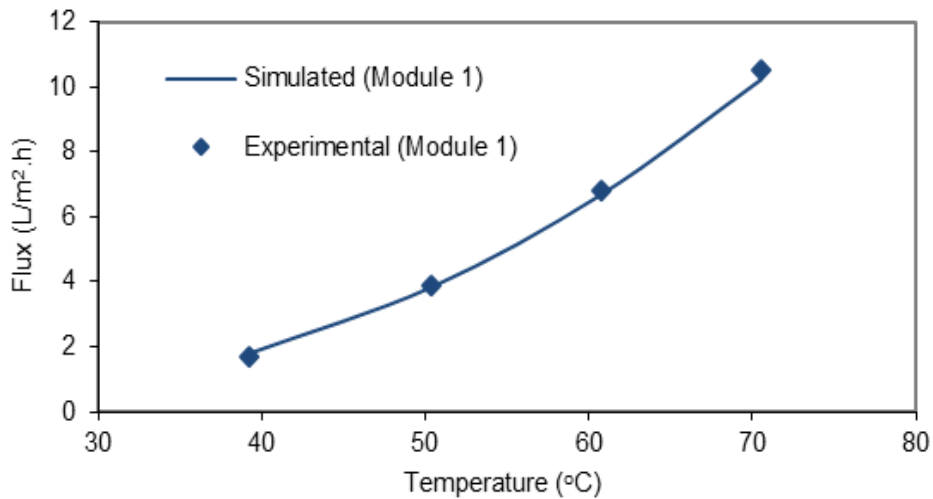
Fig. 6-5. Simulated and measured results with different feed inlet temperatures (0.69 m/s feed velocity)

Table 6-5 Relative errors between predicted and experimental results (0.69 m/s feed velocity)

Feed inlet temperature (˚C)	40	50	60	70
Error (%)	-6.93	1.58	2.25	2.89

Both Figs. 6-4 and 6-5 also show that the relative errors systematically increase from less than zero to larger than zero as the flux increases when feed velocity and feed temperature become greater. This phenomenon could be attributed to the assumption of 'no heat loss due to the permeate production from the system'. Increased flux in the experiment will result in more heat loss in the permeate gap and lower the temperature in the permeate gap. Therefore, the actual temperature in the permeate gap will be lower than the modelled temperature. Since the predicted flux is based on the temperature difference between the feed and permeate gaps, the lower predicted temperature difference would lead to a lower flux than that of the experiment.
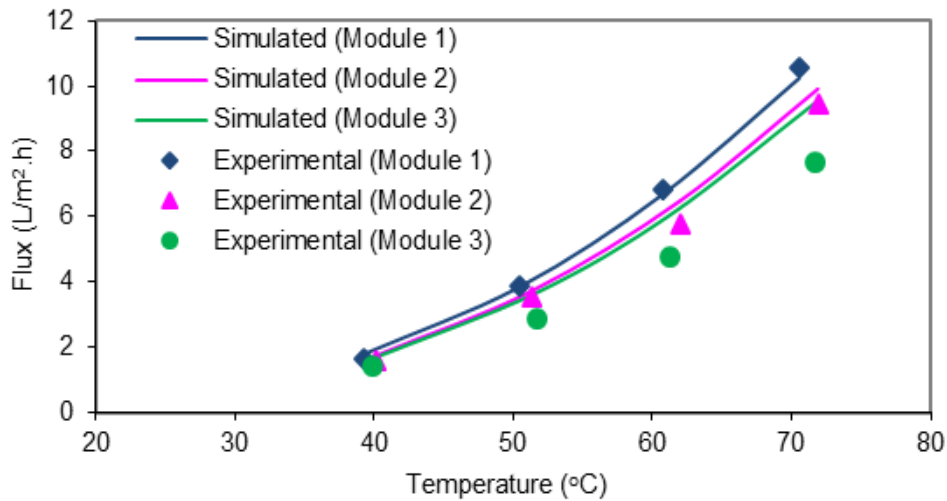
Fig. 6-6. Simulated and measured results with different hollow fibre packing densities (0.69 m/s feed velocity)

Table 6-6 Relative errors between predicted and experimental results (0.69 m/s feed velocity)

Feed inlet temperature (°C)		40	50	60	70
	Module 1	-6.93	1.58	2.25	2.89
Error (%)	Module 2	-9.22	-4.84	-10.46	-4.61
	Module 3	-15.87	-28.93	-26.55	-23.55

Experimental and simulated results of modules 1, 2 and 3 with different feed inlet temperatures are shown in Fig. 6-6. Similar to module 1, both module 2 and module 3 have 8 gap channels. For modules 2 and 3, 2 and 3 hollow fibres are contained within each gap channel, respectively. The modelled results show that the flux decreases with the increasing hollow fibre packing density, which is confirmed by the experimental results. As mentioned in Chapter 5, this phenomenon can be explained by three main reasons [108]. Firstly, module with a higher hollow fibre density has a higher permeate productivity, which results in greater temperature increase in the gap channel and reduced vapour pressure difference between membrane surfaces. In addition, with a higher hollow fibre packing density, hollow fibres contact with each other which leads to a less effective membrane surface area for permeate production than lower hollow fibre packing density. Furthermore, the module with a lower hollow fibre packing density has less dead mixing zone due to the presence of transverse flow in a loosely packed module where each fibre has full contact with fluids [60].

Table 6-6 also shows that the differences between simulated and experimental results for modules 1 and 2 are within approximately ± 10%, while the differences for module 3 are much larger (-20% to -30%). This phenomenon is consistent with our previous assumptions that hollow fibres may have contacted with each other and reduced the effective membrane surface area and create dead mixing zones. The model predicts the flux under optimal conditions where each hollow fibre has full contact with both feed and permeate. The inner and outer diameters of the HDPE gap channel and hollow fibre are 2.84 mm and 1.11 mm, respectively. Without any baffles and spacers within the permeate gap, the hollow fibres will inevitably be in contact with each other during the tests. As a result, the predicted flux values for modules with higher hollow fibre density are always higher than the experimental results, and the error of the prediction becomes greater when hollow fibre density is higher as contact between fibres becomes more likely.
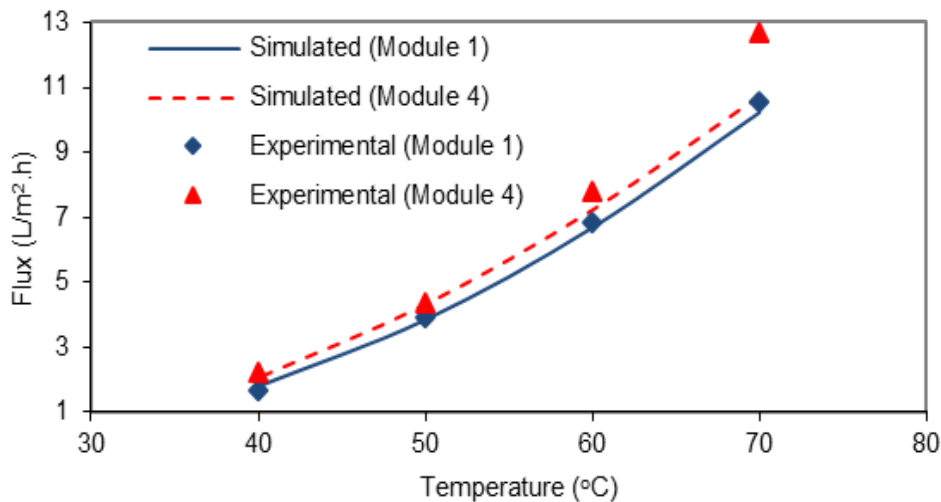
Fig. 6-7. Simulated and measured results with different cooling plate materials (0.69 m/s feed velocity)

Table 6-7 Relative errors between predicted and experimental results (0.69 m/s feed velocity)

Feed inlet temperature (°C)		40	50	60	70
Error (%)	Module 1	-6.93	1.58	2.25	2.89
	Module 4	5.49	1.25	7.42	15.24

The simulated and experimental results of modules 1 and 4 with different cooling plate materials are presented in Fig. 6-7. The model predicts that the module with a SS cooling plate has a higher flux compared to module with a HDPE cooling plate, which

is similar to the experimental results. As discussed in Chapter 5 [108], the sensible heat transfer is proportional to the $\dfrac{\lambda_4}{b_2}$, the value of $\dfrac{\lambda_4}{b_2}$ of SS cooling plate is significantly higher than that of HDPE cooling plate, indicating lower thermal resistance for module 4. This will subsequently lead to a greater vapour pressure difference across the membrane and higher flux of module 4. The difference between simulated and experimental results are all within ±10%, except for one result of module 4 at 70 ˚C hot inlet temperature (15%). Aforementioned, this high error was probably due to the combination of experimental error and higher heat loss caused by the increased flux (higher permeate production).

In addition to the thermal conductivity and thickness, the SS gap channel has different inner and outer diameters compared to HDPE gap channel, which will change the hydrodynamics within the coolant channel and permeate gap. To understand the effects of different design parameters (inner/outer diameters and conductivity of gap channel) on flux, a sensitivity study using the developed mathematical model for the heat and mass transfers in the PGMD module was undertaken, which is further discussed in Chapter 6.4.2.4.

6.4.2. Effects of design parameters and operating conditions

The validation and discussion shown in Chapter 6.4.1 demonstrated that the developed model can successfully simulate the mass and heat transfers within hollow fibre PGMD module. The model is now utilized to analyze the effects of other important module design parameters and operating conditions. The outcome will help to optimize hollow fibre PGMD process.

To facilitate the comparison and discussion, the simulated results obtained from a base case (case 1) is utilized to benchmark the performance of other designs or operating conditions. Module 1 operated at 70 ˚C hot inlet temperature and 0.69 m/s feed velocity is used as the base case (case 1).

6.4.2.1. Effect of coolant velocity
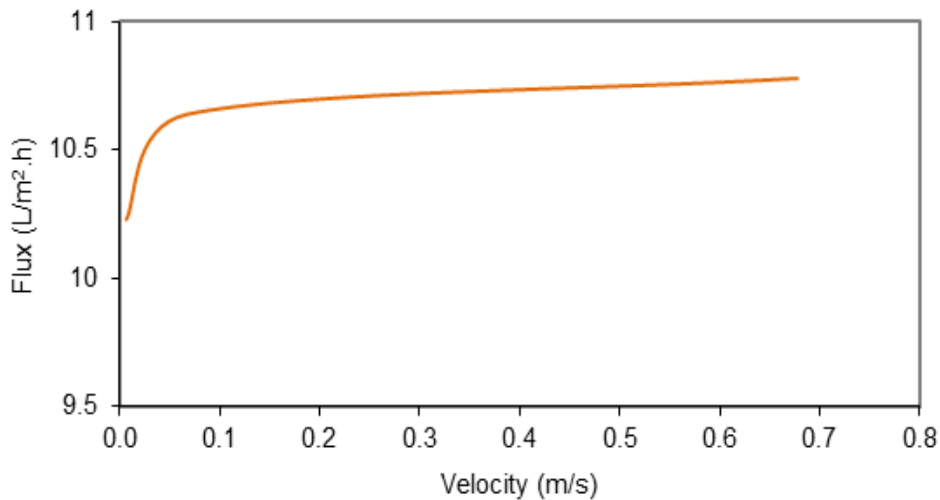
Fig. 6-8. Effect of coolant velocities on flux (70 °C hot inlet temperature and 0.69 m/s feed velocity)

Due to the unique PGMD module characteristics, the coolant is also used as the hot feed. Therefore, the PGMD module has the same flowrate for both feed and coolant flows, and the effect of coolant flow rate has not been extensively investigated compared to DCMD module.

Our hollow fibre PGMD module was tested under a one-pump system, and the brine was firstly pumped through the coolant channel and then flowed through the hot channel via an external heater. Because of the significantly larger cross sectional area of coolant channel compared to the hot channels, the volume of the coolant channel is considerably bigger than that of the feed channel, and subsequently, the coolant velocity is approximately one to two orders of magnitude lower than hot feed velocity (see Table 6-3) [108], and the flow within the coolant channel is within the laminar flow regime. The uniformity of temperature of the coolant channel is lower due to the extremely low coolant velocity (velocity: 0.003 – 0.007 m/s, Re: 30 – 74). To evaluate the effect of coolant velocity on PGMD performance, the model was used to simulate the flux with higher coolant velocity.

Fig. 6-8 shows that flux only increases 4.0% and 5.4% when the coolant velocity increases 10 (0.068 m/s) and 100 times (0.68 m/s) compared to that of case 1 (0. 0068 m/s), showing a minimum effect of coolant velocity on flux. Here, the hot feed velocity is kept at 0.69 m/s during all simulations. Khalifa [8] investigated the performance of a flat sheet PGMD module and he found the similar results. When coolant flow rate was increased from 2 L/min to 4 L/min, the flux only increased about 5%, and the flux

remained nearly the same when coolant flow rate decreased from 2 L/min to 1 L/min. Other studies [20, 100] evaluated the effect of cold permeate velocity on flux for DCMD system. They concluded that cold permeate velocity has insignificant impact on flux compared to feed velocity since the feed side is the source of vapourization and controls the permeation process [100]. For PGMD module, the coolant does not contact with membrane directly and its effect on flux is expected to be lower. Furthermore, the uniformity of temperature within the permeate gap cannot be improved by the coolant velocity, consequently, the effect of coolant velocity on permeate is minimum.

6.4.2.2.   Effect of coolant inlet temperature
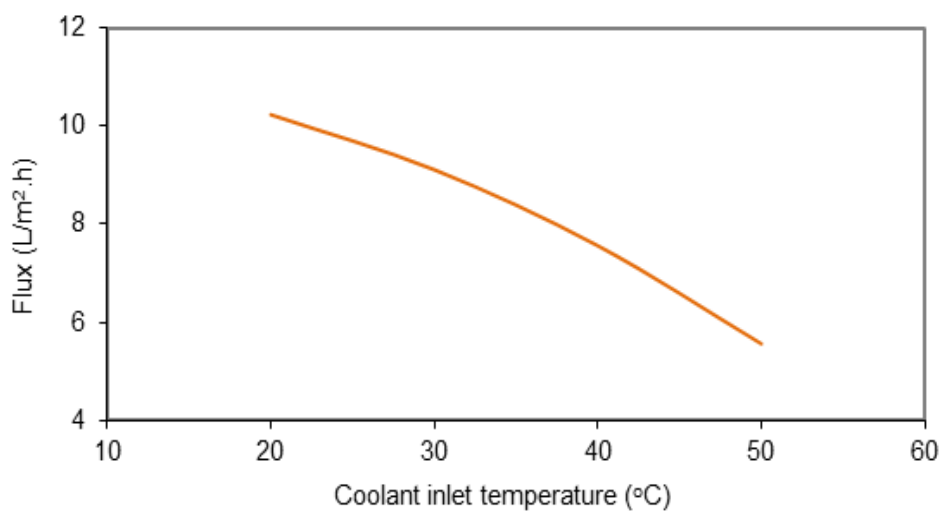
Fig. 6-9. Effect of coolant temperature on flux (0.69 m/s feed velocity)

Fig. 6-9 shows the effect of coolant inlet temperature on flux. It can be seen clearly that the flux decreases as a function of coolant inlet temperature, and it decreases more significantly at higher coolant inlet temperature. This is due to the exponential relationship between vapour pressure difference and temperature difference across the membrane. Furthermore, compared to the effect of hot inlet temperature on flux shown in Fig. 6-5, the coolant inlet temperature has a less impact on flux. Cheng et al. [14] used hollow fibre membrane module to compare the performance of AGMD with PGMD. They identified the similar results as the flux increased exponentially with increasing hot inlet temperature but only decreased gradually with increasing coolant inlet temperature.

Alklaibi et al. [20] reviewed the impacts of coolant inlet temperature of various MD studies. They suggested that changes in coolant temperature can result in more than a 1-fold increase in flux (inlet temperature difference between hot and coolant channels:

30 – 50 ˚C), although the effect of coolant inlet temperature was considerably lower compared to that of hot inlet temperature. In our study, there is less than a 1-fold improvement of flux when the coolant inlet temperature changes from 50 ˚C to 20 ˚C. This indicates that coolant inlet temperature for hollow fibre PGMD has even less effect on flux compared to DCMD. This phenomenon is due to the permeate gap of PGMD module adding to the heat transfer resistance, so a temperature decrease in the cold channel cannot effectively change the vapour pressure difference between the membrane surfaces. Furthermore, this phenomenon makes PGMD module more suitable for multi-stage application. The coolant effluent from an upstream stage is used as the coolant influent for the next stage for multi-stage processes, and the flux does not decrease significantly when coolant temperature increases along the stages.

6.4.2.3. Effect of cooling plate thermal conductivity
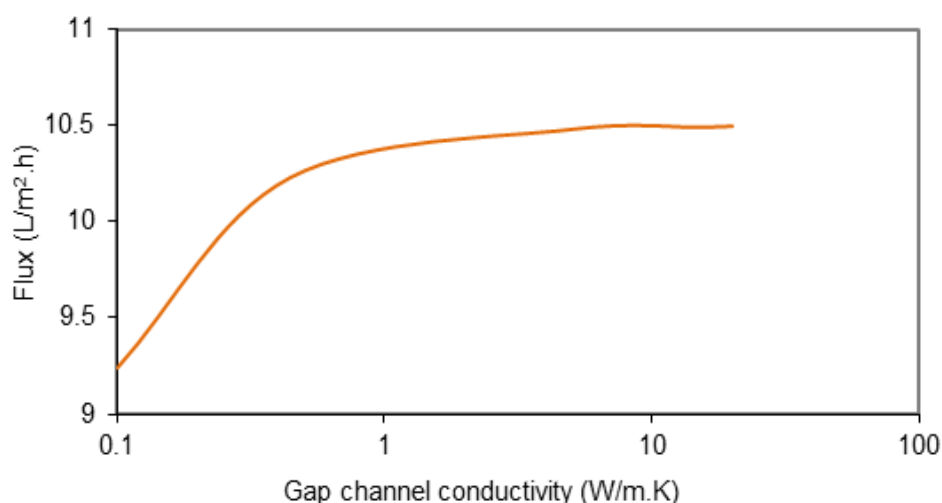
Fig. 6-10. Effect of cooling plate thermal conductivities on flux (70 ˚C hot inlet temperature and 0.69 m/s feed velocity)

The effect of cooling plate thermal conductivity on flux is shown in Fig. 6-10. A feed inlet temperature of 70 ˚C, coolant inlet temperature of 20 ˚C and feed velocity of 0.69 m/s were used as inputs for the model.

It can be clearly seen that the flux increases 14% when the cooling plate thermal conductivity increases from 0.1 W/m.K to 5 W/m.K, and there is much less increase in flux when cooling plate thermal conductivity is higher than 5 W/m.K. The high cooling plate thermal conductivity will lead to high heat transfer from the permeate gap to the coolant channel, and lower the temperature in the permeate gap. Thus, the flux will be higher at greater thermal conductivity of the cooling plate due to the greater temperature difference across the membrane. When the cooling plate thermal

conductivity is higher than 5 W/m.K, the heat transfer resistance of the cooling plate is negligible and the temperature at the interface between cooling plate and coolant (T_{cc}) and temperature at the interface between cooling plate and permeate (T_{pc}) are nearly the same (see Fig. 6-11). The temperature profile is then similar to that of the coolant channel in DCMD configuration. Further increases in cooling plate thermal conductivity will not significantly improve the heat transfer through the cooling plate and permeate gap. Swaminathan et al. [16] filled the gap of PGMD with high conductivity materials and investigated the effect of gap conductivity on flux. They also found that the effect of gap conductivity became minimum when it was higher than 10 W/m.K.

In addition to the highly conductive cooling plate, high conductivity materials (such as metal mesh) could be inserted into the permeate gap to further improve hollow fibre PGMD performance.

a) HDPE cooling plate thermal conductivity of 0.445 W/m.K
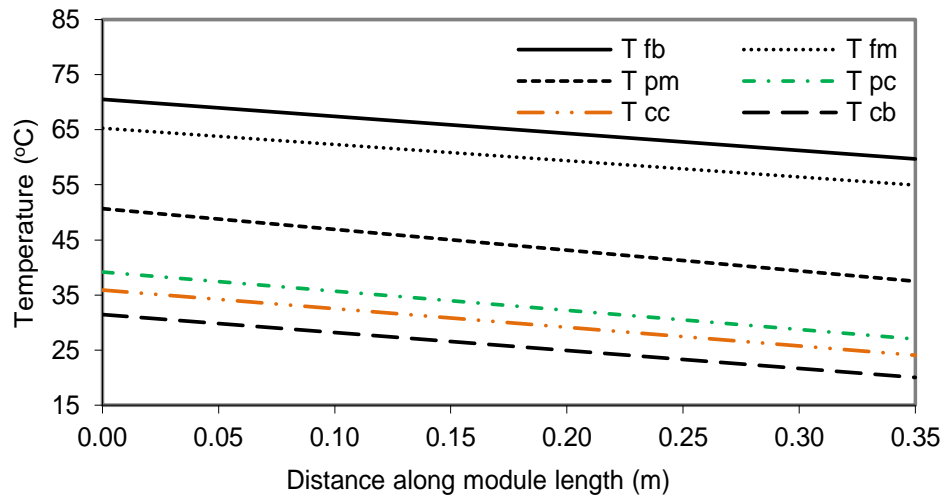
b) SS cooling plate thermal conductivity of 15 W/m.K
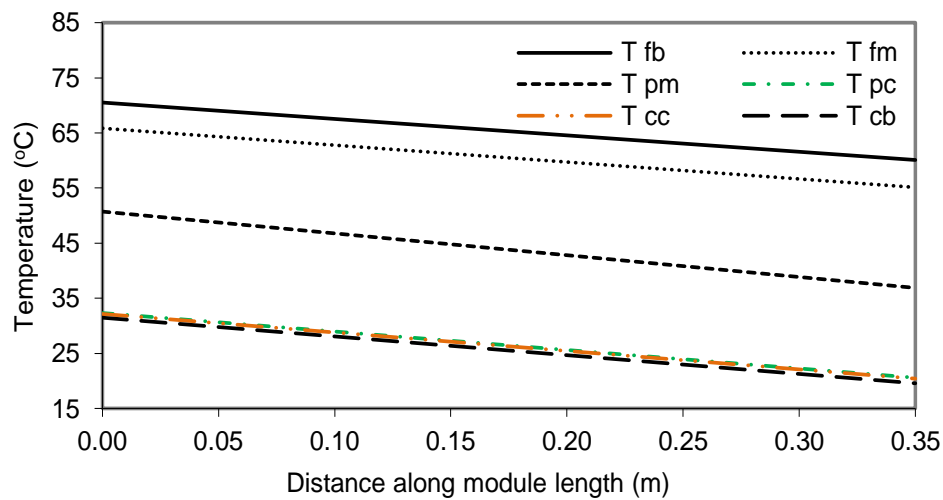
Fig. 6-11. Effect of different gap channel thermal conductivities on temperature profile (70 ˚C hot inlet temperature and 0.69 m/s feed velocity)

6.4.2.4. Sensitivity study of different gap channel properties
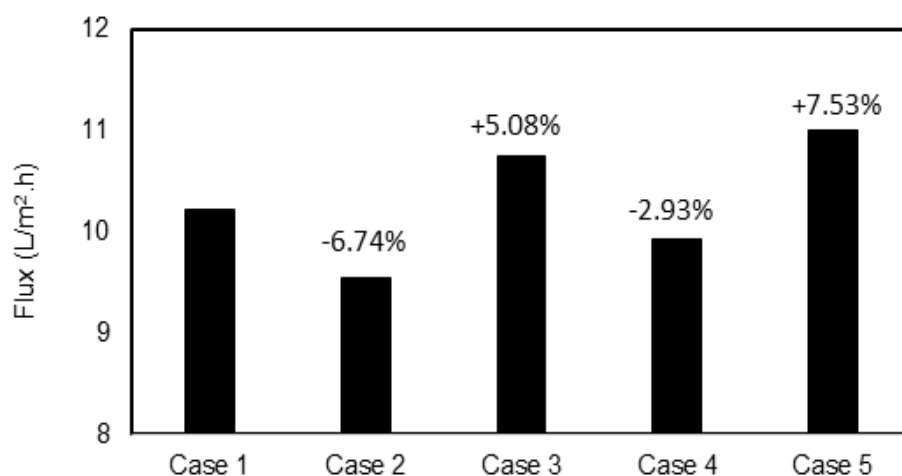
Fig. 6-12. Sensitivity study of different design parameters (inner/outer diameters and conductivity of gap channel)

During the PGMD experiments, it was identified that the flux of module 4 with SS gap channel was higher than that of module 1 with HDPE gap channel. It was suggested this is mainly caused by the higher thermal conductivity of SS compared to HDPE. The simulated results also show the similar outcomes.

The HDPE gap channel had a smaller inner/outer diameters compared to the SS gap channel, consequently, the hydrodynamics of coolant and permeate gaps will be influenced in addition to the thermal conductivity when SS gap channel is used to replace HDPE gap channel. Hence, a typical One-At-A-Time approach was used here to evaluate the effects of different parameters (gap channel conductivity, gap channel inner dimeter and outer dimeter) on PGMD performance.

Table 6-8 shows the model inputs for the design variables of 5 cases. As mentioned before, the base case (case 1) is based on module 1 with HDPE gap channel operated at 70 ˚C hot inlet temperature and 0.69 m/s feed velocity.

Table 6-8 Design parameters of sensitivity analysis

	Gap channel conductivity (W/m.K)	Gap channel inner diameter (mm)	Gap channel outer diameter (mm)
Case 1	0.445	2.84	3.40
Case 2	0.445	2.84	6.35
Case 3	15	2.84	6.35
Case 4	0.445	1.60	3.40
Case 5	15	1.60	3.40

Fig. 6-12 shows the flux of each case and the percentage of relative flux change based on case 1.

For case 2, the gap channel conductivity and gap channel inner diameter are kept the same as case 1, but the gap channel outer dimeter is increased to 6.35 mm, which is same as SS gap channel outer diameter. The simulated result show that the flux of case 2 is 6.74% lower than that of case 1. The larger outer dimeter of gap channel will result in a better hydrodynamic flow within the coolant channel due to the higher coolant velocity, but it will also lead to a higher thermal resistance of the gap due to the larger thickness. Because of lower flux of case 2, it can be concluded that the effect of a higher thermal resistance has a greater impact compared to the better hydrodynamics. There are two main reasons for this phenomenon, firstly, although the coolant velocity of case 2 (0.019 m/s) is approximately 1.8 times higher than that of case 1 (0.0068 m/s), they are still within the laminar flow regime and the uniformity of temperature is not improved significantly; secondly, the gap thermal conductivity is low and a thicker gap will result in a higher thermal resistance.

Compared to case 2, the thermal conductivity of the gap channel is increased to 15 W/m.K from 0.445 W/m.K, the inner and outer diameters of gap are still 2.84 mm and 6.35 mm for case 3. The simulated result from Fig. 6-12 shows that the flux for case 3 is 5.1% higher than that of case 1. This result demonstrates that gap channel thermal conductivity has a much greater impact on flux compared to coolant velocity.

For case 4, the gap thermal conductivity and gap channel outer dimeter are the same as those of case 1, but the gap channel inner dimeter is decreased to 1.60 mm. The model result shows a minor decrease of flux (2.93%) compared to case 1. This phenomenon can be explained by the slightly higher thermal conductivity of water (0.6 W/m.K at 20 ˚C) compared to that of HDPE gap channel (0.445 W/m.K). The flow within

the permeate gap is nearly stagnant [6], as a result, the permeate within the gap channel can be considered as an annular layer outside of the hollow fibre membrane. For case 4, when the gap channel inner dimeter is decreased, the thickness of the water annular layer is decreased and the thickness of gap channel with lower thermal conductivity is increased. Consequently, the overall thermal resistance of the gap channel and water layer is higher, and flux is decreased accordingly.

For case 5, the gap channel inner and outer diameters are the same as those of case 4, and the gap thermal conductivity is increased to 15 W/m.K. The simulated result shows a 7.53% increase in flux of case 5 compared to case 1. Similarly, this phenomenon is due to the overall less thermal resistance of the gap channel and water layer.

Both Francis et al. [7] and Khalifa [8] investigated the effect of gap width on PGMD performance using flat sheet membrane modules. Francis et al. [7] identified that the gap width seems to have insignificant effect on flux. On the contrary, Khalifa [8] found that increasing the gap width generally reduced the flux, which was attributed to the increased heat transfer resistance. Compared to the above flat sheet PGMD studies, the changes in gap channel of hollow fibre PGMD module in our study result in a more complex combination (hydrodynamics in coolant and permeate gaps and thickness of gap channel). Based on the above discussion, it is suggested that the larger outer diameter of the gap channel can benefit the hydrodynamic flow within coolant channel, but its effect on flux is very low when the gap channel thermal conductivity is low. The effect of gap channel inner diameter on permeate gap hydrodynamic flow is negligible due to the nearly stagnant flow. Overall, the gap thermal resistance plays a more important role in PGMD performance.

6.4.2.5   Effect of multi-stage process on energy efficiency
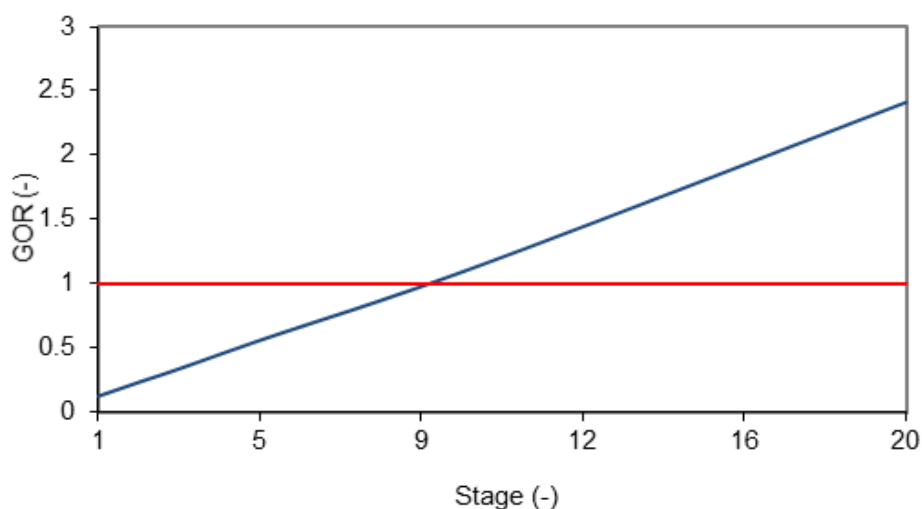
Fig. 6-13. Effect of number of stages on energy efficiency

Compared to a single stage process, a multi-stage process will maximize the internal heat recovery of PGMD to improve energy efficiency. Furthermore, a higher velocity can still be used to improve the uniformity of temperature and improve flux [108].

Here, the developed model is used to evaluate the effect of multi-stage process on energy efficiency of module 1. In the simulation, multiple PGMD modules (module 1) are connected in series, the coolant is pumped into the coolant channel of first module via a chiller, it flows through the coolant channel of each module and comes out from the coolant channel of the last module. Afterwards, it is heated to a pre-set temperature and pumped into the hot channel of the last module. It flows reversely to the first module through the hot channel of each module. A feed velocity of 0.69 m/s, coolant velocity of 0.0068 m/s, hot inlet temperature of 70 ˚C, and coolant inlet temperature of 20 ˚C are used as the model inputs (here, the flowrates of feed and coolant are identical).

The Gain Output Ratio (GOR) is used here to indicate the energy efficiency of hollow fibre PGMD module. When GOR is higher than 1, it demonstrates the thermal energy savings compared to the pure evaporation process without any heat recovery [101].

Fig. 6-13 shows that the GOR increases as the number of stages increase, from 0.12 with a 1 stage unit to 2.4 with a 20 stage unit. When there are more than 9 stages of PGMD modules, the GOR becomes higher than 1. Cipollina et al. [13] used a predictive model to simulate the behavior of multi-stage flat sheet PGMD and found that GOR

can increase 20 times from a 1 stage unit to a 9 stage unit, and may reach a value between 3 and 4. With a similar flowrate (200 mL/min), GOR from their study became more than 1 with a 3 stage unit, which is much less than that of our study. They suggested that the most energy efficient system should have more stages with larger membrane surface area. The effective membrane surface area of the single module from their study is 0.042 m^2, which is approximately 5 times larger than that of our hollow fibre PGMD module. Consequently, the GOR of their module reaches 1 with only 3 stages. Module 1 from this study has relatively low gap channel density and hollow fibre density, but a full scale hollow fibre membrane module normally has a higher packing density and large specific surface area [108], which will lead to a higher GOR value.

6.5. Summary

In this chapter, a mathematical model was developed to simulate mass and heat transfers for desalination using hollow fibre PGMD modules. The model has been validated by experimental results, and the difference between simulated results and experimental results were within the experimental error range except for high hollow fibre packing densities when the model overestimates the flux. The main reason for this phenomenon is that the model simulates the flux under optimal situation where hollow fibre has the full contact with both feed and permeate, but actually the fibres may touch each other leading to a reduced effective membrane area.

The validated model was then used to investigate effects of different design parameters and operating conditions on hollow fibre PGMD performance. It was suggested that coolant velocity and coolant temperature had less impacts on flux compared to those of DCMD, because the coolant of DCMD contacts with membrane directly. Furthermore, the coolant velocity of PGMD is extremely low, so the uniformity of temperature within the coolant channel cannot be effectively improved.

The model also suggested that increasing the cooling plate thermal conductivity will result in a higher flux. However, when the cooling plate thermal conductivity is higher than 5 W/m.K, the temperature difference across the cooling plate is minimum and further increases in the cooling plate thermal conductivity has a negligible impact on flux. In application, the use of high conductive material needs to be balanced with the cost.

A sensitivity study was undertaken to analyze the combined effects of gap channel inner/outer diameters and gap channel thermal conductivity on flux. It is concluded that

the gap thermal conductivity plays a more important role in PGMD performance compared to the hydrodynamic flow within permeate and coolant channels.

The effect of multi-stage process on energy efficiency was evaluated by the developed model. The results suggest that the GOR increases as a function of number of stages, and reaches 2.4 for a 20 stage unit. The energy performance can be further improved for the module with a higher hollow fibre packing density/gap channel density.

It is worthwhile mentioning that the developed model package is only validated under current experimental conditions, however, the trends shown in this study should be representative. Furthermore, the model could be easily updated to accommodate different operating conditions, such as different salinities. However, it is suggested to re-validate the updated model before the application.

Chapter 7 Conclusions and recommendations

In this study, a specifically designed hollow fibre PGMD has been systematically investigated using both experimental and mathematical approaches. There are four main components of this study: firstly of all, the employed hollow fibre membrane has been characterized to confirm its suitability for MD application; secondly, a specifically designed hollow fibre PGMD module has been experimentally investigated and its performance has been compared with that of (a) same module operated in DCMD and SGMD modes; and (b) other spiral wound and flat sheet PGMD studies; thirdly, the effects of hollow fibre packing density, gap channel density and gap materials on PGMD performance have been assessed, in terms of productivity and energy efficiency; and finally, a mathematical model has been developed to predict the permeation flux based on the theoretical analysis of mass and heat transfers within hollow fibre PGMD module, the developed model has also been utilized to identify further optimization opportunities.

For the first component, based on the membrane characterization, it is confirmed that the employed membrane has a unique three-layer morphology: a finger-like macro-void inner and outer layers, a sponge-like middle layer. The tortuosity of the finger-like macro-void layer is close to 1 and that of sponge-like middle layer is much greater than 1. Additionally, the porosity of the macro-void finger-like layers is much higher than that of sponge-like middle layer. The higher porosity and smaller tortuosity within the finger-like layers will increase the flux and lower the sensible heat loss. The smaller porosity and larger tortuosity of the sponge-like middle layer can provide the desired mechanical strength.

The membrane mean pore size was measured to be about 0.15 μm, which is within the typical mean pore size range of 0.07 – 0.32 μm for PVDF membrane employed in MD process. The measured contact angles for inner and outer surfaces were 132°±3° and 94°±2°, respectively, showing hydrophobic characteristics. The larger inner surface contact angle indicates a higher hydrophobicity, which can effectively prevent water from penetrating into the membrane pores as the feed solution is pumped through the hollow fiber lumen. Based on these results, it is concluded that the employed hollow fibre membrane is suitable for MD applications.

For the second component, a new hollow fibre PGMD module was successfully developed and tested with different feed velocities and feed inlet temperatures. The same module was also operated under DCMD and SGMD modes to enable the performance comparison.

The results showed that the maximum hollow fiber PGMD flux of 9.4 L/m^2.h was obtained for the experimental conditions of 70˚C feed inlet temperature and 0.81 m/s feed velocity, which was 27% and 1.6% lower than the maximum flux of DCMD and SGMD respectively. This phenomenon was due to the higher coolant velocity for DCMD and applied airflow in the gap channel of the SGMD. The experiments also showed that the STEC of PGMD was higher than that of DCMD but lower than that of SGMD, which was mainly due to the higher flux of DCMD. The EE of PGMD was always higher than that of DCMD and lower than that of SGMD, which was attributed to the lower heat loss due to heat conduction for SGMD.

The mass transfer coefficient was used as an indicator to compare performance among PGMD, DCMD and SGMD. For PGMD, the mass transfer coefficient increased with the increasing feed velocity and stabilized at higher feed velocity. Additionally, the mass transfer coefficient increased initially at the lower feed inlet temperature and then decreased when the feed inlet temperature was higher than 60˚C, which could be attributed to the combined effects of transverse vapor flux and the uniformity of the temperature. On the contrary, the global mass transfer coefficients of the DCMD and SGMD decreased slightly as a function of feed inlet temperature, which was probably due to the lower uniformity of temperature in the feed channel at higher temperature. The different trends of global mass transfer coefficients versus feed inlet temperature for PGMD, DCMD and SGMD was probably due to the nearly stagnant permeate overflow within the permeate channel for PGMD compared to the much higher coolant circulation velocity and air velocity for DCMD and SGMD, respectively.

Compared to other studies, our results successfully demonstrated that PGMD has the potential to effectively combine the advantages of different conventional MD processes, a lower STEC compared to DCMD and SGMD when flux was the same. Furthermore, the hollow fiber PGMD module could achieve a better balance between flux and STEC compared to flat sheet and spiral wound PGMD modules.

In order to investigate the effects of different PGMD module designs on water productivity and energy efficiency, five different hollow fibre PGMD modules were manufactured and tested under identical operating conditions. The results showed that module with lower hollow fibre packing density or gap channel density had a higher flux and better energy efficiency, while modules with higher hollow fibre packing density or gap channel density exhibited a more energy efficient use of membrane surface area and higher productivity.

Additionally, the module with a more conductive cooling plate had a higher flux and lower STEC, which was mainly attributed to the lower thermal resistance of the cooling plate. Due to the nearly stagnant velocities within the gap and coolant channels, the impact of cooling plate material on PGMD performance was greater than that of hollow fibre packing density and gap channel density.

The GOR obtained for the hollow fibre PGMD module was relatively low compared to that from other MD studies, which was mainly attributed to the small membrane surface area, high heat loss for two steps of heat transfer and insufficient internal heat recovery. However, the PGMD module performance cannot be assessed purely based on GOR. A trade-off between GOR and flux for MD modules is generally required, and the flux obtained from the hollow fibre PGMD module was relatively high.

Finally, a set of mathematical models were developed to simulate the mass and heat transfer phenomenon in the PGMD process. The model was validated by the experimental data and was employed to evaluate the impacts of important MD design parameters on module performance, which provided a guidance for hollow fibre PGMD module optimization.

In general, it is found that the predicted results from the model agree with the experimental results very well (within the experimental error range), except for high hollow fibre packing density module when the model overestimated the flux. The main reason for this phenomenon was that the model simulated the flux under optimal situation where hollow fibre had the full contact with both feed and permeate, but actually the fibres may touch each other in the small space of the gap channel, and thus, leading to a reduced effective membrane area.

Furthermore, the results from the validated model showed that the coolant velocity and coolant temperature had less impact on flux compared to those of DCMD, because the coolant of DCMD contacts with membrane directly. The coolant velocity of PGMD was extremely low, so the uniformity of the temperature within the coolant channel cannot be effectively improved.

The model also suggested that increasing the cooling plate thermal conductivity can result in a higher flux. However, when the cooling plate thermal conductivity was higher than 5 W/m.K, the temperature difference across the cooling plate was minimum and further increases in the cooling plate thermal conductivity had a negligible impact on flux. In application, the use of highly conductive material needs to be balanced with the cost.

A sensitivity study was undertaken to analyze the combined effects of gap channel inner/outer diameters and gap channel thermal conductivity on flux. It is concluded that the gap thermal conductivity played a more important role in PGMD performance compared to the hydrodynamic flow within permeate and coolant channels.

The effect of multi-stage process on energy efficiency was evaluated by the developed model. The results suggested that the GOR increased as a function of number of stages, and reached 2.4 for a 20 stages unit.

Based on this study, the following key advantages of hollow fibre PGMD module have been identified:

- The heat recovery is integrated within the PGMD module, the external heat exchanger is not required;

- Coolant is also used as the hot feed, therefore, only a single pump is required to circulate both hot feed and coolant;

- PGMD has the potential to effectively combine the advantages of different conventional MD processes, a lower STEC compared to DCMD and SGMD when flux is the same; and

- Hollow fiber PGMD module could achieve a better balance between flux and STEC compared to flat sheet and spiral wound PGMD modules.

In addition, the following limitations have been identified for hollow fibre PGMD module based on the current design:

- The energy consumption is relatively high compared to other MD studies, mainly due to the small membrane surface area;

- The uniformity of the temperature within the permeate gap and coolant channel are low, mainly due to the nearly stagnant flows within the permeate gap and coolant channel; and

- The hollow fibres (gap channels) may have contacted each other, it will result in a reduced effective surface area for membrane (gap channel).

In the future work, the following improvements could be implemented to further optimize the hollow fibre PGMD module.

Firstly, the hollow fibre packing density and gap channel density used in this study are very low compared to the commercialized hollow fibre module products. It is realized

from this study that membrane surface area plays an important role in permeate productivity and energy efficiency. A module with higher hollow fibre packing density and gap channel density could be manufactured and tested to prove the economic feasibility of hollow fibre PGMD concept.

Secondly, the hollow fibre (gap channel) could contact with each other if high hollow fibre packing density (gap channel density) is used. This will lead to a reduced effective membrane surface area (cooling plate surface area). Therefore, baffles and spacers could be integrated into hollow fibre PGMD module to ensure the full contact between membrane and permeate (cooling plate with coolant).

Thirdly, it is identified that the flow within the permeate gap is nearly stagnant, which leads to a lower uniformity of the temperature within the permeate gap. Modified design should be considered to improve the hydrodynamics within the permeate gap. If air could be used to sweep the permeate out of the gap channels, higher flux could be obtained. In the meantime, internal heat recovery can still be realized, which is considered as a key advantage compared to conventional SGMD.

Fourthly, modelling results suggest that multi-stage process can bring various benefits, such as energy efficiency and productivity improvements. Actual multi-stage experiment could be conducted to validate the modelling results and test different multi-stage configurations.

Fifthly, a few assumptions have been made to develop the PGMD mathematical model, which could limit the model applications. For example, heat loss due to the permeate production is not considered during the model development. This can lead to an inaccurate modelled result when permeate production is high as heat loss increases as a function of flux. More effort should be made to eliminate these limitations and ensure an accurate outcome over broader operating conditions.

Finally, artificial brine has been used for all experiments in this study. The investigation of membrane fouling and long term operation with actual wastewater was not included in this study. These factors should be considered in the future investigation.

Nomenclature

α_c	Heat transfer coefficient at coolant side (W/m^2.K)
α_f	Heat transfer coefficient at hot feed side (W/m^2.K)
ε	Membrane porosity (%)
λ_{air}	Thermal conductivity for air (W/m.K)
λ_m	Thermal conductivity for membrane material (W/m.K)
λ_1	Thermal conductivity of the feed brine (W/m.K)
λ_2	Thermal conductivity for hollow fibre membrane (W/m.K)
λ_3	Thermal conductivity for permeate (W/m.K)
λ_4	Thermal conductivity for cooling plate (W/m.K)
τ	Average tortuosity of the membrane pores (-)
γ_1	Surface tension of the solution (N/m)
θ	Contact angle between solution and membrane surface (^{o})
ρ	Density of the fluid (kg/m^3)
π	Ratio of the circumference of a circle to its diameter (-)
μ	Viscosity of the fluids (Pa.s)
A	Cross sectional area of the channel (m^2)
A_1	Cross sectional area for hot channel based on its inner diameter (m^2)
A_m	The membrane surface area (m^2)
b_1	Thickness of the membrane (m)
B	Geometric factor of pore (-)
C_{global}	Global mass transfer coefficient (L/m^2.h.Pa)

C_p | Specific heat capacity (J/kg. ˚C)

$C_{pfb,i}$ | Specific heat capacity of feed bulk flow coming out of slice i (J/kg. ˚C)

$C_{pfb,i-1}$ | Specific heat capacity of feed bulk flow coming into slice i (J/kg. ˚C)

$C_{pcb,i}$ | Specific heat capacity of coolant bulk flow coming out of slice i (J/kg. ˚C)

$C_{pcb,i+1}$ | Specific heat capacity of coolant bulk flow coming into the slice i (J/kg. ˚C)

dx_i | Length of the slice i (m)

d | Mean pore diameter of employed membrane (m)

d_h | Hydraulic diameter of the flowing channel (m)

d_{hf} | Hydraulic diameter for the hot channel (m)

d_{fi} | Inner diameter for the hollow fibre (m)

d_{fo} | Outer diameter for the hollow fibre (m)

d_{gi} | Inner diameter for the gap channel (m)

d_{go} | Outer diameter for the gap channel (m)

d_{pi} | Inner diameter for the PE pipe (m)

D_{AB} | Diffusivity of the water vapour (A) relative to air (B) (m^2/s)

F | Force from surface tension (N)

g | Acceleration due to the gravity (m/s^2)

h | Height difference between the top of the fibre and water surface (m)

h_{latent} | Latent heat of vaporization of water (J/kg)

i | i^{th} slice (-)

J_{vm}	Vapour flux through the membrane (kg/m².h)
$J_{fb,i}$	Vapour flux in the hot feed channel (kg/m².h)
$J_{pg,i}$	Vapour flux in permeate gap (kg/m².h)
Kn	Knudsen number (-)
l	Membrane module length (m)
l_f	Mean free path of the transferred gas molecules (m)
L_1	Circumference of hollow fibre membrane based on its inner diameter (m)
L_2	Average circumference based on average radius r_2 (m)
Δm	The mass change due to the force from surface tension (kg)
M	The molecular mass of the water vapour (g/mol)
$\Delta \dot{m}_{fb,i}$	Change of mass flow rate for the feed bulk flow (kg/s)
$\dot{m}_{fb,i}$	Mass flow rate of bulk feed flow coming out of slice i (kg/s)
$\dot{m}_{fb,i-1}$	Mass flow rate of bulk feed flow coming into the slice i (kg/s)
$\dot{m}_{pg,i}$	Mass flow rates of the permeate coming out the slice i (kg/s)
$\dot{m}_{pg,i+1}$	Mass flow rates of the permeate coming into the slice i (kg/s)
$\dot{m}_{cb,i}$	Mass flow rate of coolant bulk flow coming out of slice i (kg/s)
$\dot{m}_{cb,i+1}$	Mass flow rate of coolant bulk flow coming into the slice i (kg/s)
$\dot{m}_{feed}$	Feed mass flow rate (kg/s)
$\dot{m}_{permeate}$	Mass flow rate of the produced permeate (kg/s)
N	Mass transfer coefficient for hollow fibre membrane (L/m².h.Pa)
N_{Kn}	Mass transfer coefficient for Knudsen mechanism (L/m².h.Pa)
N_m	Mass transfer coefficient for molecular diffusion mechanism (L/m².h.Pa)

Nu	Nusselt's number (-)
Nu_f	Nusselt's number of the hot feed (-)
N_f	Number of hollow fibre (-)
N_g	Number of gap channel (-)
ΔP_{avg}	Average vapour pressure difference between the feed bulk flow and the permeate gap (Pa)
P	Total pressure (Pa)
P_{fm}	Vapour pressure at membrane interface temperature at hot feed side (Pa)
P_{pm}	Vapour pressure at membrane interface temperature at permeate side (Pa)
$P_{T_{fb}}$	Vapour pressure based on feed bulk temperature (Pa)
$P_{T_{pb}}$	Vapour pressure based on permeate bulk temperature (Pa)
P_{H_i}	Vapour pressure at inlet of feed channel (Pa)
P_{H_o}	Vapour pressure at outlet of feed channel (Pa)
P_{P_o}	Vapour pressure at overflow point of permeate channel (Pa)
P_{P_s}	Vapour pressure at bottom of permeate channel (Pa)
P_{vacuum}	Vacuum pressure at permeate side (Pa)
P_v	Water vapour partial pressure (Pa)
Pw	Wetted perimeter of the cross section (m)
Pr	Prandtl number (-)
Q_{trans}	Total heat transfer (J)
$\dot{Q}_{heat}$	External thermal energy input (J)
$\dot{Q}_{total.heat.loss}$	Total heat loss of the feed (J)

Q_1	Total heat transfer rate in the hot feed channel (J)
Q_2	Total heat transfer from the bulk hot flow to the membrane surface (J)
Q_3	Total heat transfer through the hollow fibre membrane (J)
Q_4	Total heat transfer within the permeate gap (J)
Q_5	Total heat transfer through the cooling plate (J)
Q_6	Total heat transfer from the cooling plate surface to the coolant bulk flow (J)
Q_7	Total heat transfer for the coolant bulk flow (J)
R	Universal gas constant (J/mol.K.)
Re	Reynolds number (-)
r_1	Inner radius of hollow fibre (m)
r_2	Average radius based on the inner (r_1) and outer (r_3) radius of the hollow fibre membrane (m)
r_3	Outer radius of hollow fibre (m)
r_5	Inner radius of the cooling plate (m)
r_7	Outer radius of the cooling plate (m)
r_{max}	Maximum pore radius (m)
S	Indicator for effective use of membrane surface area (kWh/kg.m^2)
T	Mean temperature in membrane pores (˚C)
T_{Hi}	Inlet temperature of the feed channel (˚C)
T_{Ho}	Outlet temperature of the feed channel (˚C)
T_{Co}	Outlet temperature of the coolant channel (˚C)
T_{Po}	Overflow temperature of the permeate gap (˚C)

T_{Ps}	Bottom temperature of the permeate gap (˚C)
T_{fb}	Feed bulk temperature (˚C)
T_{cb}	Coolant bulk temperature (˚C)
T_{pb}	Permeate bulk temperature (˚C)
T_{fm}	Interface temperature between membrane and feed solution (˚C)
T_{pm}	Interface temperature between permeate and membrane (˚C)
T_{pc}	Interface temperature between cooling plate and permeate (˚C)
T_{cc}	Interface temperature between coolant and cooling plate (˚C)
T_{cm}	Interface temperature between membrane and coolant (˚C)
v	Velocity (m/s)
V_{mass}	Mass volume of the hollow fibre (m^3)
V_{total}	Total volume of the hollow fibre (m^3)
χ_A	Mole fraction of the water vapour (%)

Reference

[1] A. Alkhudhiri, N. Darwish, N. Hilal, Membrane distillation: A comprehensive review, Desalination, 287 (2012) 2-18.

[2] M. Khayet, T. Matsuura, Membrane Distillation Principles and Applications, Elsevier, Amsterdam, 2011.

[3] P. Wang, T.-S. Chung, Recent advances in membrane distillation processes: Membrane development, configuration design and application exploring, Journal of Membrane Science, 474 (2015) 39-56.

[4] L. Camacho, L. Dumée, J. Zhang, J.-d. Li, M. Duke, J. Gomez, S. Gray, Advances in Membrane Distillation for Water Desalination and Purification Applications, Water, 5 (2013) 94-196.

[5] J. Zhang, N. Dow, M. Duke, E. Ostarcevic, J.-D. Li, S. Gray, Identification of material and physical features of membrane distillation membranes for high performance desalination, Journal of Membrane Science, 349 (2010) 295-303.

[6] L. Gao, J. Zhang, S. Gray, J.-D. Li, Experimental study of hollow fiber permeate gap membrane distillation and its performance comparison with DCMD and SGMD, Separation and Purification Technology, 188 (2017) 11-23.

[7] L. Francis, N. Ghaffour, A.A. Alsaadi, G.L. Amy, Material gap membrane distillation: A new design for water vapor flux enhancement, Journal of Membrane Science, 448 (2013) 240-247.

[8] A.E. Khalifa, Water and air gap membrane distillation for water desalination – An experimental comparative study, Separation and Purification Technology, 141 (2015) 276-284.

[9] F. Mahmoudi, H. Siddiqui, M. Pishbin, G. Goodarzi, S. Dehghani, A. Date, A. Akbarzadeh, Sustainable Seawater Desalination by Permeate Gap Membrane Distillation Technology, Energy Procedia, 110 (2017) 346-351.

[10] A. Ruiz-Aguirre, J.A. Andrés-Mañas, J.M. Fernández-Sevilla, G. Zaragoza, Modeling and optimization of a commercial permeate gap spiral wound membrane distillation module for seawater desalination, Desalination, 419 (2017) 160-168.

[11] M. Essalhi, M. Khayet, Application of a porous composite hydrophobic/hydrophilic membrane in desalination by air gap and liquid gap membrane distillation: A comparative study, Separation and Purification Technology, 133 (2014) 176-186.

[12] V.V. Ugrozov, I.B. Elkina, V.N. Nikulin, L.I. Kataeva, Theoretical and experimental research of liquid-gap membrane distillation process in membrane module, Desalination, 157 (2003) 325-331.

[13] A. Cipollina, M.G. Di Sparti, A. Tamburini, G. Micale, Development of a Membrane Distillation module for solar energy seawater desalination, Chemical Engineering Research and Design, 90 (2012) 2101-2121.

[14] L. Cheng, Y. Zhao, P. Li, W. Li, F. Wang, Comparative study of air gap and permeate gap membrane distillation using internal heat recovery hollow fiber membrane module, Desalination, 426 (2018) 42-49.

[15] F. Mahmoudi, G.M. Goodarzi, S. Dehghani, A. Akbarzadeh, Experimental and theoretical study of a lab scale permeate gap membrane distillation setup for desalination, Desalination, 419 (2017) 197-210.

[16] J. Swaminathan, H.W. Chung, D.M. Warsinger, F.A. AlMarzooqi, H.A. Arafat, J.H. Lienhard V, Energy efficiency of permeate gap and novel conductive gap membrane distillation, Journal of Membrane Science, 502 (2016) 171-178.

[17] D. Winter, J. Koschikowski, S. Ripperger, Desalination using membrane distillation: Flux enhancement by feed water deaeration on spiral-wound modules, Journal of Membrane Science, 423-424 (2012) 215-224.

[18] D. Winter, J. Koschikowski, M. Wieghaus, Desalination using membrane distillation: Experimental studies on full scale spiral wound modules, Journal of Membrane Science, 375 (2011) 104-112.

[19] N. Thomas, M.O. Mavukkandy, S. Loutatidou, H.A. Arafat, Membrane distillation research & implementation: Lessons from the past five decades, Separation and Purification Technology, 189 (2017) 108-127.

[20] A.M. Alklaibi, N. Lior, Membrane-distillation desalination: Status and potential, Desalination, 171 (2005) 111-131.

[21] A.E. Khalifa, S.M. Alawad, Air gap and water gap multistage membrane distillation for water desalination, Desalination, 437 (2018) 175-183.

[22] G. Zaragoza, A. Ruiz-Aguirre, E. Guillén-Burrieza, Efficiency in the use of solar thermal energy of small membrane desalination systems for decentralized water production, Applied Energy, 130 (2014) 491-499.

[23] Q. Liu, C. Liu, L. Zhao, W. Ma, H. Liu, J. Ma, Integrated forward osmosis-membrane distillation process for human urine treatment, Water Res, 91 (2016) 45-54.

[24] T. Husnain, Y. Liu, R. Riffat, B. Mi, Integration of forward osmosis and membrane distillation for sustainable wastewater reuse, Separation and Purification Technology, 156 (2015) 424-431.

[25] P. Wang, Y. Cui, Q. Ge, T. Fern Tew, T.-S. Chung, Evaluation of hydroacid complex in the forward osmosis–membrane distillation (FO–MD) system for desalination, Journal of Membrane Science, 494 (2015) 1-7.

[26] K.Y. Wang, M.M. Teoh, A. Nugroho, T.-S. Chung, Integrated forward osmosis–membrane distillation (FO–MD) hybrid system for the concentration of protein solutions, Chemical Engineering Science, 66 (2011) 2421-2430.

[27] R. Creusen, J. van Medevoort, M. Roelands, A. van Renesse van Duivenbode, J.H. Hanemaaijer, R. van Leerdam, Integrated membrane distillation–crystallization: Process design and cost estimations for seawater treatment and fluxes of single salt solutions, Desalination, 323 (2013) 8-16.

[28] X. Ji, E. Curcio, S. Al Obaidani, G. Di Profio, E. Fontananova, E. Drioli, Membrane distillation-crystallization of seawater reverse osmosis brines, Separation and Purification Technology, 71 (2010) 76-82.

[29] J. Kim, H. Kwon, S. Lee, S. Lee, S. Hong, Membrane distillation (MD) integrated with crystallization (MDC) for shale gas produced water (SGPW) treatment, Desalination, 403 (2017) 172-178.

[30] H. Geng, J. Wang, C. Zhang, P. Li, H. Chang, High water recovery of RO brine using multi-stage air gap membrane distillation, Desalination, 355 (2015) 178-185.

[31] H.C. Duong, A.R. Chivas, B. Nelemans, M. Duke, S. Gray, T.Y. Cath, L.D. Nghiem, Treatment of RO brine from CSG produced water by spiral-wound air gap membrane distillation — A pilot study, Desalination, 366 (2015) 121-129.

[32] J.A. Sanmartino, M. Khayet, M.C. García-Payo, H. El-Bakouri, A. Riaza, Treatment of reverse osmosis brine by direct contact membrane distillation: Chemical pretreatment approach, Desalination, 420 (2017) 79-90.

[33] R. Schwantes, K. Chavan, D. Winter, C. Felsmann, J. Pfafferott, Techno-economic comparison of membrane distillation and MVC in a zero liquid discharge application, Desalination, 428 (2018) 50-68.

[34] I. Vergili, Y. Kaya, U. Sen, Z.B. Gönder, C. Aydiner, Techno-economic analysis of textile dye bath wastewater treatment by integrated membrane processes under the zero liquid discharge approach, Resources, Conservation and Recycling, 58 (2012) 25-35.

[35] K. Barr, G.J. Millar, I.D.R. Mackinnon, Desalination by a solar thermal membrane distillation process, in: Membranes & Desalination Conference 2013, Brisbane Convention & Exhibition Centre, Brisbane, Australia, 2013.

[36] A. Chafidz, E.D. Kerme, I. Wazeer, Y. Khalid, A. Ajbar, S.M. Al-Zahrani, Design and fabrication of a portable and hybrid solar-powered membrane distillation system, Journal of Cleaner Production, 133 (2016) 631-647.

[37] A.M. Elzahaby, A.E. Kabeel, M.M. Bassuoni, A.R.A. Elbar, Direct contact membrane water distillation assisted with solar energy, Energy Conversion and Management, 110 (2016) 397-406.

[38] S.E. Moore, S.D. Mirchandani, V. Karanikola, T.M. Nenoff, R.G. Arnold, A. Eduardo Sáez, Process modeling for economic optimization of a solar driven sweeping gas membrane distillation desalination system, Desalination, 437 (2018) 108-120.

[39] K. Rahaoui, L.C. Ding, L.P. Tan, W. Mediouri, F. Mahmoudi, K. Nakoa, A. Akbarzadeh, Sustainable Membrane Distillation Coupled with Solar Pond, Energy Procedia, 110 (2017) 414-419.

[40] R. Schwantes, A. Cipollina, F. Gross, J. Koschikowski, D. Pfeifle, M. Rolletschek, V. Subiela, Membrane distillation: Solar and waste heat driven demonstration plants for desalination, Desalination, 323 (2013) 93-106.

[41] Y. Zhang, L. Liu, K. Li, D. Hou, J. Wang, Enhancement of energy utilization using nanofluid in solar powered membrane distillation, Chemosphere, 212 (2018) 554-562.

[42] A.E. Amali, S. Bouguecha, M. Maalej, Experimental study of air gap and direct contact membrane distillation configurations: application to geothermal and seawater desalination, Desalination, 168 (2004) 357.

[43] B. Ozbey-Unal, D.Y. Imer, B. Keskinler, I. Koyuncu, Boron removal from geothermal water by air gap membrane distillation, Desalination, 433 (2018) 141-150.

[44] R. Sarbatly, C.-K. Chiam, Evaluation of geothermal energy in desalination by vacuum membrane distillation, Applied Energy, 112 (2013) 737-746.

[45] R. Long, X. Lai, Z. Liu, W. Liu, Direct contact membrane distillation system for waste heat recovery: Modelling and multi-objective optimization, Energy, 148 (2018) 1060-1068.

[46] X. Lai, R. Long, Z. Liu, W. Liu, A hybrid system using direct contact membrane distillation for water production to harvest waste heat from the proton exchange membrane fuel cell, Energy, 147 (2018) 578-586.

[47] R.D. Gustafson, S.R. Hiibel, A.E. Childress, Membrane distillation driven by intermittent and variable-temperature waste heat: System arrangements for water production and heat storage, Desalination, 448 (2018) 49-59.

[48] N. Dow, S. Gray, J.-d. Li, J. Zhang, E. Ostarcevic, A. Liubinas, P. Atherton, G. Roeszler, A. Gibbs, M. Duke, Pilot trial of membrane distillation driven by low grade waste heat: Membrane fouling and energy assessment, Desalination, 391 (2016) 30-42.

[49] O.R. Lokare, S. Tavakkoli, G. Rodriguez, V. Khanna, R.D. Vidic, Integrating membrane distillation with waste heat from natural gas compressor stations for produced water treatment in Pennsylvania, Desalination, 413 (2017) 144-153.

[50] E. Curcio, E. Drioli, Membrane Distillation and Related Operations—A Review, Separation & Purification Reviews, 34 (2005) 35-86.

[51] M.M. Teoh, S. Bonyadi, T.-S. Chung, Investigation of different hollow fiber module designs for flux enhancement in the membrane distillation process, Journal of Membrane Science, 311 (2008) 371-379.

[52] A. Ali, P. Aimar, E. Drioli, Effect of module design and flow patterns on performance of membrane distillation process, Chemical Engineering Journal, 277 (2015) 368-377.

[53] A. Ruiz-Aguirre, D.-C. Alarcón-Padilla, G. Zaragoza, Productivity analysis of two spiral-wound membrane distillation prototypes coupled with solar energy, Desalination and Water Treatment, 55 (2014) 2777-2785.

[54] L. Eykens, K.D. Sitter, C. Dotremont, W.D. Schepper, L. Pinoy, B.V.D. Bruggen, Wetting Resistance of Commercial Membrane Distillation Membranes in Waste Streams Containing Surfactants and Oil, Applied Sciences, 7 (2017).

[55] Z.D. Hendren, J. Brant, M.R. Wiesner, Surface modification of nanostructured ceramic membranes for direct contact membrane distillation, Journal of Membrane Science, 331 (2009) 1-10.

[56] C.-C. Ko, A. Ali, E. Drioli, K.-L. Tung, C.-H. Chen, Y.-R. Chen, F. Macedonio, Performance of ceramic membrane in vacuum membrane distillation and in vacuum membrane crystallization, Desalination, 440 (2018) 48-58.

[57] M.-Y. Yang, J.-W. Wang, L. Li, B.-B. Dong, X. Xin, S. Agathopoulos, Fabrication of low thermal conductivity yttrium silicate ceramic flat membrane for membrane distillation, Journal of the European Ceramic Society, (2018).

[58] E. Drioli, A. Ali, F. Macedonio, Membrane distillation: Recent developments and perspectives, Desalination, 356 (2015) 56-84.

[59] J. Zhang, Theoretical and experimental investigation of membrane distillation, in: Institute for Sustainability and Innovation, Victoria University, 2011.

[60] X. Yang, R. Wang, L. Shi, A.G. Fane, M. Debowski, Performance improvement of PVDF hollow fiber-based membrane distillation process, Journal of Membrane Science, 369 (2011) 437-447.

[61] J. Zhang, S. Gray, J.-D. Li, Modelling heat and mass transfers in DCMD using compressible membranes, Journal of Membrane Science, 387-388 (2012) 7-16.

[62] J. Zhang, J.-D. Li, M. Duke, M. Hoang, Z. Xie, A. Groth, C. Tun, S. Gray, Modelling of vacuum membrane distillation, Journal of Membrane Science, 434 (2013) 1-9.

[63] A.S. Alsaadi, N. Ghaffour, J.D. Li, S. Gray, L. Francis, H. Maab, G.L. Amy, Modeling of air-gap membrane distillation process: A theoretical and experimental study, Journal of Membrane Science, 445 (2013) 53-65.

[64] I. Hitsov, T. Maere, K. De Sitter, C. Dotremont, I. Nopens, Modelling approaches in membrane distillation: A critical review, Separation and Purification Technology, 142 (2015) 48-64.

[65] H. Chang, C.-D. Ho, J.-A. Hsu, Analysis of Heat Transfer Coefficients in Direct Contact Membrane Distillation Modules Using CFD Simulation, Journal of Applied Science and Engineering, 19 (2016) 197-206.

[66] J. Phattaranawik, Effect of pore size distribution and air flux on mass transport in direct contact membrane distillation, Journal of Membrane Science, 215 (2003) 75-85.

[67] M. Khayet, C. Cojocaru, Artificial neural network model for desalination by sweeping gas membrane distillation, Desalination, 308 (2013) 102-110.

[68] M. Khayet, C. Cojocaru, Artificial neural network modeling and optimization of desalination by air gap membrane distillation, Separation and Purification Technology, 86 (2012) 171-182.

[69] M. Khayet, C. Cojocaru, C. Garcı́a-Payo, Application of Response Surface Methodology and Experimental Design in Direct Contact Membrane Distillation, Ind. Eng. Chem. Res., 46 (2007) 5673-5685.

[70] D. Cheng, W. Gong, N. Li, Response surface modeling and optimization of direct contact membrane distillation for water desalination, Desalination, 394 (2016) 108-122.

[71] J. Zhang, J.-D. Li, S. Gray, Effect of applied pressure on performance of PTFE membrane in DCMD, Journal of Membrane Science, 369 (2011) 514-525.

[72] S. Srisurichan, R. Jiraratananon, A. Fane, Mass transfer mechanisms and transport resistances in direct contact membrane distillation process, Journal of Membrane Science, 277 (2006) 186-194.

[73] W. Kast, C.-R. Hohenthanner, Mass transfer within the gas-phase of porous media, International Journal of Heat and Mass Transfer, 43 (2000) 807-823.

[74] J. Zhang, J.-D. Li, M. Duke, Z. Xie, S. Gray, Performance of asymmetric hollow fibre membranes in membrane distillation under various configurations and vacuum enhancement, Journal of Membrane Science, 362 (2010) 517-528.

[75] G.K.Batchelor, An Introduction in Fluid Dynamics, 1st ed. ed., Cambridge University Press, London, 1970.

[76] P. Wang, M.M. Teoh, T.S. Chung, Morphological architecture of dual-layer hollow fiber for membrane distillation with higher desalination performance, Water Res, 45 (2011) 5489-5500.

[77] S. Bonyadi, T.-S. Chung, Highly porous and macrovoid-free PVDF hollow fiber membranes for membrane distillation by a solvent-dope solution co-extrusion approach, Journal of Membrane Science, 331 (2009) 66-74.

[78] S. Bonyadi, T.S. Chung, Flux enhancement in membrane distillation by fabrication of dual layer hydrophilic–hydrophobic hollow fiber membranes, Journal of Membrane Science, 306 (2007) 134-146.

[79] L.-H. Cheng, P.-C. Wu, C.-K. Kong, J. Chen, Spatial variations of DCMD performance for desalination through countercurrent hollow fiber modules, Desalination, 234 (2008) 323-334.

[80] K. Yu Wang, T.-S. Chung, M. Gryta, Hydrophobic PVDF hollow fiber membranes with narrow pore size distribution and ultra-thin skin for the fresh water production through membrane distillation, Chemical Engineering Science, 63 (2008) 2587-2594.

[81] M. Gryta, M. Barancewicz, Influence of morphology of PVDF capillary membranes on the performance of direct contact membrane distillation, Journal of Membrane Science, 358 (2010) 158-167.

[82] D. Hou, J. Wang, X. Sun, Z. Ji, Z. Luan, Preparation and properties of PVDF composite hollow fiber membranes for desalination through direct contact membrane distillation, Journal of Membrane Science, 405-406 (2012) 185-200.

[83] J. Phattaranawik, R. Jiraratananon, Direct contact membrane distillation: effect of mass transfer on heat transfer, Journal of Membrane Science, 188 (2001) 137-143.

[84] H.C. Duong, P. Cooper, B. Nelemans, T.Y. Cath, L.D. Nghiema, Optimising thermal efficiency of direct contact membrane distillation by brine recycling for small-scale seawater desalination, Desalination, 374 (2015) 1-9.

[85] S. Al-Obaidani, E. Curcio, F. Macedonio, G.D. Profio, H. Al-Hinai, E. Drioli, Potential of membrane distillation in seawater desalination: Thermal efficiency, sensitivity study and cost estimation, Journal of Membrane Science, 323 (2008) 85-98.

[86] S. Zhao, P.H.M. Feron, Z. Xie, J. Zhang, M. Hoang, Condensation studies in membrane evaporation and sweeping gas membrane distillation, Journal of Membrane Science, 462 (2014) 9-16.

[87] M. Khayet, C. Cojocaru, A. Baroudi, Modeling and optimization of sweeping gas membrane distillation, Desalination, 287 (2012) 159-166.

[88] R. Aryapratama, H. Koo, S. Jeong, S. Lee, Performance evaluation of hollow fiber air gap membrane distillation module with multiple cooling channels, Desalination, 385 (2016) 58-68.

[89] H.C. Duong, P. Cooper, B. Nelemans, T.Y. Cath, L.D. Nghiem, Evaluating energy consumption of air gap membrane distillation for seawater desalination at pilot scale level, Separation and Purification Technology, 166 (2016) 55-62.

[90] J. Swaminathan, H.W. Chung, D.M. Warsinger, J.H.L. V, Membrane distillation model based on heat exchanger theory and configuration comparison, Applied Energy, 184 (2016) 491-505.

[91] J. Zheng, Y. Xu, Z. Xu, Flow distribution in a randomly packed hollow fiber membrane module, Journal of Membrane Science, 211 (2003) 263-269.

[92] A.S. Alsaadi, L. Francis, G.L. Amy, N. Ghaffour, Experimental and theoretical analyses of temperature polarization effect in vacuum membrane distillation, Journal of Membrane Science, 471 (2014) 138-148.

[93] L. Martinez-Diez, M.I. Vazquez-Gonzalez, Temperature and concentration polarization in membrane distillation of aqueous salt solutions, Journal of Membrane Science, 156 (1999) 265-273.

[94] M.D. Lechner, Polymers, in: W.Martienssen, H.Warlimont (Eds.) Spring Handbook of Condensed Matter and Materials Data, Springer Berlin Heidelberg, New York, 2005, pp. 484.

[95] F. Goodwin, S. Guruswamy, K.U. Kainer, C. Kammer, W. Knabl, A. Koethe, G. Leichtfried, G. Schlamp, R. Stickler, H. Warlimont, Metals, in: W.Martienssen, H.Warlimont (Eds.) Springer Handbook of Condensed Matter and Materials Data, Springer Berlin Heidelberg, New York, 2005, pp. 256.

[96] A. Criscuoli, Improvement of the Membrane Distillation performance through the integration of different configurations, Chemical Engineering Research and Design, 111 (2016) 316-322.

[97] E.K. Summers, H.A. Arafat, J.H. Lienhard, Energy efficiency comparison of single-stage membrane distillation (MD) desalination cycles in different configurations, Desalination, 290 (2012) 54-66.

[98] K. Zhao, W. Heinzl, M. Wenzel, S. Büttner, F. Bollen, G. Lange, S. Heinzl, N. Sarda, Experimental study of the memsys vacuum-multi-effect-membrane-distillation (V-MEMD) module, Desalination, 323 (2013) 150-160.

[99] Z. Liu, Q. Gao, X. Lu, L. Zhao, S. Wu, Z. Ma, H. Zhang, Study on the performance of double-pipe air gap membrane distillation module, Desalination, 396 (2016) 48-56.

[100] A. Khalifa, H. Ahmad, M. Antar, T. Laoui, M. Khayet, Experimental and theoretical investigations on water desalination using direct contact membrane distillation, Desalination, 404 (2017) 22-34.

[101] D. Winter, J. Koschikowski, F. Gross, D. Maucher, D. Düver, M. Jositz, T. Mann, A. Hagedorn, Comparative analysis of full-scale membrane distillation contactors - methods and modules, Journal of Membrane Science, 524 (2017) 758-771.

[102] D. Cheng, N. Li, J. Zhang, Modeling and multi-objective optimization of vacuum membrane distillation for enhancement of water productivity and thermal efficiency in desalination, Chemical Engineering Research and Design, 132 (2018) 697-713.

[103] V. Oddone, B. Boerner, S. Reich, Composites of aluminum alloy and magnesium alloy with graphite showing low thermal expansion and high specific thermal conductivity, Science and Technology of Advanced Materials, 18 (2017) 180-186.

[104] L. Chen, Z. Li, Z.-Y. Guo, Experimental investigation of plastic finned-tube heat exchangers, with emphasis on material thermal conductivity, Experimental Thermal and Fluid Science, 33 (2009) 922-928.

[105] N. Song, X. Hou, L. Chen, S. Cui, L. Shi, P. Ding, A Green Plastic Constructed from Cellulose and Functionalized Graphene with High Thermal Conductivity, ACS Appl. Mater. Interfaces, 9 (2017) 17914-17922.

[106] Y. Zhang, Y. Peng, S. Ji, Z. Li, P. Chen, Review of thermal efficiency and heat recycling in membrane distillation processes, Desalination, 367 (2015) 223-239.

[107] M. Khayet, Membranes and theoretical modeling of membrane distillation: A review, Advances in Colloid and Interface Science, 164 (2011) 56-88.

[108] L. Gao, J. Zhang, S. Gray, J.-D. Li, Influence of PGMD module design on the water productivity and energy efficiency in desalination, Desalination, 452 (2019) 29-39.

[109] J. Xu, Y.B. Singh, G.L. Amy, N. Ghaffour, Effect of operating parameters and membrane characteristics on air gap membrane distillation performance for the treatment of highly saline water, Journal of Membrane Science, 512 (2016) 73-82.

Appendix

PGMD model based on MATLAB program

Mass transfer script

```
global Ru M_H2O h_fg0 Patm
global k_m k_g Vh Vc
global r1 r3 r5 r7 r8 L Ng Nf dh35 L35
global dm delta epsilon tau dh1 dh2 dx


N=10000;
beta=1.0;


M_H2O=18;


Ru=8314;


dm=0.00000015;
epsilon=0.817;
tau=1.71;


d1=0.00081;
d3=0.00111;
d5=0.00284;
d7=0.00340;
d8=0.025;
r1=0.000405;
r3=0.000555;
r5=0.00142;
r7=0.00170;
r8=0.0125;


delta=r3*log(r3/r1);


Ng=8;
Nf=1;
```

```
dh1=2*r1;
dh2=(r8*r8-Ng*r7*r7)/(2*r8+Ng*2*r7);


if Nf==1
    dh35=r3*log(r5/r3);
else
    dh35=(r5^2-Nf*r3^2)/(r5+Nf*r3);
end
L35=2*pi*r3*Nf;




L=0.35;
L2=2*pi*r3;
dx=L/(N-1);
x=[0:dx:L];


Patm=101.325;
Qh_0=170;
Qc_0=-170;


Qp_0=0;


mh_0=0.002833333;
mc_0=-0.0028333333;


mh(1:N)=mh_0;
mc(1:N)=mc_0;
mp(1:N)=0;


Th_in=70.52;
Tc_in=20.01;


Th(1:N)=Th_in;
Tc(1:N)=Tc_in;


T_fm(1:N)=0;
T_pm(1:N)=0;
T_cc(1:N)=0;
T_pc(1:N)=0;
```

```
Tmean=0.5*(Th_in+Tc_in);


[vis_a,cp_a,k_a]=airproperties(Tmean);


k=0.2622;
k_m=(1-epsilon)*k+epsilon*k_a;
k_g=0.445;


[rho_h,vis_h,cp_h,k_h]=waterproperties(Th_in);
[rho_c,vis_c,cp_c,k_c]=waterproperties(Tc_in);


Vh=mh_0/1000/(pi*r1*r1*Ng*Nf)
Vc=abs(mc_0)/1000/(pi*r8*r8-Ng*pi*r7*r7)


Re_h=Vh*dh1*rho_h/vis_h;
Pr_h=cp_h*vis_h/k_h;


Re_c=Vc*dh2*rho_c/vis_c;
Pr_c=cp_c*vis_c/k_c;


h_fg0=latentheat(0);


Tup=Th_in;
Tlow=Tc_in;


error=1.0;
m_total=0.0;


while error>0.000001
    mh(1:N)=mh_0;
    mp(1:N)=0;
    m_total=0.0;


    Tguess=0.5*(Tup+Tlow);


    Th(1)=Th_in;
    Tc(1)=Tguess;
```

```matlab
    [Tfm,Tpm,Tcc,Tpc,dmdx,dQ,cp_h,cp_p]=HeatTransfer_1(Th(1),Tc(1));
    T_fm(1)=Tfm;
    T_pm(1)=Tpm;
    T_cc(1)=Tcc;
    T_pc(1)=Tpc;
    mp(1)=dmdx;
    m_total=m_total+dmdx*dx*L2*Ng*Nf;


    for i=2:N
        mh(i)=mh(i-1)-dmdx*dx*L2*Ng*Nf;


        Th(i)=Th(i-1)*mh(i-1)/mh(i)-dQ/(mh(i)*cp_h);
        Tc(i)=Tc(i-1)+dQ/(mc(i)*cp_c);

[Tfm,Tpm,Tcc,Tpc,dmdx,dQ,cp_h,cp_c]=HeatTransfer_1(Th(i),Tc(i));
        T_fm(i)=Tfm;
        T_pm(i)=Tpm;
        T_cc(i)=Tcc;
        T_pc(i)=Tpc;
        mp(i)=dmdx;


        m_total=m_total+dmdx*dx*L2*Ng*Nf;
    end


    if Tc(N)>Tc_in
        Tup=Tguess;
    else
        Tlow=Tguess;
    end


    error=abs(Tc_in-Tc(N))/(Tc_in+273.15)
end


plot(x,Th,'r');
hold on
plot(x,Tc,'r');
plot(x,T_pm,'r');
plot(x,T_fm,'r');
plot(x,T_cc,'b');
plot(x,T_pc,'b');
```

```
flux=m_total*3600/(L*L2*Ng*Nf)
```

Heat transfer script

```
function [Tfm,Tpm,Tcc,Tpc,m,dQ,cp_h,cp_c]=HeatTransfer_1(Th,Tc)


global Ru M_H2O h_fg0 Patm
global k_m k_g Vh Vc
global r1 r3 r5 r7 r8 L Ng Nf dh35 L35
global dm delta epsilon tau dh1 dh2 dx


[rho_h,vis_h,cp_h,k_h]=waterproperties(Th);


[rho_c,vis_c,cp_c,k_c]=waterproperties(Tc);


Re_h=Vh*dh1*rho_h/vis_h;
Pr_h=cp_h*vis_h/k_h;


Re_c=Vc*dh2*rho_c/vis_c;
Pr_c=cp_c*vis_c/k_c;


Nu_h=4.36+0.036*Re_h*Pr_h*dh1/L/(1+0.0011*(Re_h*Pr_h*dh1/L)^0.8);
Nu_c=4.36+0.036*Re_c*Pr_c*dh2/L/(1+0.0011*(Re_c*Pr_c*dh2/L)^0.8);


 h_h=Nu_h*k_h/dh1;
 h_c=Nu_c*k_c/dh2;


 L1=2*pi*r1;
 L2=2*pi*r3;
 L7=2*pi*r7;


U=1.0/(1/(h_c*L7*Ng*dx)+log(r7/r5)/(2*pi*k_g*dx*Ng)+dh35/(k_h*L35*dx*
Ng)+delta/(k_m*dx*L2*Ng*Nf)+1/(h_h*dx*L1*Ng*Nf));


dQ=U*(Th-Tc);
Tfm=Th-dQ/(h_h*dx*L1*Ng*Nf);
Tcc=Tc+dQ/(h_c*dx*L7*Ng);
Tpc=Tcc+dQ*log(r7/r5)/(2*pi*k_g*dx*Ng);
Tpm=Tpc+dQ*dh35/(k_h*L35*dx*Ng);


Tmean=0.5*(Tfm+Tpm);
```

```
error=1.0;

iter=0;

Patm1=Patm*1000;

    while error>0.000001 && iter<100

        Tfm1=Tfm;
        Tpm1=Tpm;

        Tmean1=Tmean+273.15;

        Dv=0.0003939*Tmean1^1.5;

        Pmean_sat=SaturationPressure(Tmean)*1000;

        Ph_sat=SaturationPressure(Tfm)*1000;
        Pc_sat=SaturationPressure(Tpm)*1000;

        [vis_v,cp_v,k_v]=vapourproperties(Tmean);
        hfg=h_fg0+cp_v*Tmean;

mass_coeff=((Patm1-
Pmean_sat)*tau*Ru*Tmean1/(M_H2O*epsilon*Dv)+0.75*tau*sqrt(2*pi*Ru*Tme
an1/M_H2O)/(epsilon*dm))^(-1)/delta;

        m=mass_coeff*(Ph_sat-Pc_sat);

U=1.0/(1/(h_c*L7*Ng*dx)+log(r7/r5)/(2*pi*k_g*dx*Ng)+dh35/(k_h*L35*dx*
Ng)+delta/(k_m*dx*L2*Ng*Nf)+1/(h_h*dx*L1*Ng*Nf));

        dQ=U*(Th-Tc+hfg*m*delta/k_m);

        Tfm=Th-dQ/(h_h*dx*L1*Ng*Nf);
        Tcc=Tc+dQ/(h_c*dx*L7*Ng);
        Tpc=Tcc+dQ*log(r7/r5)/(2*pi*k_g*dx*Ng);
```

```
Tpm=Tpc+dQ*dh35/(k_h*L35*dx*Ng);


Tmean=0.5*(Tfm+Tpm);
iter=iter+1;


error=0.5*abs(Tfm1-Tfm)/(Tfm1+Tfm)+0.5*abs(Tpm1-
Tpm)/(Tpm1+Tpm);


end
```